

# The Commander and Chief: Redefining Light Business Jet Excellence

TEAM YEHUDI LIGHT: PREFERRED CONCEPT REPORT

AE 442: Aerospace Systems Design | November 29, 2016

## **Team Yehudi Light:**

- Aarav Balsu
- Patchara Choakpichitchai
- Kevin Dvorak
- Kevin MacDuff
- Liam McHugh
- Alicia Qiu
- Martynas Vasiliasukas
- Hyung Woo You

## Table of Contents

Nomenclature.....	iv
Acronyms.....	iv
List of Figures.....	v
List of Tables.....	vii
Compliance Checklist.....	ix
Executive Summary.....	x
1 Introduction (Dvorak).....	1
1.1 Key Performance Requirements.....	1
1.2 Configuration Description.....	1
1.3 Configuration 3-View Drawing.....	2
1.4 Configuration Integration.....	3
2 Concept of Operations (McHugh).....	3
2.1 Goals.....	4
2.2 Requirements and Constraints.....	5
2.2.1 Warmup, Taxi, Takeoff & Landing.....	6
2.2.2 Cruise.....	6
2.2.3 Further Requirements.....	6
2.3 Fielding and Maintenance.....	6
3 Configuration (Choakpichitchai & You).....	8
3.1 Draft.....	8
3.1.1 Chief 3 View.....	9
3.1.2 The Commander 3 View.....	10
3.1.3 The Chief – Internal Configuration.....	11
3.1.4 The Commander – Internal Configuration.....	12
3.1.5 The Chief – Cockpit Configuration.....	13
3.1.6 The Commander – Cockpit Configuration.....	14
3.1.7 The Chief – Landing Gear Configuration.....	15
3.1.8 The Commander – Landing Gear Configuration.....	16
3.2 Morphology.....	17
3.2.1 Fuselage Configuration.....	17
3.2.2 Engine Configuration.....	18
3.2.3 Wing Configuration.....	19
3.2.4 Empennage Configuration.....	20
3.2.5 Landing Gear Configuration.....	22
3.2.6 Integrated Configuration Possibilities.....	22
3.3 Internal Configuration.....	23
3.3.1 Seat Selection.....	23
3.3.2 Fuselage for the Commander.....	25

3.3.3	Empennage.....	26
3.3.4	Cockpit.....	27
3.3.5	Fuselage for the Chief.....	30
3.4	Future Work.....	31
4	Weights, Center of Gravity and Balance (Choakpichitchai & Dvorak).....	32
4.1	Component Weights and Location.....	32
4.2	Weight and Balance.....	40
5	Aerodynamics (MacDuff).....	41
5.1	Airfoil Selection.....	41
5.2	Wing Selection and Shape.....	43
5.3	Aircraft Drag Buildup.....	43
5.4	Aircraft Lift Curves and Drag Polars.....	45
5.5	Trade Studies.....	48
5.6	Future Work.....	49
6	Performance (Dvorak & Vasiliauskas).....	50
6.1	Initial Sizing.....	50
6.2	Constraint Analysis.....	52
6.3	Mission Performance.....	54
6.4	Passenger Sensitivity Trade Study.....	57
6.5	Fuel Burn.....	59
6.6	Future Work.....	61
7	Stability and Control (Vasiliauskas).....	61
7.1	Tail Configuration Selection.....	61
7.2	Tail Airfoil Selection.....	63
7.3	Horizontal Tail Sizing.....	65
7.4	Vertical Tail Sizing.....	66
7.5	Control Surface Sizing.....	67
7.6	Pitching Moment and Trim.....	69
7.7	Static Margin.....	71
7.8	Future Work.....	71
8	Propulsion (Balsu).....	72
8.1	Introduction.....	72
8.2	Engine Selection.....	72
8.2.1	Trade Study: Engine Selection Process for the Commander.....	74
8.3	Engine Description for the Commander.....	75
8.4	Engine Performance for the Commander.....	76
8.4.1	Thrust.....	76
8.4.2	Thrust Specific Fuel Consumption for the Commander.....	78
8.5	Trade Study: Engine Selection Process for the Chief.....	80
8.6	Engine Description for the Chief.....	82
8.7	Engine Performance for the Chief.....	83

8.7.1	Thrust .....	83
8.7.2	Thrust Specific Fuel Consumption for the Chief .....	84
8.8	Future Work .....	84
9	Structures (Klepacki & Qiu).....	85
9.1	Introduction .....	86
9.2	Wing Structures.....	90
9.2.1	Wing Primary Structures.....	90
9.2.2	Wing Secondary Structures.....	92
9.3	Fuselage Structures .....	93
9.3.1	Longerons and Floor .....	93
9.3.2	Stringers and Skins .....	96
9.3.3	Cockpit and Empennage Structures .....	100
9.3.4	Vertical Tail and Horizontal Stabilizer Structures.....	102
9.4	Primary Structures Commonality Design .....	103
9.5	Primary Structures Summary and Weight Analysis.....	104
9.6	V-n Diagram.....	107
9.7	Landing Gear.....	110
9.7.1	Gear Configuration Trade Study.....	110
9.7.2	Shock Absorption Trade Study.....	112
9.7.3	Components .....	114
9.7.4	Loads.....	115
9.7.5	Wheel Sizing.....	117
9.7.6	Shock Strut and Height Sizing.....	118
9.8	Future Work .....	119
10	Costs (McHugh).....	120
10.1	Basis for Estimation.....	120
10.2	Method #1: Comparison to other Light Jets .....	120
10.3	Method #2: Weighted Normal Distribution of Comparable Jets.....	121
10.4	Method #3: RAND Corporation's Cost Estimating Relationships.....	122
10.5	Market Analysis.....	124
10.6	RDT&E and Flyaway Costs .....	125
11	Avionics (Balsu) .....	126
11.1	Introduction .....	126
11.2	Avionics Cockpit Package.....	126
11.3	Connectivity Package .....	127
11.4	Upgrades.....	128
12	Conclusion .....	128
	References.....	128

## Nomenclature

$b$	=	wing span
$C_{Lmax}$	=	maximum lift coefficient
$\bar{c}$	=	wing average chord
$CG$	=	center of gravity
$E_t$	=	maximum kinetic energy
$g$	=	gravity
$l$	=	horizontal tail moment arm
$l_{opt}$	=	optimum moment arm
$l_v$	=	vertical tail moment arm
$L/D$	=	lift to drag ratio
$m$	=	mass of aircraft
$n$	=	load factor
$n_{max}$	=	maximum load factor
$n_s$	=	number of main gear struts
$N_g$	=	landing gear load factor
$P_n$	=	nose gear force
$P_m$	=	main gear force
$s_s$	=	maximum allowable tire deflection
$s_t$	=	stroke of the shock absorber
$S$	=	wing area
$S_v$	=	planform area of the vertical tail
$(t/c)_{max}$	=	maximum thickness to chord
$T/W$	=	thrust to weight ratio
$V$	=	airspeed
$V_h$	=	horizontal tail volume coefficient
$V_v$	=	vertical tail volume coefficient
$V^*$	=	maneuver point airspeed
$W$	=	weight of business jet
$w_t$	=	vertical touchdown rate
$\delta_{max}$	=	maximum longitudinal deflection
$\eta_t$	=	energy absorption efficiency of the shock absorber
$\eta_t$	=	tire energy absorption efficiency
$\rho$	=	density
$\rho_0$	=	density at sea level

## Acronyms

AOA	=	Angle of Attack
APU	=	Auxiliary Power Unit
AR	=	Aspect Ratio
CAD	=	Computer Aided Design
CER	=	Cost Estimation Relationships
CFR	=	Code of Federal Regulations

CP	=	Center of Pressure
DFM	=	Design for Manufacturability
EIS	=	Entry Into Service
FAA	=	Federal Aviation Administration
FAR	=	Federal Aviation Regulation
HP	=	High Pressure
IFR	=	Instrument Flight Rules
LP	=	Low Pressure
LRC	=	Long Range Cruise
MMH/FH	=	Maintenance Man-Hours per Flight-Hour
MOS	=	Margin of Safety
MTOW	=	Maximum Takeoff Weight
NACA	=	National Advisory Committee for Aeronautics
NASA	=	National Aeronautics and Space Administration
NBAA	=	Nautical Business Aviation Association
PCR	=	Preferred Concept Report
RDT&E	=	Research, Development, Test & Evaluation
RFP	=	Request for Proposal
TOGW	=	Takeoff Gross Weight
TSFC	=	Thrust Specific Fuel Consumption

## List of Figures

Figure 1.1. 3-View drawing of the Chief.....	2
Figure 1.2. 3-View drawing of the Commander.....	3
Figure 2.1. Mission profile for the Commander and the Chief aircraft series.....	5
Figure 3.1. Possible fuselage configurations considered.....	17
Figure 3.2. Possible engine mount configurations.....	19
Figure 3.3. Possible wing structure configurations.....	19
Figure 3.4. Possible wing locations.....	20
Figure 3.5. Possible empennage configurations.....	21
Figure 3.6. Possible tail configurations.....	21
Figure 3.7. Combinations of all possible configurations before integration.....	23
Figure 3.8. CAD model of a seat.....	24
Figure 3.9. Implementation of the seats in the fuselage.....	25
Figure 3.10. Three views of the fuselage with empennage.....	27
<b>Figure 3.12. Initial concept sketch of the cockpit.....</b>	<b>28</b>
Figure 3.13. CAD draft of the cockpit.....	29
Figure 3.14. Final CAD model draft of the cockpit.....	30
Figure 3.15. The Chief's fuselage.....	31
Figure 5.1. Airfoil lift curve and drag polar.....	43
Figure 5.2. Diagram of the high lift system.....	45
Figure 5.5. Aircraft lift curve and drag polar at takeoff.....	46
Figure 5.6. Aircraft lift curve and drag polar at cruise.....	47
Figure 5.7. Aircraft lift curve and drag polar at landing.....	48

Figure 5.8. Comparing the Aerodynamic Properties of the Airfoils.....	49
Figure 6.1. Worst-case scenario mission profile.....	51
Figure 6.2. The Commander constraint analysis and design space. ....	53
Figure 6.3. The Chief constraint and analysis and design space. ....	54
Figure 6.4. Landing field length vs. weight. ....	56
Figure 6.5. Aircraft range vs. passenger load. ....	58
Figure 7.1. NACA 0009 section lift coefficient plotted against angle of attack and section drag coefficient [25]. ....	65
<b>Figure 7.2. Elevator and rudder diagram.....</b>	<b>68</b>
<b>Figure 7.3. Main wing ailerons and flaps diagram. ....</b>	<b>68</b>
Figure 7.4. Horizontal tail airfoil trade study. ....	70
Figure 8.1. Comparing Various Engine Candidates .....	<b>Error! Bookmark not defined.</b>
Figure 8.2. TFE731-5R engine. ....	75
Figure 8.3. Specifications of TFE731-5R.....	<b>Error! Bookmark not defined.</b>
Figure 8.4. Uninstalled thrust vs. Mach number at varying altitudes from sea level (0 ft) to service ceiling (45,000 ft).....	77
<b>Figure 8.5. Installed thrust vs. Mach number at varying altitudes from sea level (0 ft) to service ceiling (45,000 ft). ....</b>	<b>78</b>
Figure 8.6. TSFC vs. Mach number at standard temperature.....	79
Figure 8.7. TSFC vs. Mach number at cold temperature.....	79
Figure 8.8. TSFC vs. Mach number at hot temperature.....	80
Figure 8.9. Comparing Various Engine Candidates for the Chief.....	<b>Error! Bookmark not defined.</b>
Figure 8.10. Cutaway of TFE731-4R.....	82
Figure 8.11. Specifications of TFE731-4R.....	<b>Error! Bookmark not defined.</b>
Figure 8.12. Uninstalled Thrust vs. Mach Number at varying altitudes from Sea Level (0 ft) to Service Ceiling (45,000 ft) .....	84
Figure 8.13. Installed thrust vs. Mach number at varying altitudes from sea level (0 ft) to service ceiling (45,000 ft). ....	84
Figure 9.1. Complete structures CAD assembly.....	<b>Error! Bookmark not defined.</b>
Figure 9.2. Isometric view of all primary structures.....	87
Figure 9.3. Top view of all primary structures. ....	88
Figure 9.4. Side view of all primary structures.....	89
Figure 9.5. Aerospace certified material properties and allowables for AL 7075-T6. ....	89
Figure 9.6. Limited Load Cases for Wing Primary Structures .....	<b>Error! Bookmark not defined.</b>
Figure 9.7. Primary I-beam dimensions [19]. ....	91
Figure 9.8. Stresses and deflections of a cantilevered beam with a point load.....	92
Figure 9.9. Final primary wing beam dimensions. ....	92
Figure 9.10. Detailed view of wing primary and secondary structures. ....	93
Figure 9.11. Upper longerons (including T-beam cross section) and main floor beam. ....	94
Figure 9.12. Fuselage bending diagram [19]. ....	94
Figure 9.13. Primary C-channel dimensions and geometry.....	95
Figure 9.14. Primary Longerons Dimensions.....	<b>Error! Bookmark not defined.</b>
Figure 9.15. Primary Floor Beam Dimensions .....	<b>Error! Bookmark not defined.</b>

Figure 9.16. Fuselage Margins and Limit Load Deflections .....	<b>Error! Bookmark not defined.</b>
Figure 9.17. Stringer spacing diagram and interfaces.....	97
Figure 9.18. Top view of fuselage structures.....	98
Figure 9.19. Isometric view of fuselage structures.....	99
Figure 9.20. Detailed view of wing spar and fuselage interfaces.....	99
Figure 9.21. Detailed isometric view of cockpit primary and secondary structures.....	101
Figure 9.22. Stringer locations for cockpit, fuselage, and empennage.....	102
Figure 9.23. Tail section primary and secondary structures.....	103
Figure 9.24. Section view of primary structures design and integration within full aircraft assembly.....	104
Figure 9.25. User-created iterative solver and automated design tool input screen.....	105
Figure 9.26. User-created iterative solver and automated design tool detailed analysis screen.....	105
Figure 9.27. Tabulated Weights and Margins of Safety for all Primary and Secondary Structures .....	<b>Error! Bookmark not defined.</b>
Figure 9.28. Relative weight distribution for primary and secondary structures.....	107
Figure 9.29. V-n diagram.....	108
Figure 9.30. Taildragger landing gear configuration [17].....	110
Figure 9.31. Bicycle landing gear configuration [17].....	111
Figure 9.32. Tricycle landing gear configuration [17].....	112
Figure 9.33. Schematic of shock strut absorber [17].....	114
Figure 9.34. Nose Landing Gear and Main Landing Gear Load Calculations for the Chief.....	<b>Error! Bookmark not defined.</b>
Figure 9.35. Nose Landing Gear and Main Landing Gear Load Calculations for the Commander .....	<b>Error! Bookmark not defined.</b>
Figure 9.36. Maximum Kinetic Energy and Shock Absorber Length and Diameter Calculations .....	<b>Error! Bookmark not defined.</b>
Figure 10.1. Cost Over Weight Ratios for Light Jets .....	<b>Error! Bookmark not defined.</b>
Figure 10.2. Multi-Variable Comparison of Similar Jets .....	<b>Error! Bookmark not defined.</b>
Figure 10.3. Quantity of aircraft produced versus RDT&E plus flyaway costs for the Commander.....	<b>Error! Bookmark not defined.</b>
Figure 10.4. Breakdown of RDT&E Plus Flyaway Costs for the Commander..	<b>Error! Bookmark not defined.</b>

## List of Tables

Table 2.1. Mission Leg Descriptions.....	5
Table 3.1. Seat Dimensions .....	24
Table 3.2. Initial Dimensions of the Cockpit.....	28
Table 4.1. Weights and Center of Gravity of the Chief.....	32
Table 4.2. Weights and Center of Gravity of the Commander.....	36
Table 4.3. The Commander Center of Gravity Travel.....	40
Table 4.4. The Chief Center of Gravity Travel.....	40
Table 5.1. Drag Coefficient Values for Takeoff, Cruise, and Landing for The Commander.....	45



Table 5.2. Drag Coefficient Value for The Chief Fuselage for Takeoff, Cruise, and Landing ....	45
Table 6.1. Mission Profile Performance Summary.....	52
Table 6.2. Drag per Segment .....	57
Table 6.3. Commander Maximum Cruise Range. ....	58
Table 6.4. Chief Maximum Cruise Range. ....	58
Table 6.5. The Commander Stage Fuel Burn .....	59
Table 6.6. The Chief Stage Fuel Burn .....	59

## **Engineering Team**

### **Kevin Dvorak**

Team Leader/Weights/Performance

### **Aarav Balsu**

Propulsion/Avionics

### **Patchara Choakpichitchai**

Configurations

### **Anthony Klepacki**

Structures

### **Kevin MacDuff**

Aerodynamics

### **Liam McHugh**

Concept of Operations/Cost

### **Alicia Qiu**

Book Captain/Structures

### **Martynas Vasiliauskas**

Performance/Stability and Control

### **Hyung Woo You**

Configuration

## Compliance Checklist

Parameter	Requirement	Results	Section
Range	2500 nm	2500 nm	
Capacity	Chief: 6 passengers Commander: 8 passengers	Chief: 6 passengers Commander: 8 passengers	Config.
Cruise Speed	Mach 0.85	Mach 0.85	
Cruise Altitude	35,000 ft above sea level	35,000 ft above sea level	
Rate of Climb	3500 ft per minute	Chief: Commander:	6.3
Service Ceiling	45,000 ft above sea level	45,000 ft above sea level	
Takeoff Balanced Field Length	4000 ft	Chief: 3455 ft Commander: 3390 ft	6.3
Landing Field Length	3600 ft	Chief: 2880 ft Commander: 3190 ft	6.3
Baggage Capacity	Chief: 500 lb, 30 $ft^3$ Commander: 1000 lb, 60 $ft^3$	Chief: 500 lb, 30 $ft^3$ Commander: 1000 lb, 60 $ft^3$	
FAA Regulations	Chief: Title 14 CFR Part 23 Commander: Title 14 CFR Part 25	Chief: Title 14 CFR Part 23 Commander: Title 14 CFR Part 25	CWL
Family Commonality	70% of airframe structure and systems weight	-----	
Entry into Service	First Aircraft EIS: 2010 Second Aircraft EIS: 2022	Commander EIS: 2020 Chief EIS: 2022	Intro

## **Executive Summary**

The recent economic downturn has caused a shift in business jet demand to focus on smaller, lighter business jets that are more affordable to own and operate while still providing unmatched luxury and convenience. Modern small business jets are able to operate from shorter runways, which makes them more flexible and allows them to utilize smaller airports than are traditionally available for business jets. A family of light business jets was developed to meet this demand while providing customers with an affordable product to meet their needs.

The family will initially consist of two aircraft; the Chief will seat up to six passengers, while the Commander will seat up to eight passengers. Both aircraft were designed to minimize maintenance and operation costs in order to provide the best value for the customer, and there is a high level of commonality between the Chief and Commander in order to reduce development and production costs. The Commander is expected to have a maximum gross takeoff weight of 19,517 lb with a wingspan of 55 ft and an overall length of 50 ft. The Chief will utilize the same wings, tail, cockpit, and fuselage cross-section as used in the Commander, but the fuselage will be 2.5 ft shorter. The Chief will have a maximum gross takeoff weight of 17,673.83 lb, a wingspan of 55 ft, and a length of 47 ft.

With a build order of 300 aircraft, the Commander will have a unit price of \$11,000,000 and will cost \$9,600,000 to manufacture each aircraft, including distributed research and development costs. The reuse of the wings, tail, cockpit, and fuselage design will allow the Chief to be sold for \$10,500,000 and will cost \$9,200,000 to produce each aircraft with a total build order of 300 aircraft.

## **1 Introduction (Dvorak)**

Smaller business jets offer several advantages over larger business jets, and the market for these lighter jets continues to grow. Smaller jets have significantly lower costs of ownership and operation, and they are able to access smaller, regional airports that are not able to accommodate larger business aircraft. By introducing a family of smaller business jets with coast-to-coast range and comfortable cabins, our aircraft will serve an unmet need in the business aircraft market and provide affordable and convenient transportation to businesses and individuals. The aircraft in the family have significant structural and systems commonality, which reduces development costs and simplifies maintenance and spare part inventories. An initial Entry Into Service of 2020 for the Commander is challenging due to lengthy testing and FAA certification processes, but the use of common materials, systems, and construction techniques will facilitate enable this goal to be met. The Chief will EIS in 2022, which will allow more time to optimize the design and lower the production cost using the lessons learned from the production and fielding of the Commander. This longer development cycle will make the Chief more accessible to a larger market by lowering the purchase and operational costs.

### **1.1 Key Performance Requirements**

The key performance requirements for our aircraft were a range of 2500 nm while cruising at Mach 0.85 at 35,000 ft above mean sea level. The aircraft must also perform this mission while operating from short runways. These requirements were driven by the intended use of the aircraft to fly coast-to-coast at high speed while operating from a wide variety of airports, some of which may have shorter runways. The aircraft must also comply with FAA Regulations to allow them to operate unrestricted in the United States.

### **1.2 Configuration Description**

After conducting an extensive design morphology, it was decided to use a common business jet design to minimize costs and accelerate the development, testing, and production processes. A low-wing, T-tail design with aft-mounted turbofan engines was found to satisfy the requirements and provide the best value to the customer. A circular aluminum fuselage provides ample room for passengers and reduces production and maintenance costs due to its ubiquity in aviation industry. This fuselage design also allows the easy design and production of a family of two light business jets to serve the six-passenger and eight-passenger markets because different lengths of the same fuselage can be used for both aircraft.

### 1.3 Configuration 3-View Drawing

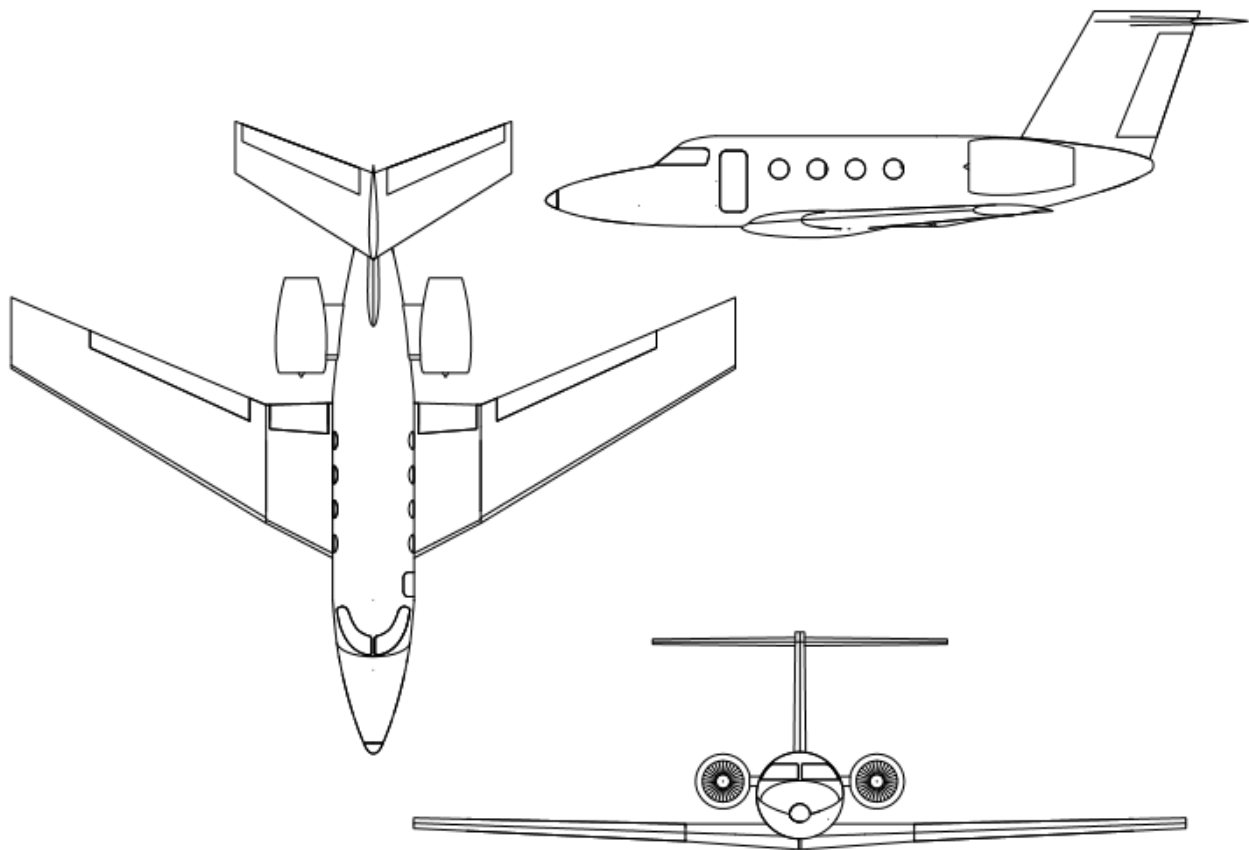


**Figure 1.1. 3-View drawing of the Chief.**

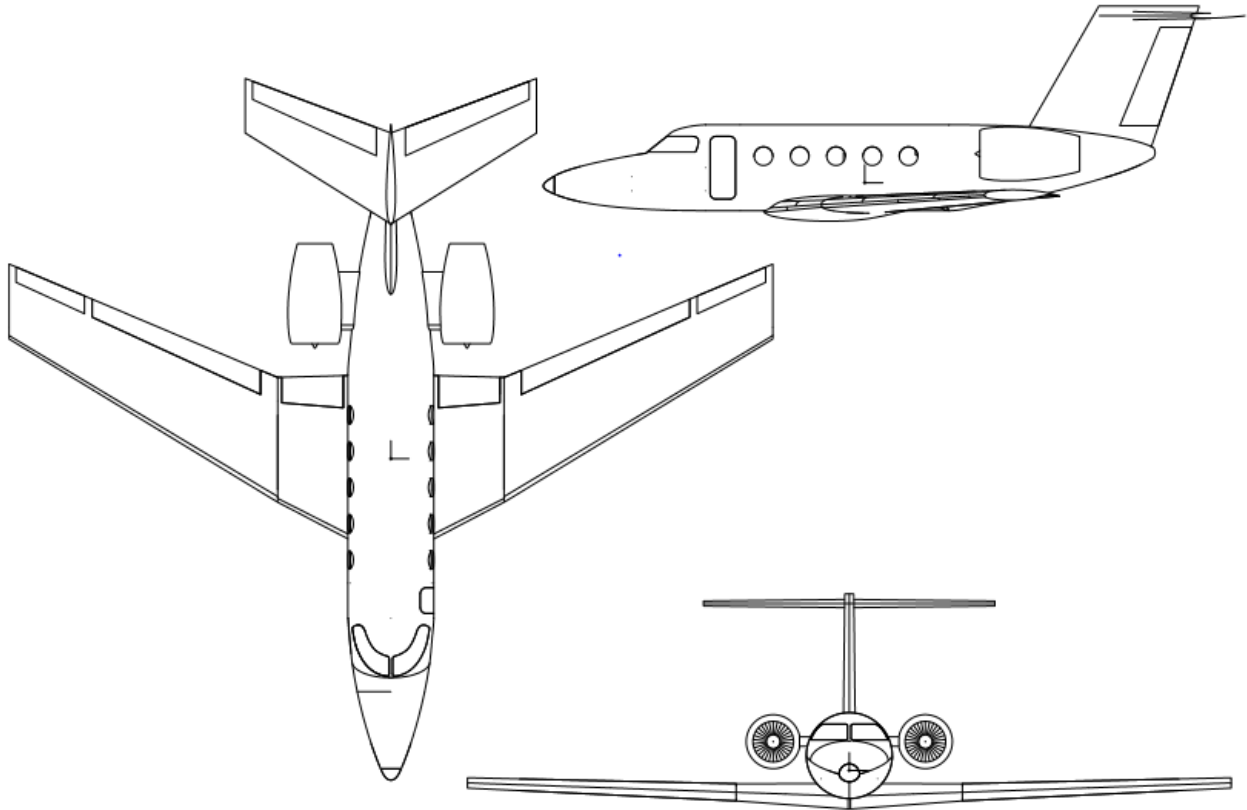


**Figure 1.2. 3-View drawing of the Commander.**

#### **1.4 Configuration Integration**

During the design process, strong cooperation among subsystems due to the significant dependence of each component on other systems. The configuration and overall dimensions had a significant impact on aerodynamics, which in turn determined effected stability and control. This required teamwork to ensure that each subsystem delivered the required performance without interfering with the operation of other subsystems. By communicating the challenges each subsystem faced, team members were able to collaborate and brainstorm new ideas to overcome these challenges. Team members also altered their designs to compensate for changes in other subsystems as well as fluctuations in aircraft weight, aerodynamic properties, and configuration.

## **2 Concept of Operations (McHugh)**

## **2.1 Goals**

In recent times the business aviation market has suffered as a result of the worst economic downturn in decades. Consequently, many of the corporations and high end consumers which were once the lifeblood of this industry have faltered and failed causing devastating effects for aviation companies. Like all luxury markets, the business aviation market suffered disproportionately during this period and is experiencing a much longer regrowth period.

However in the past two years, economic growth has reached what experts call an “escape velocity.” With global activity expanding at an annualized rate of 4.1%, economic growth has finally begun to spread back into luxury markets which has prompted some aviation companies to begin, once again, releasing new aircraft. The underwhelming reception to these releases creates an opportunity for the next generation of aircraft to leapfrog the current competition and capitalize on a weakened market.

As such, a design has been commissioned for the Commander and the Chief aircraft series, a two-member family of fixed-wing, business jets, one with eight seats to be released in 2020 and the other with six seats to be released in 2022. In order to leapfrog the current generation of aircraft, it is necessary for this new family of aircraft to appeal to consumers on their primary motivations for choosing business jet travel. The priorities should be short trip times, a connected and comfortable cabin environment, great value and short runway capability. The most important of these goals should be the pursuit of great value which will depend on minimizing the acquisition and operating costs. This will be achieved by maximizing the opportunities presented by producing a family of aircraft. This includes having a high level of commonality between both aircraft to minimize development and production costs as well as re-using many of the major airframe components such as the wings, tail and landing gear.

## 2.2 Requirements and Constraints

In order to effectively meet the goals set forth by the RFP it is necessary to establish the requirements and constraints for this aircraft series. These parameters will be influenced by a variety of sources including FAA regulations, consumer expectations and current industry standards.

The mission profile is established through interpretations of consumer demands. While the Commander & Chief aircrafts will be capable of a variety of missions, there are certain capabilities which consumers find more appealing and which should therefore be prioritized and defined through a mission profile.

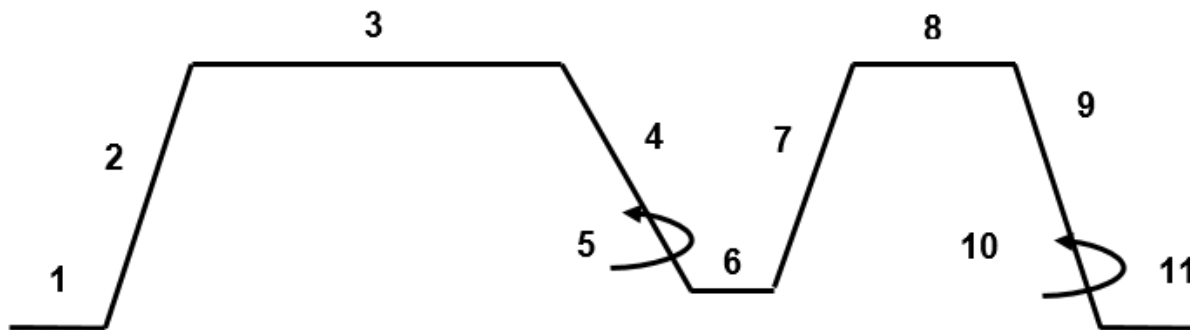


**Figure 2.1. Mission profile for the Commander and the Chief aircraft series.**

Figure 2.1 shows the mission profile for both the Commander and the Chief. The payload is assumed to be four passengers for the eight seat model and two passengers for the six seat model while all other requirements are constant between the two aircraft and specified in **Error!**  
**Reference source not found..**

**Figure 2.2. Mission Leg Descriptions**

<b>Mission Leg</b>	<b>Description</b>	<b>Altitude [ft]</b>	<b>Speed</b>	<b>Range</b>	<b>Time [min]</b>
1	Warmup, Taxi & Takeoff	-	-	< 4000 ft	8
2	Climb	-	3,500 fpm	-	-
3	Cruise	35,000	490 knots	2,500 nm	308
4 & 5	Descent & Loiter	5,000	-	-	30



6 & 7	Aborted landing & Climb	-	-	-	-
8	Cruise	35,000	490 knots	100 nm	12
9 & 10	Descent & Loiter	5,000	-	-	30
11	Landing	-	-	< 3600 ft	-

**2.2.1 Warmup, Taxi, Takeoff & Landing**

The primary driver in these legs is minimizing a flight’s turn-around time, to meet customer’s expectations for short notice flights. Takeoff should be possible in less than 4000 ft with maximum gross weight on a dry pavement and landing should be possible within 3600 ft. Our aircraft should prove capable of achieving this takeoff requirement at altitudes of up to one mile. These requirements will maximize the number of useable airports thereby making these aircraft more convenient for customers unwilling to travel long distances between their destinations and airports.

**2.2.2 Cruise**

In order to facilitate the shorter trip times demanded by the current market, a maximum cruise Mach number of 0.85 at 35000 ft is chosen. This is assuming a typical payload of four passengers and with half of the luggage weight. In fact, our aircraft series should exceed these expectations with the capability to achieve a cruise Mach number of 0.85 at 40000 ft and carry more passengers. Both aircraft should also be capable of a service ceiling of 45000 ft.

**2.2.3 Further Requirements**

In the pursuit of minimizing costs, the Commander and the Chief must share at least 70% of their airframe structure and systems by weight. It is also vital that the six and eight seat models meet the FAR Part 23 and FAR Part 25, respectively.

**2.3 Fielding and Maintenance**

There are many products for which the manufacturer’s responsibilities continue for years after the point of sale. But there are few products for which the stakes of proper maintenance and

fielding are comparable to those in the airline industry. Just one mistake or oversight in one aircraft can not only be detrimental to a company's brand but it can be fatal for their customers. It is for this reason that the responsibilities of fielding and maintenance are so highly prioritized by aircraft manufacturers and so heavily controlled by the FAA.

Raymer Chapter 8 [17] provides details on the two types of maintenance, scheduled and unscheduled. The impact of unscheduled maintenance depends on the average cost of repairs and how often the aircraft breaks, or in other words, how reliable it is. The burden of scheduled maintenance is quantified by the MMH/FH metric. It is the goal of aircraft design to drive this number down.

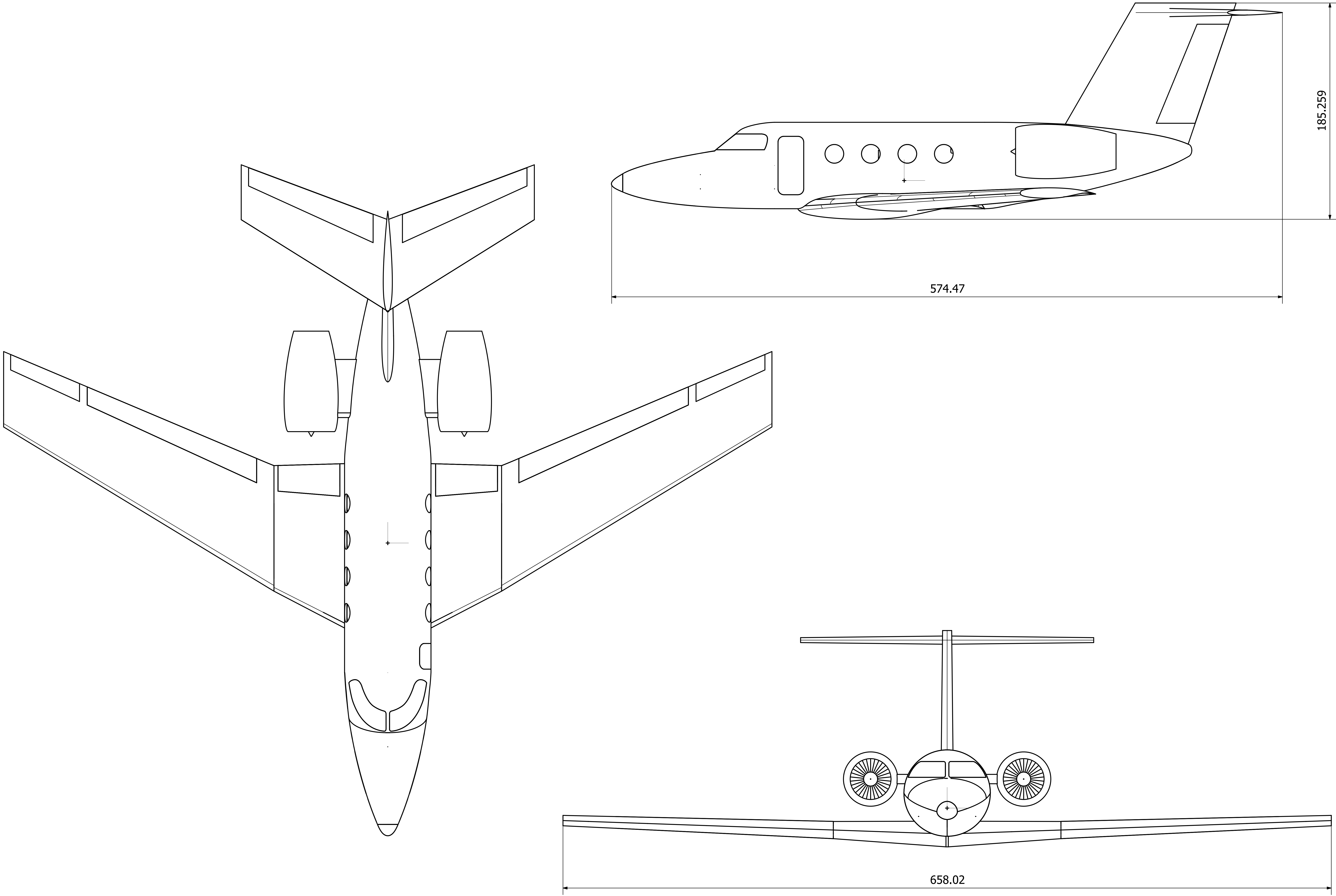
The reliability of an aircraft is dictated by the depth and detail of a number of design decisions. With this in mind, delicate components such as avionics should be positioned such that they are insulated from any vibrations or heat sources which might damage them. The cost to fix an aircraft is a function of its maintainability which is directly related to the accessibility of its internal components. For this reason, the placement of major components should be "one-deep" and within arm's reach of access doors so that they can be readily repaired or easily replaced. Maintenance space around these components will also be included in the design so that engineers have freedom of movement around them which will make repairs easier and further decrease periods of inoperability.

As a result of the risks and liabilities associated with air travel the maintenance of aircraft is regulated by the FAA through mandates set forth in FAR Part 43. While inspections and certification are encompassed within this oversight, it is still the responsibility of the customer and primarily the manufacturer to ensure proper maintenance of their aircraft. A company can achieve this by providing the necessary facilities and expertise directly to their customers, at a cost.

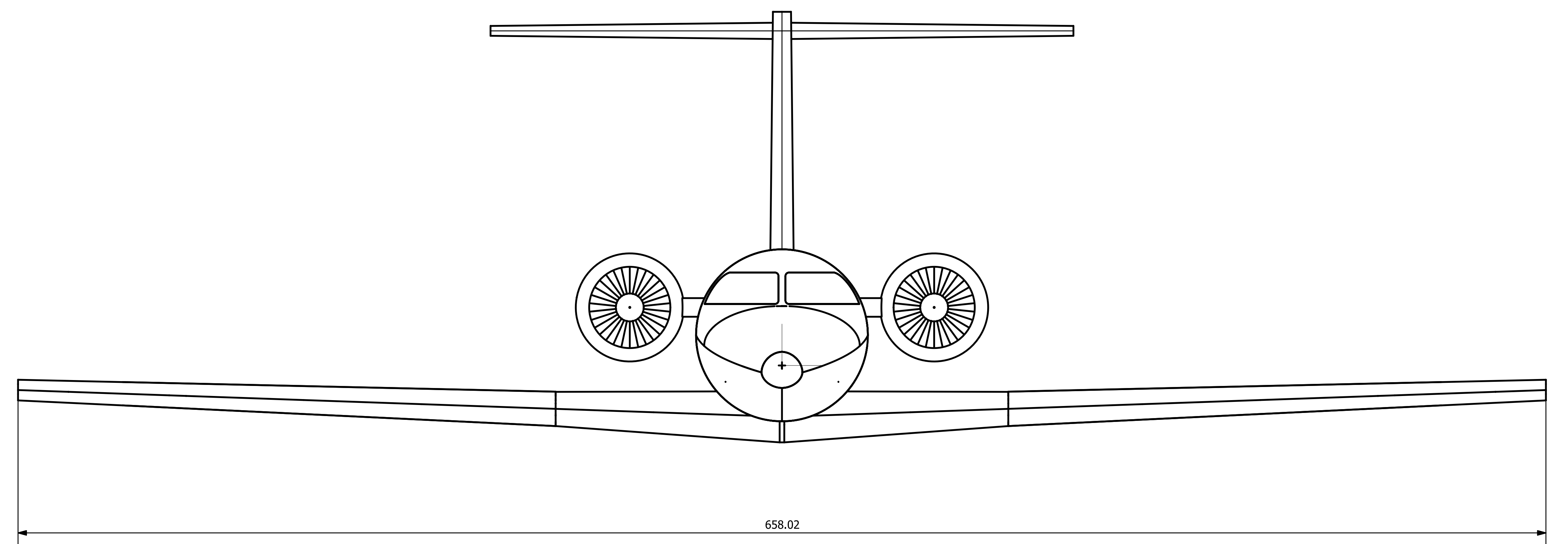
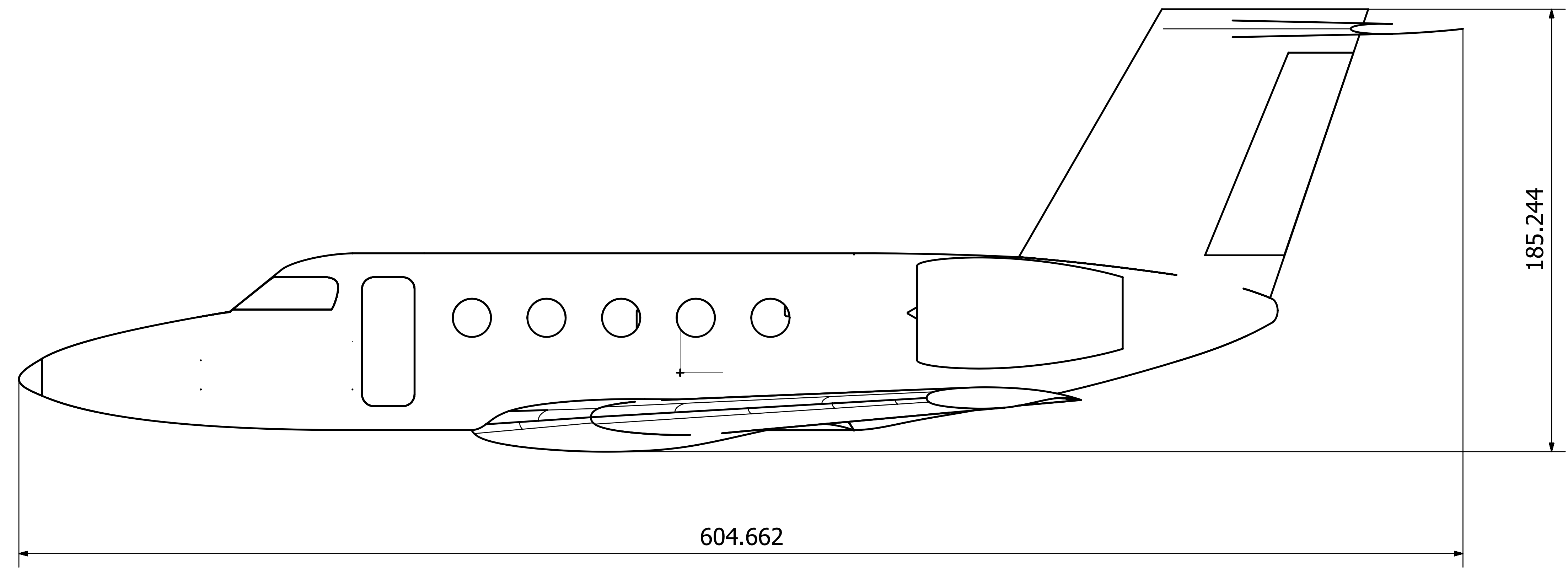
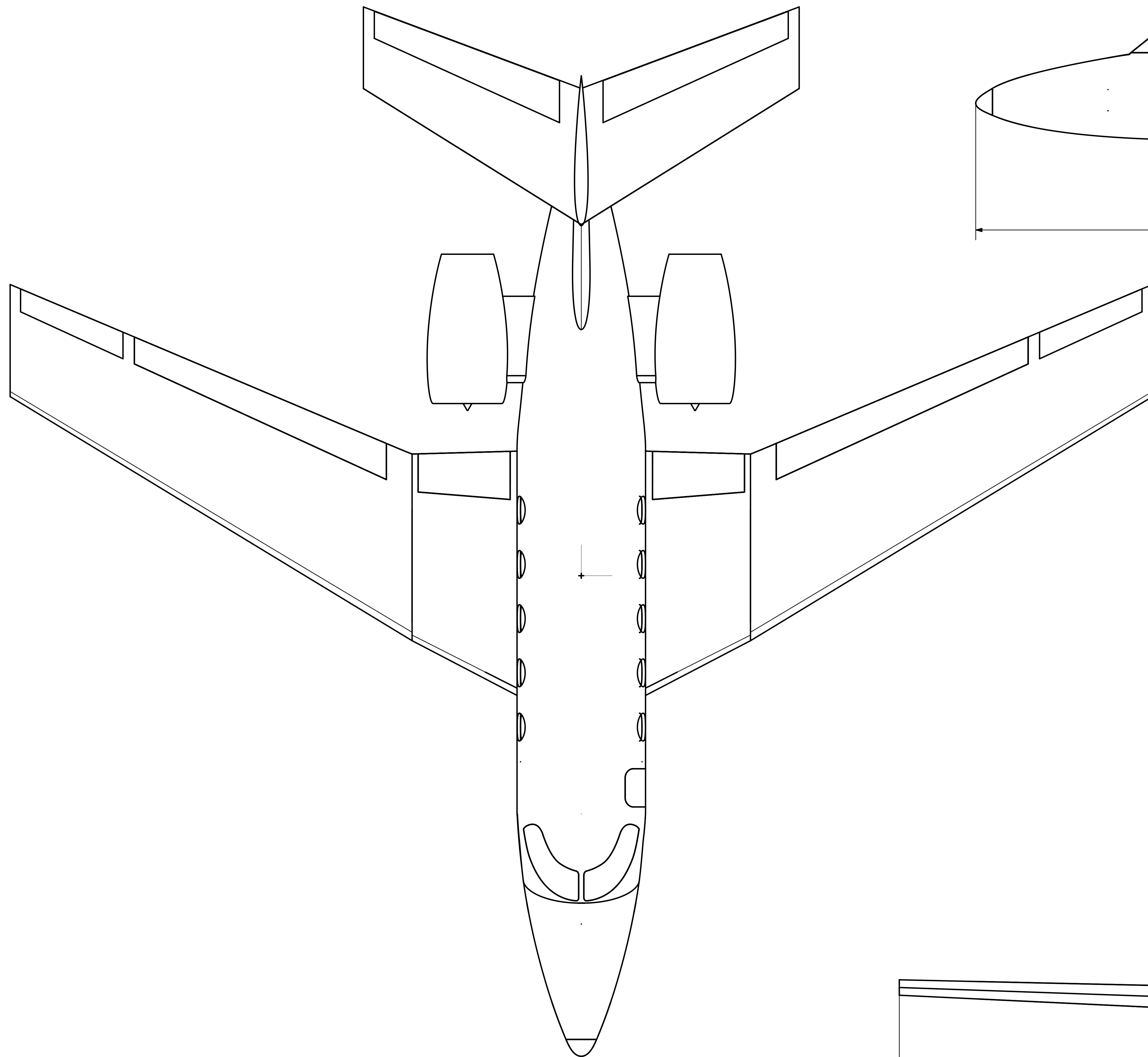
### **3 Configuration (Choakpichitchai & You)**

#### **3.1 Draft**

3.1.1. The Chief - 3 View

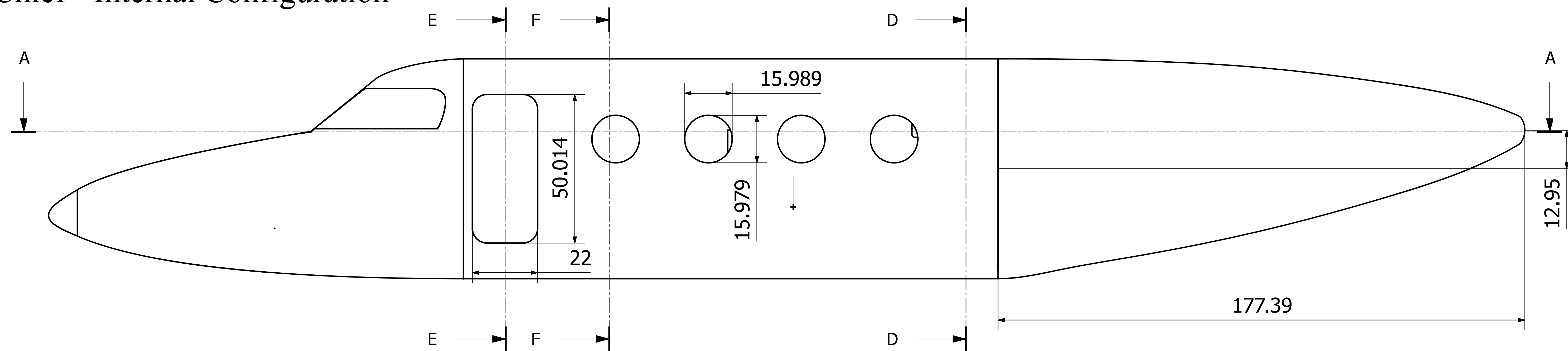
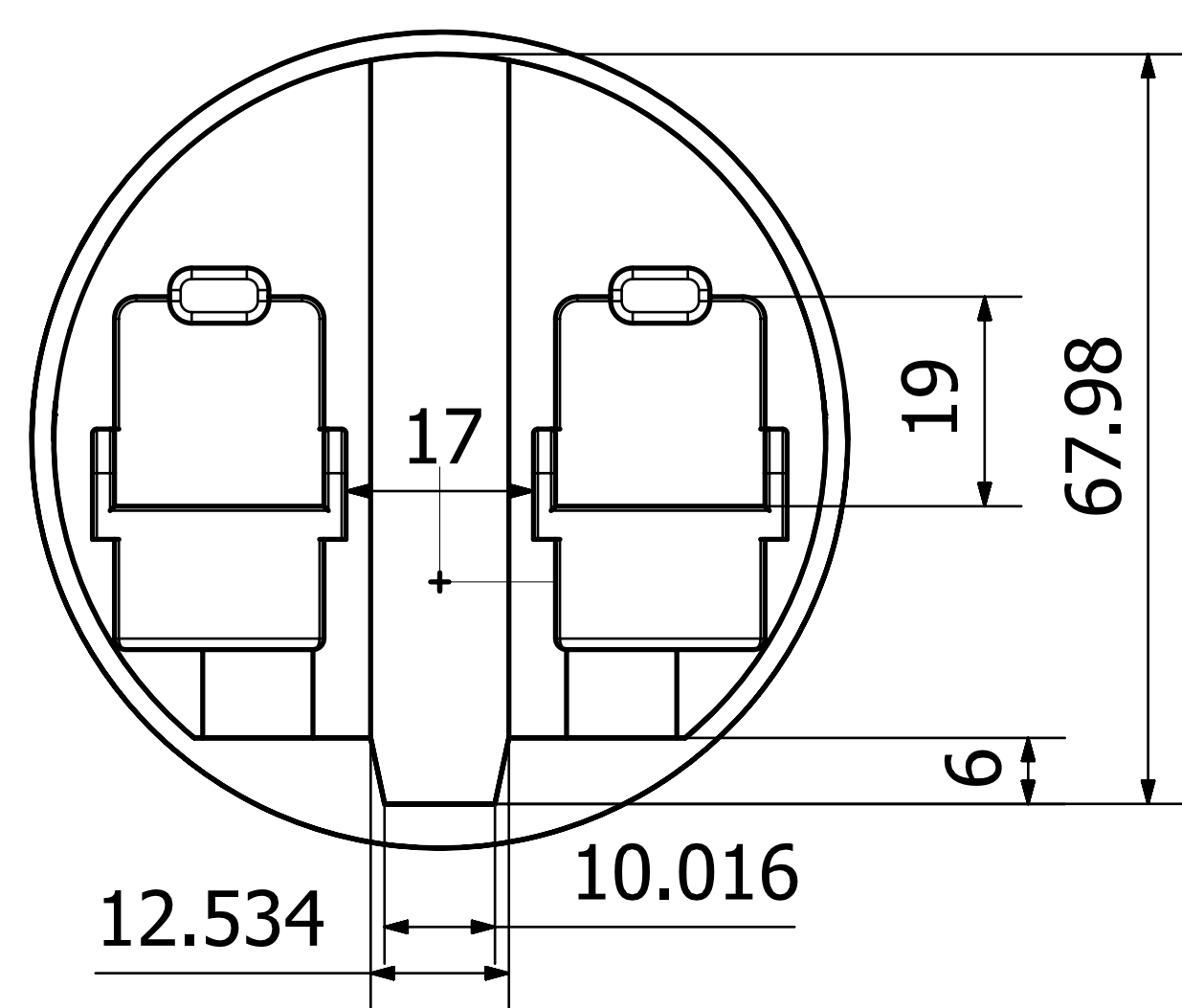


### 3.1.2. The Commander - 3 View

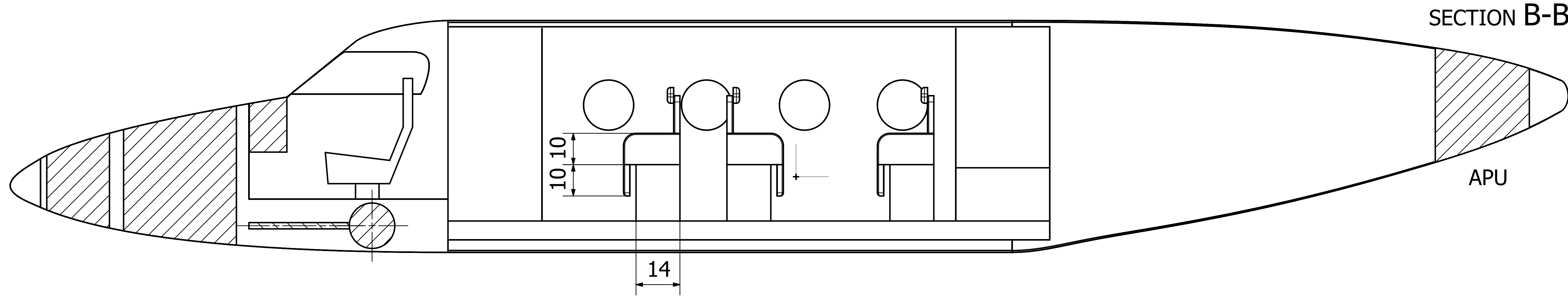
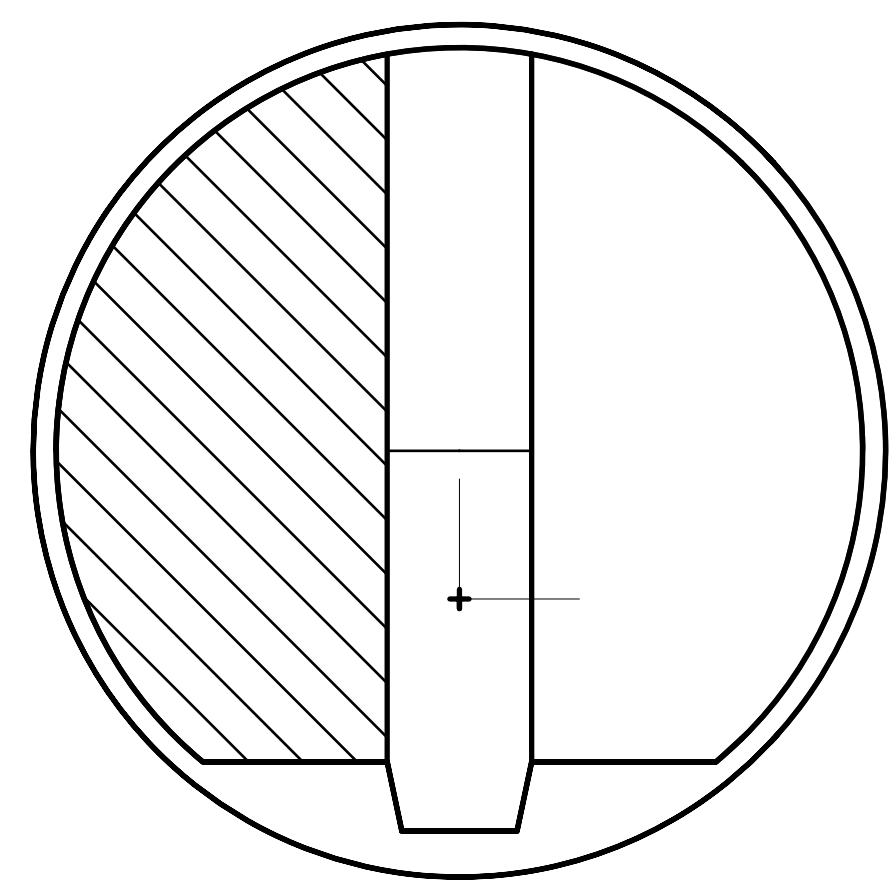


### 3.1.3. The Chief - Internal Configuration

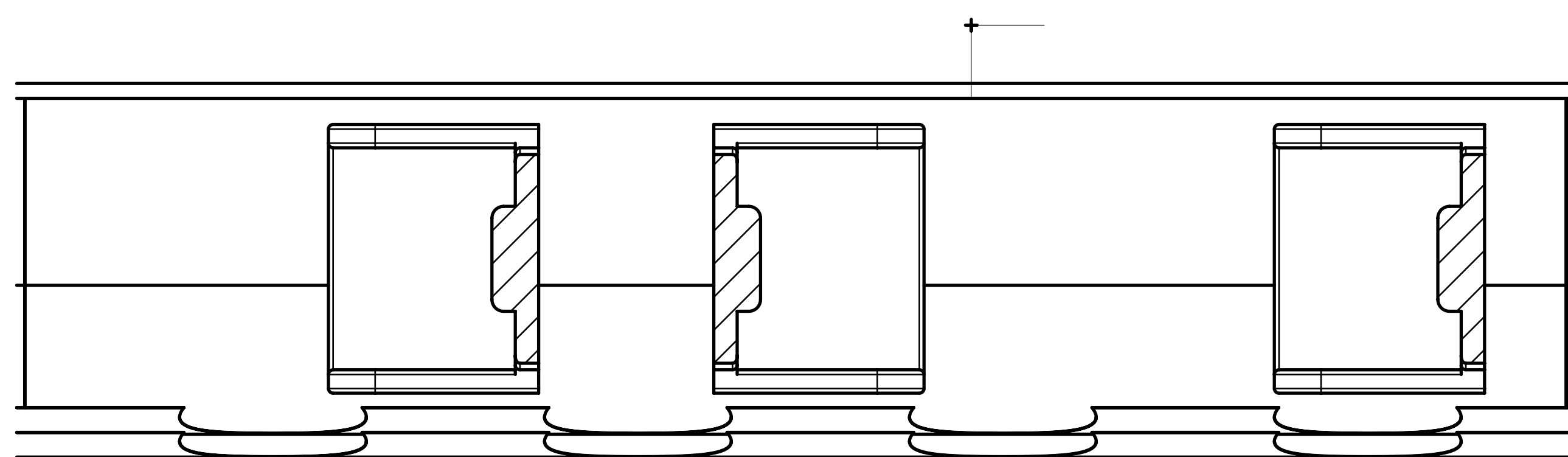
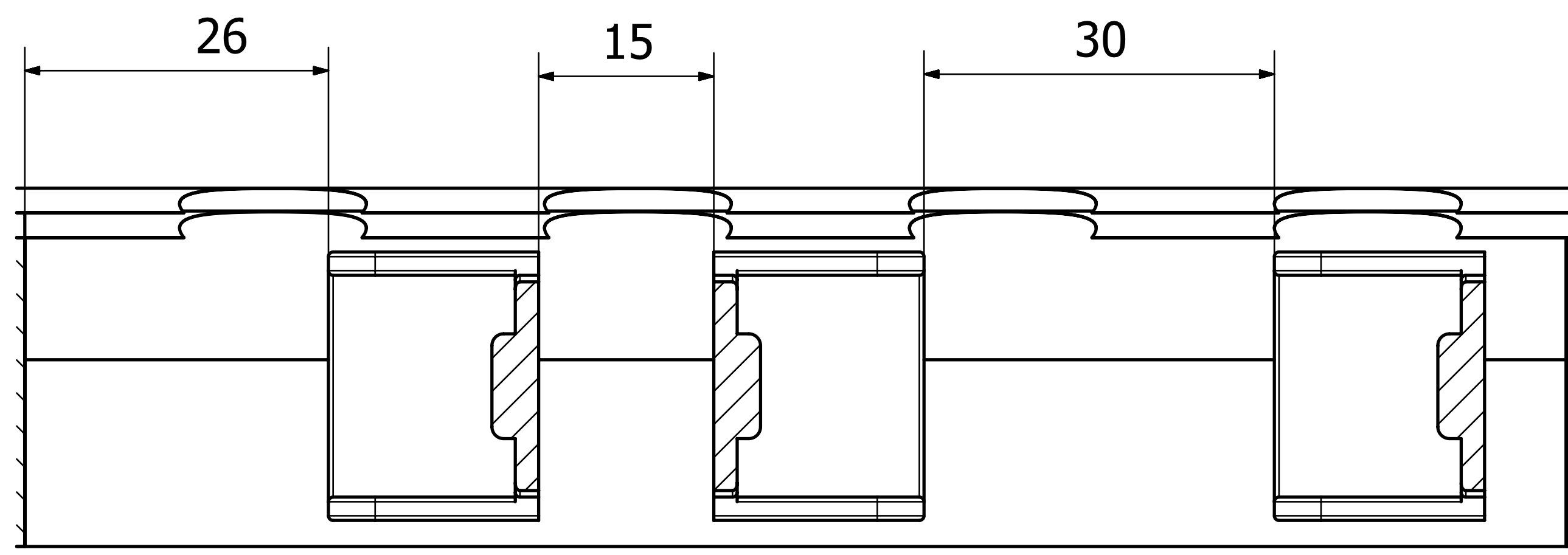
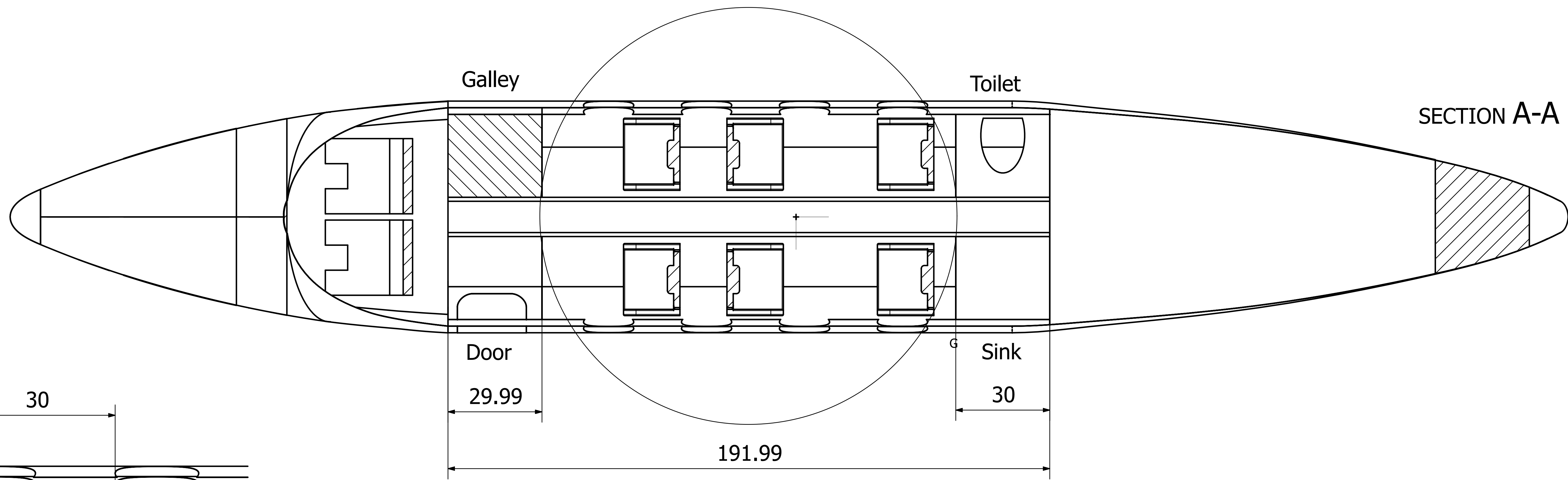
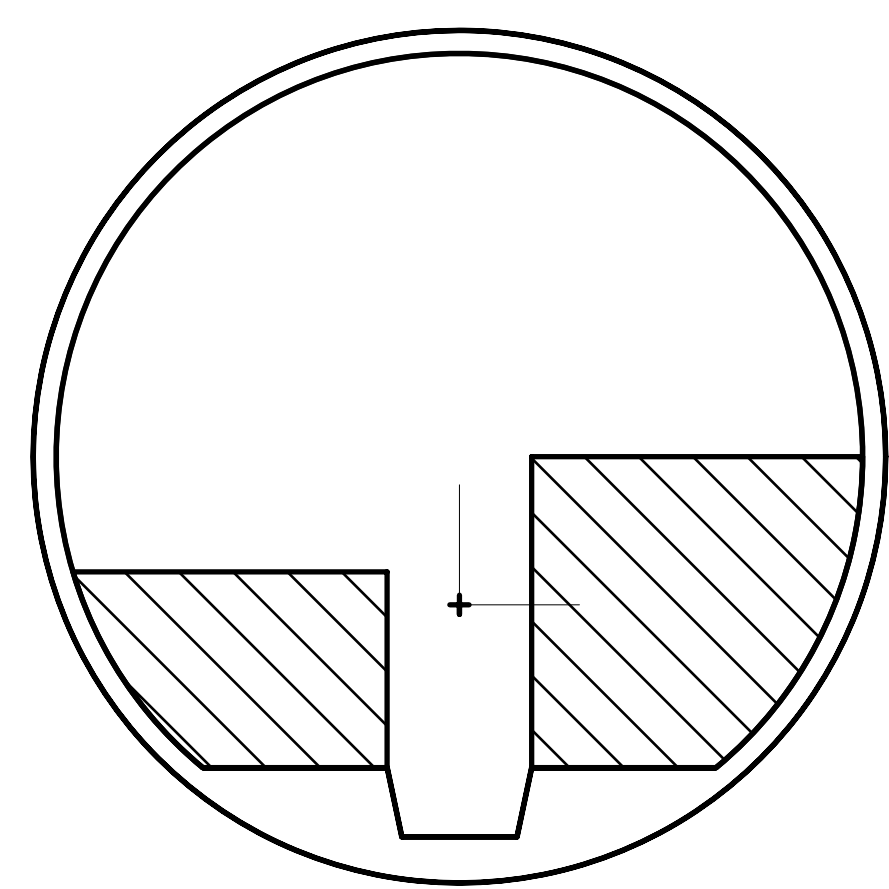
SECTION F-F



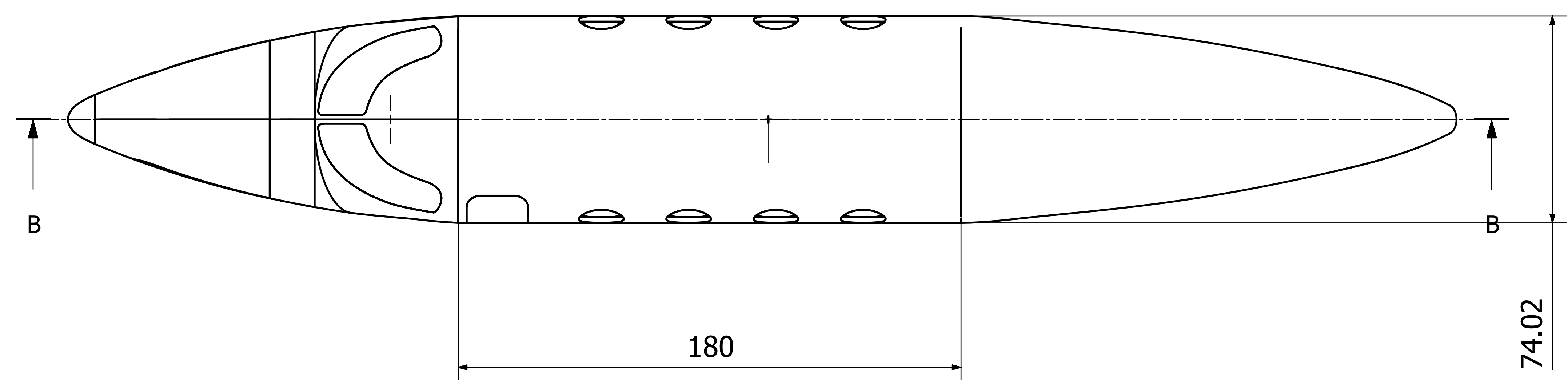
SECTION E-E



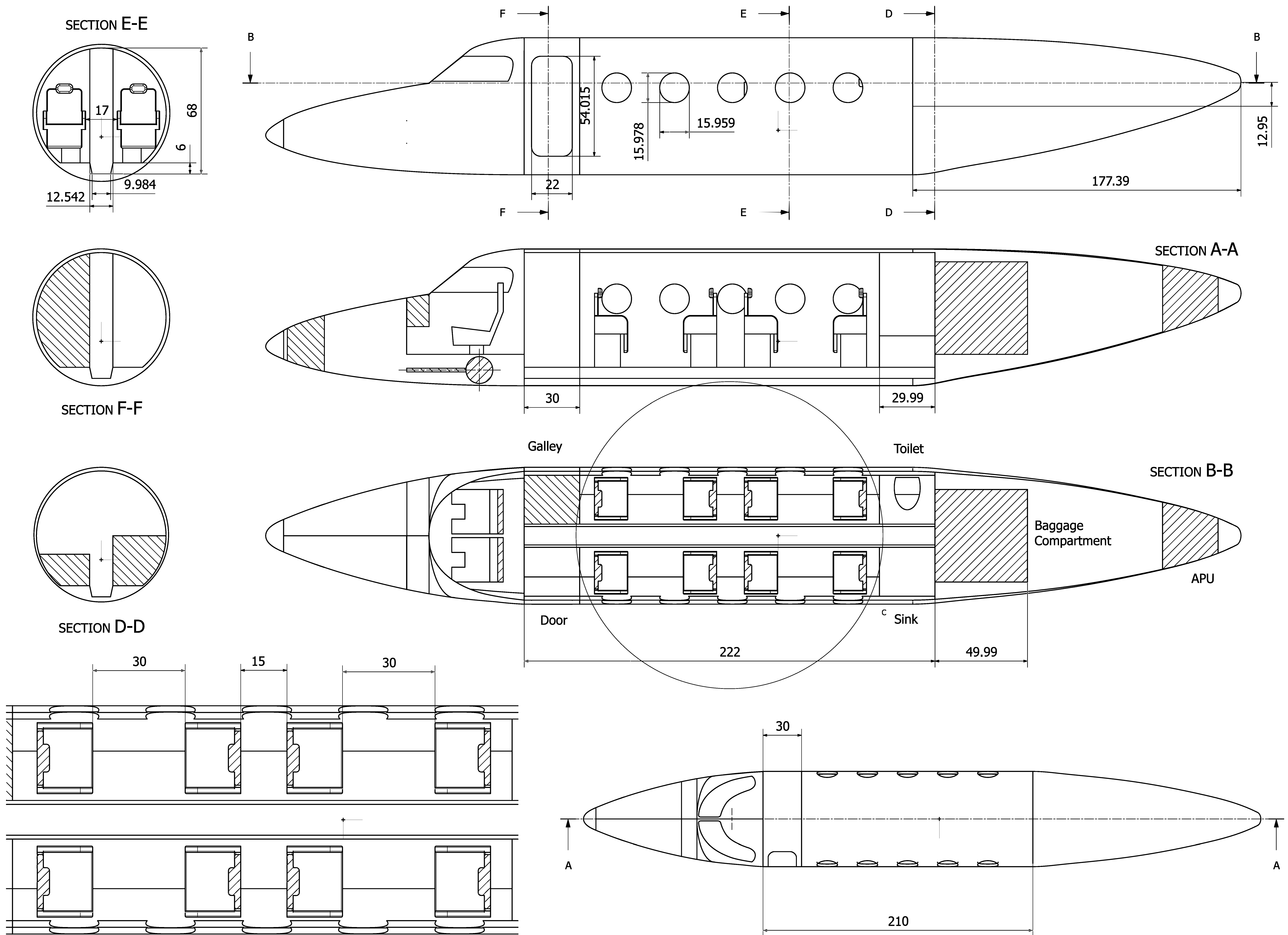
SECTION D-D



DETAIL G  
SCALE 1:10



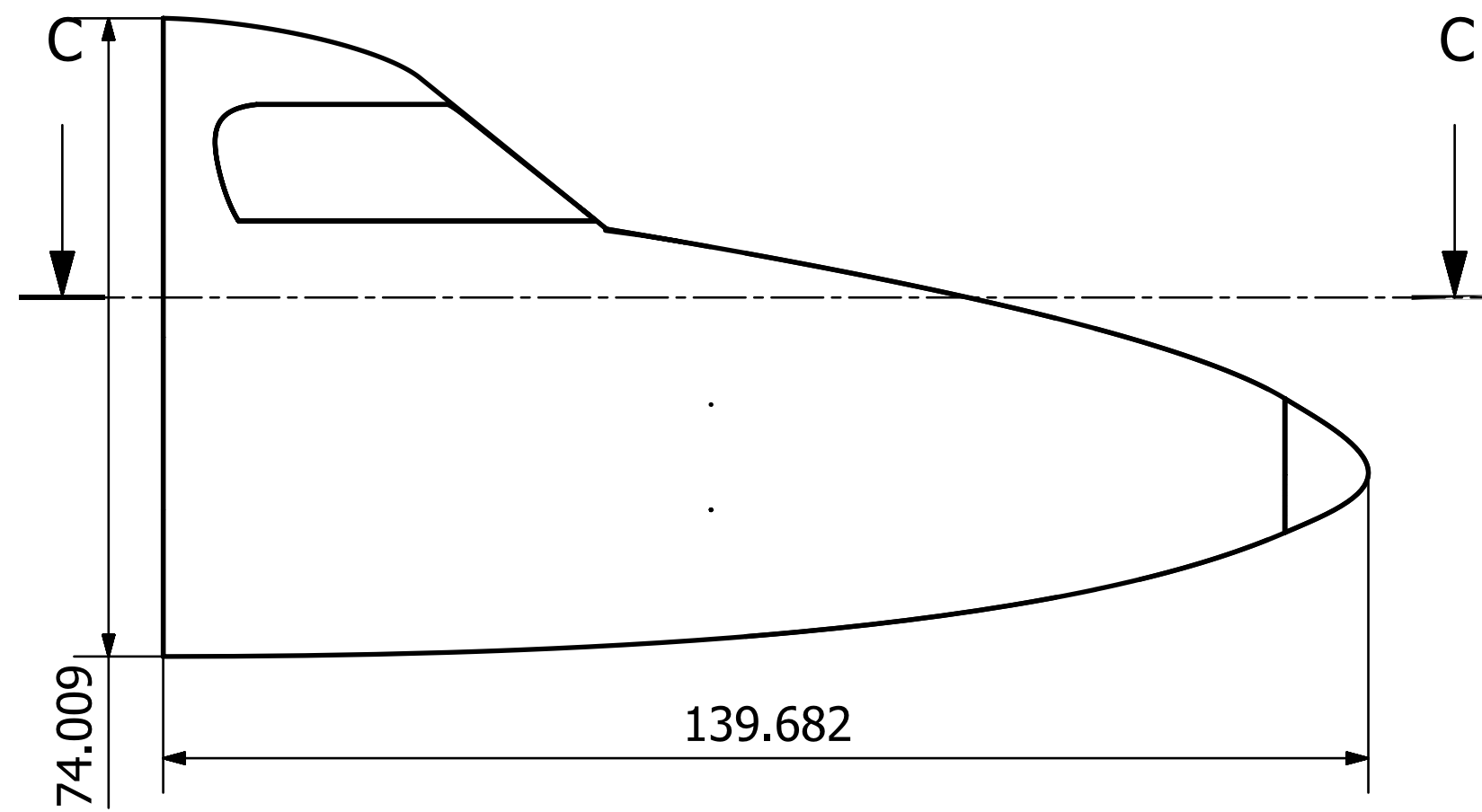
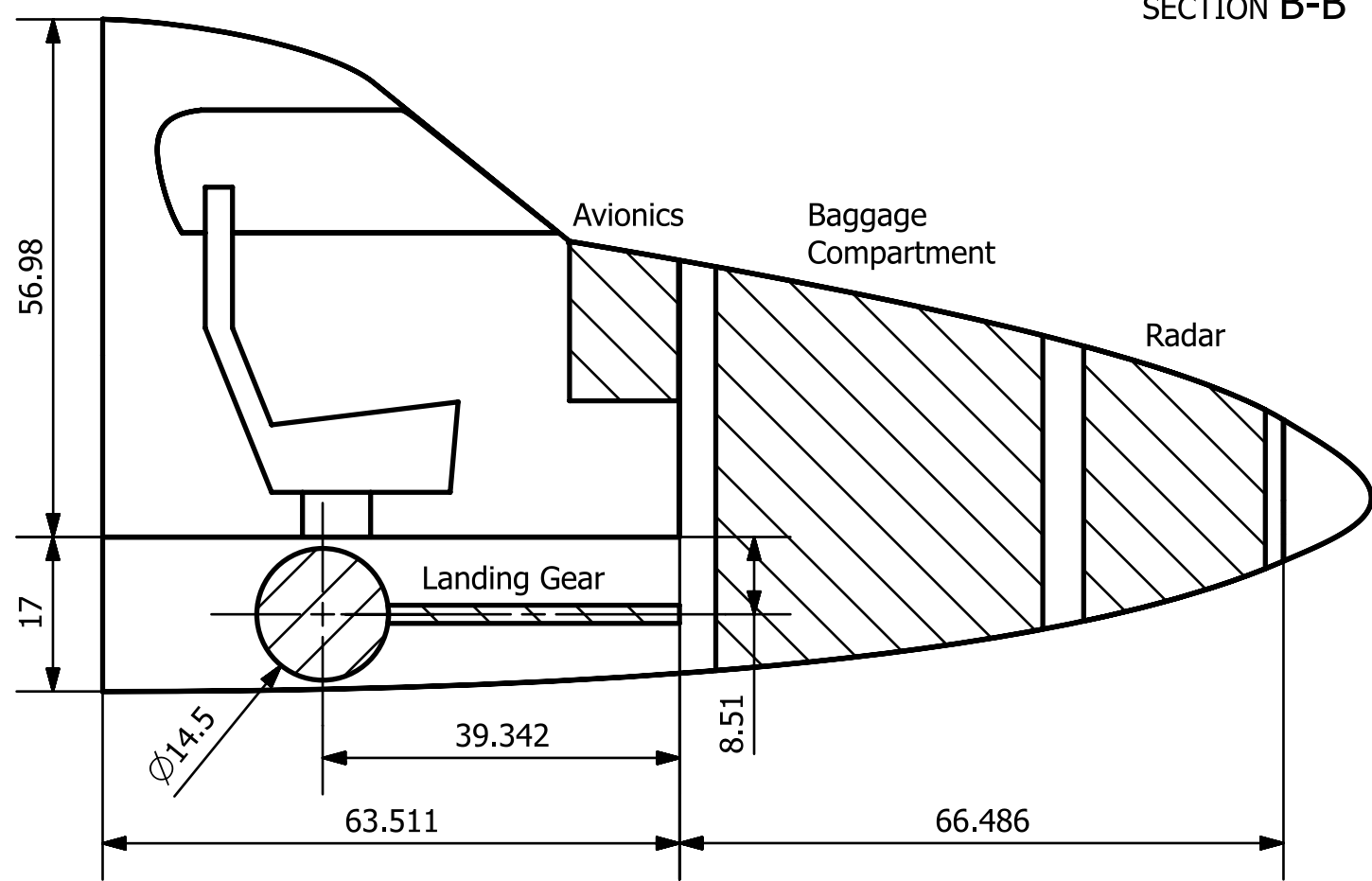
### 3.1.4. The Commander - Internal Configuration



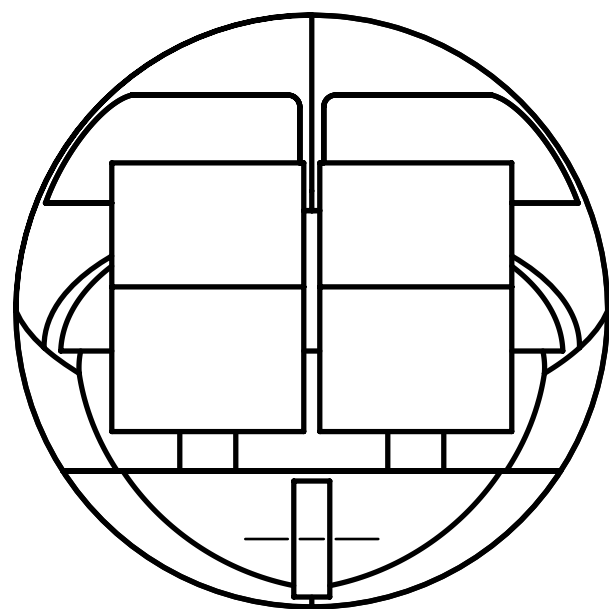
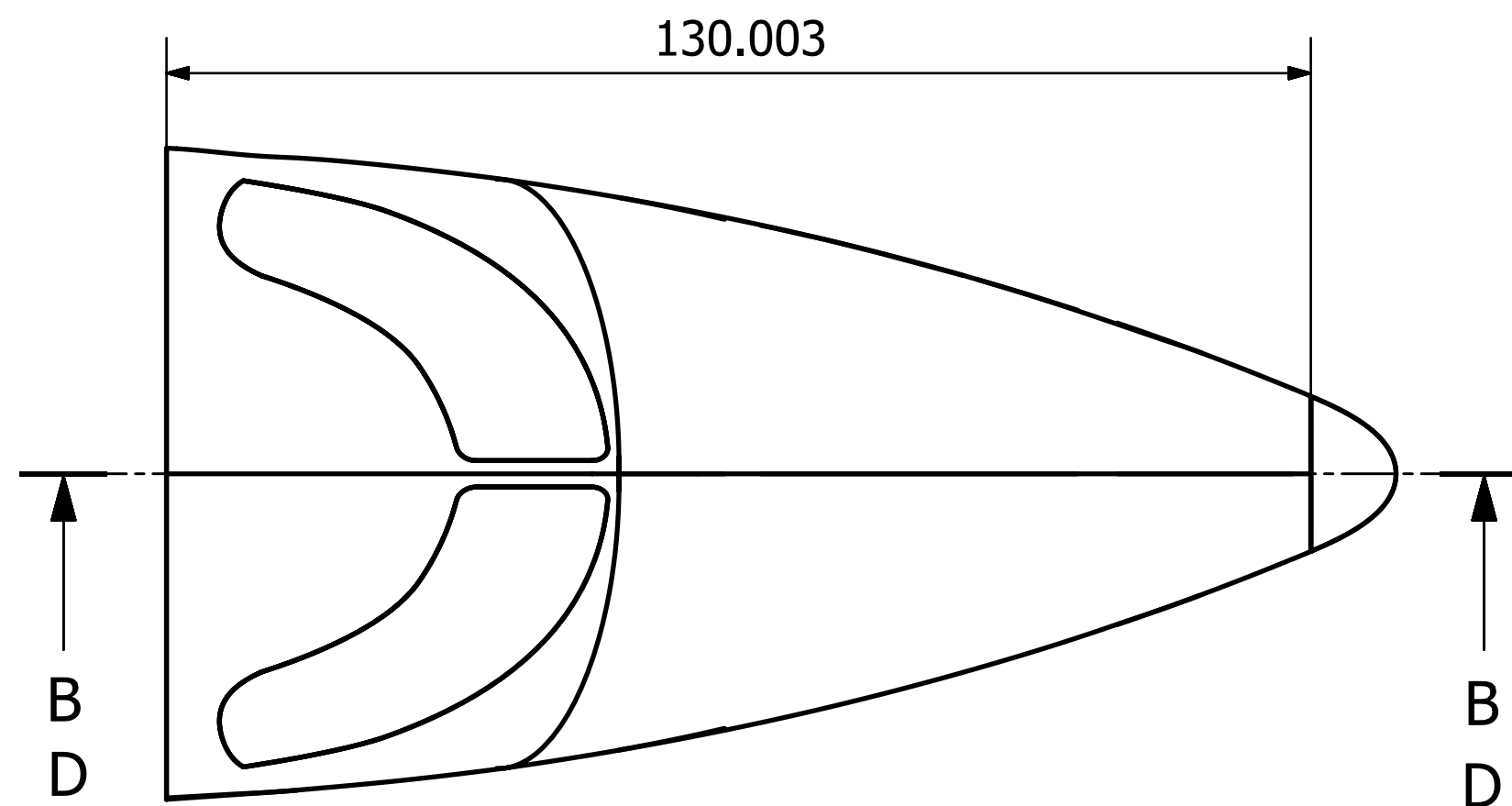
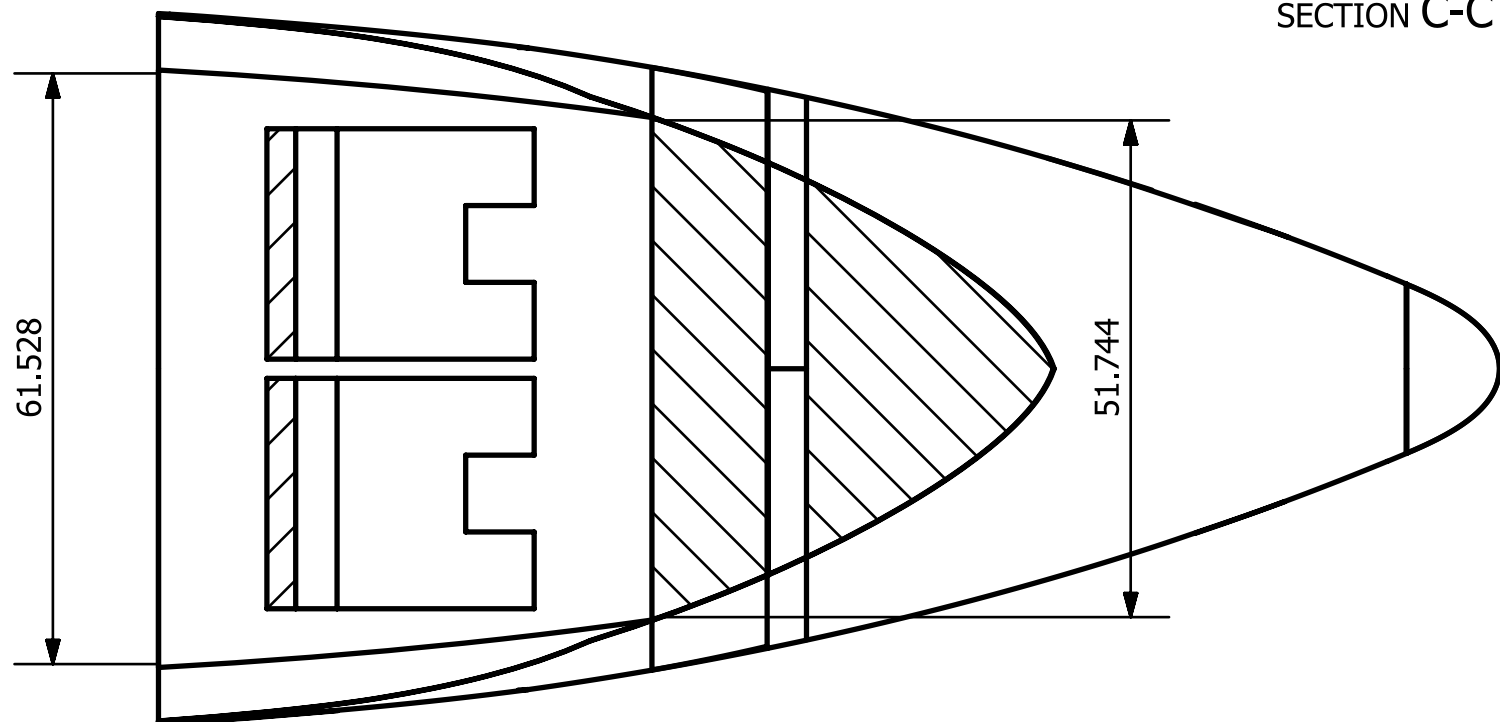
DETAIL C  
SCALE 1:10

### 3.1.5. The Chief - Cockpit Configuration

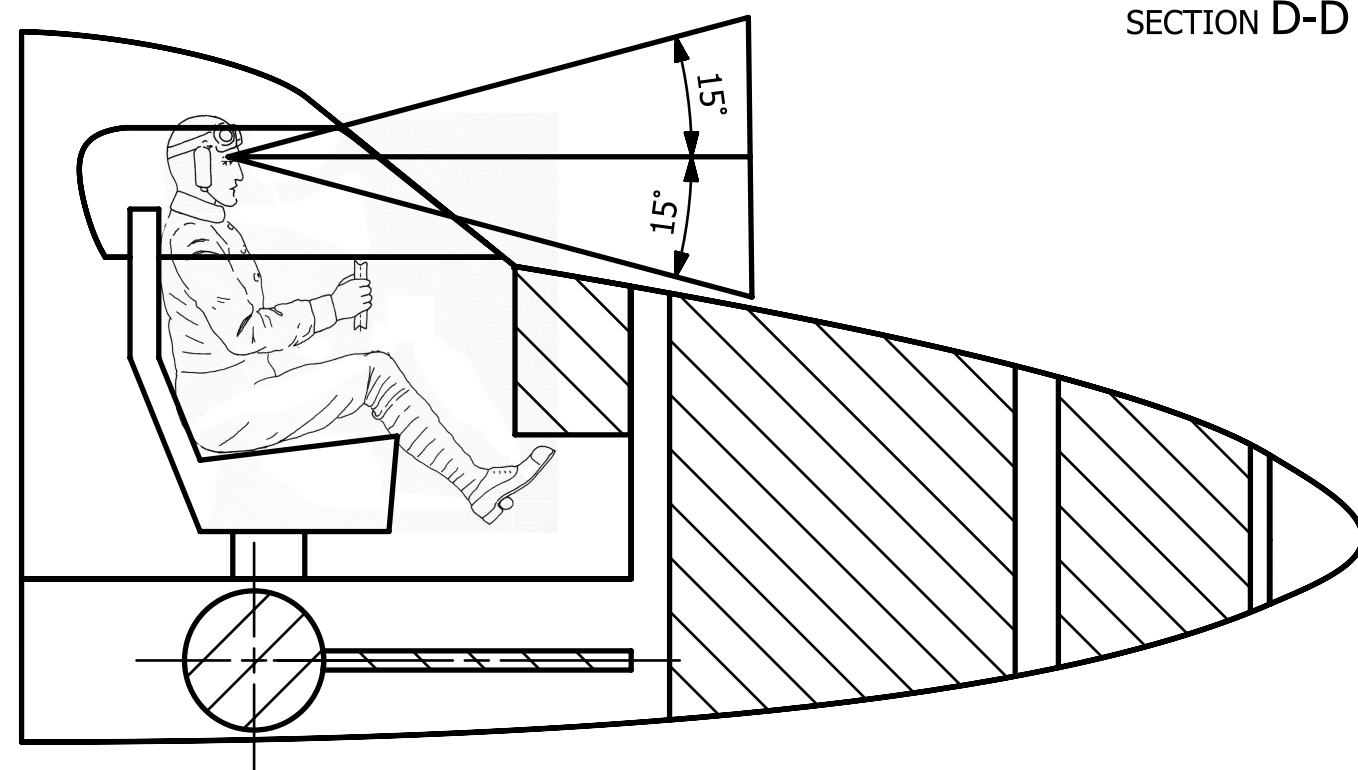
SECTION B-B



SECTION C-C

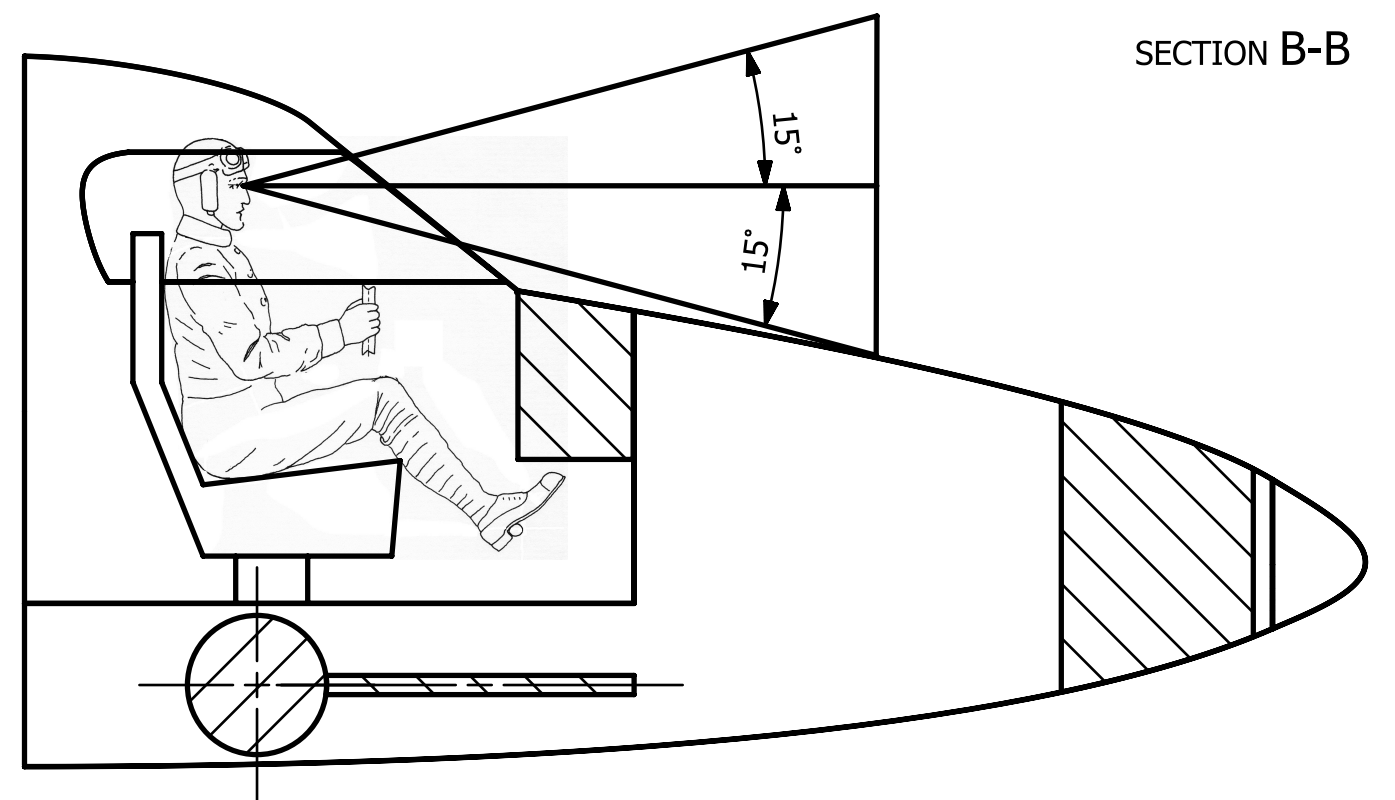
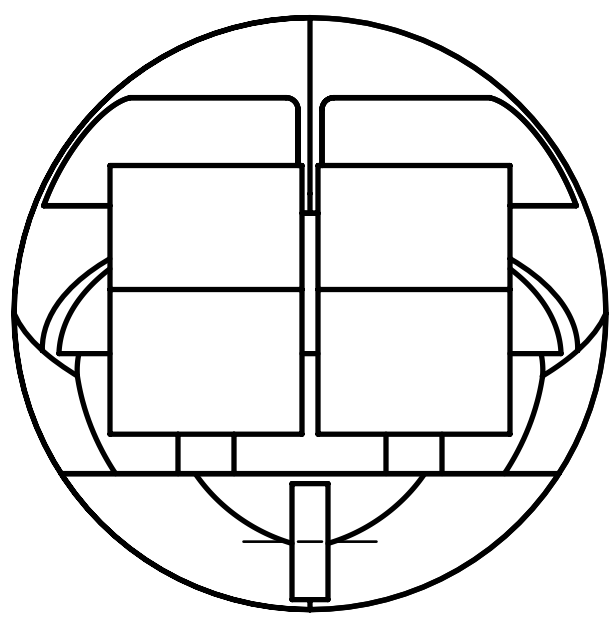
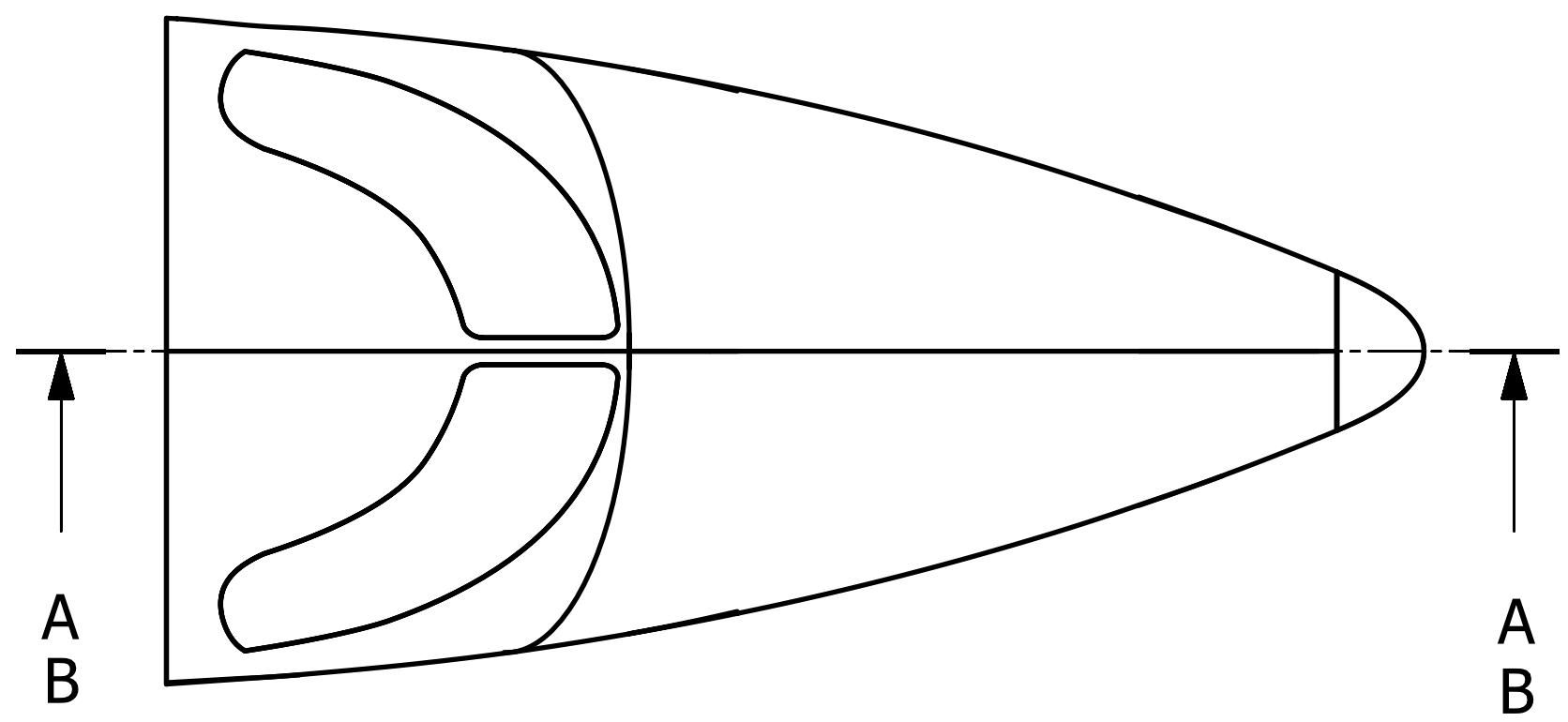
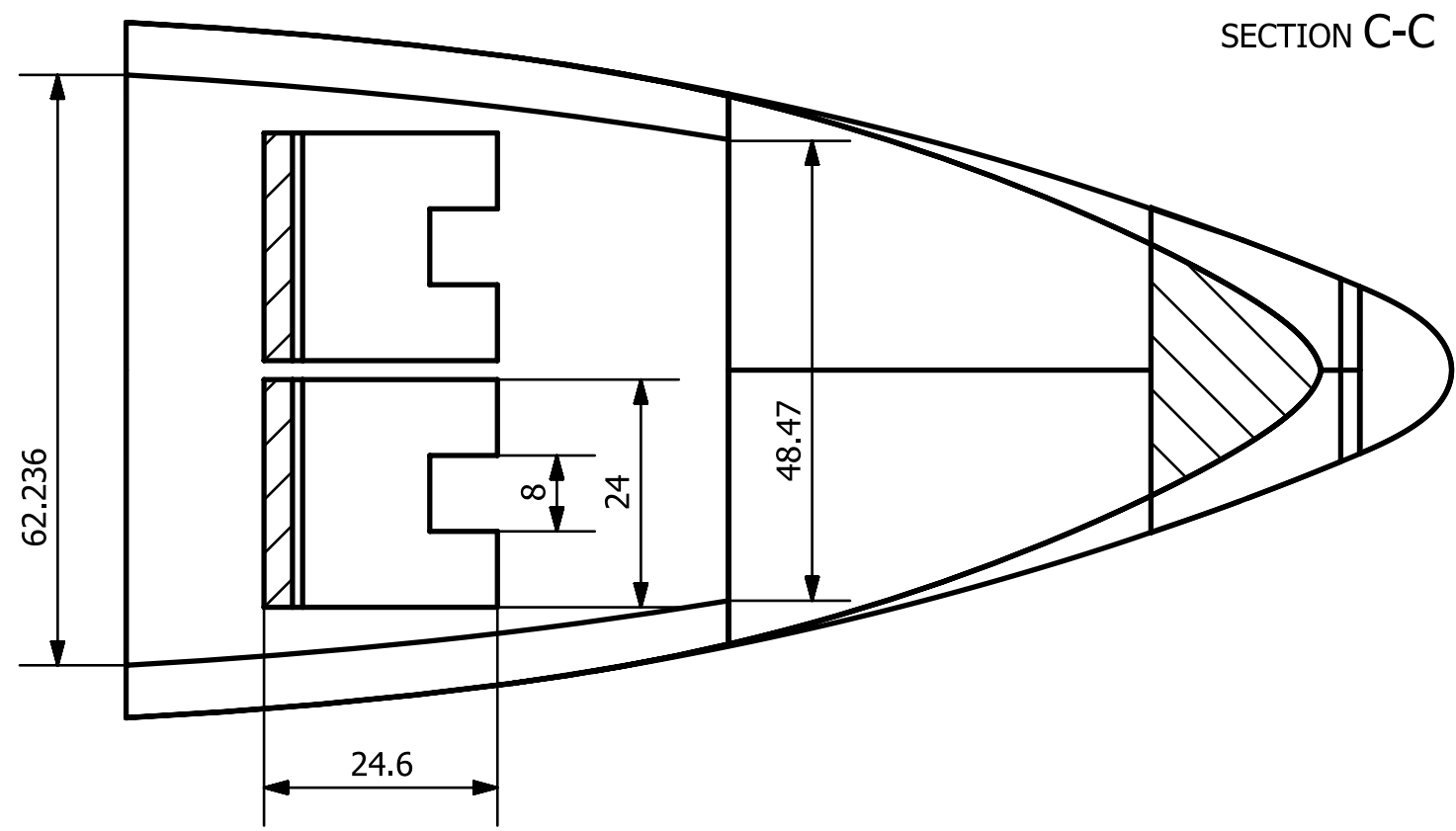
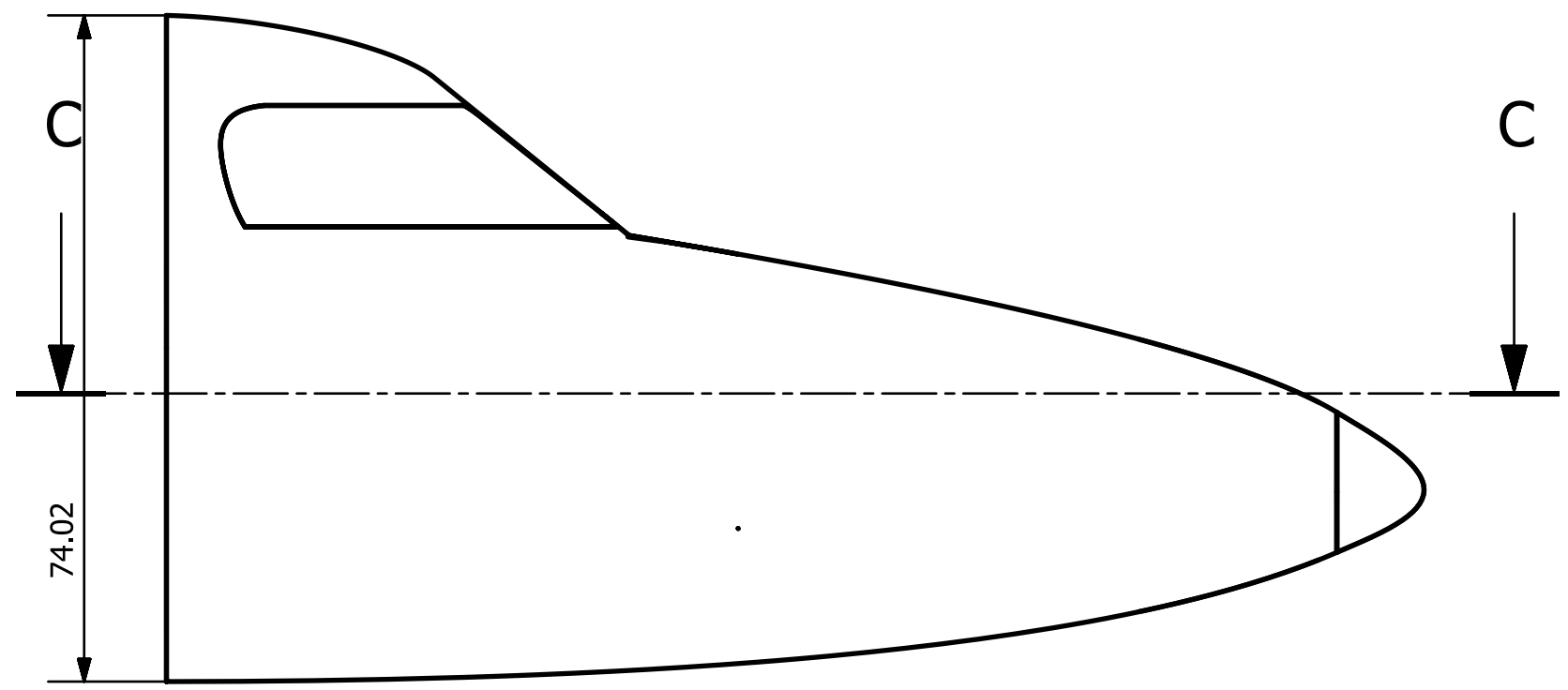
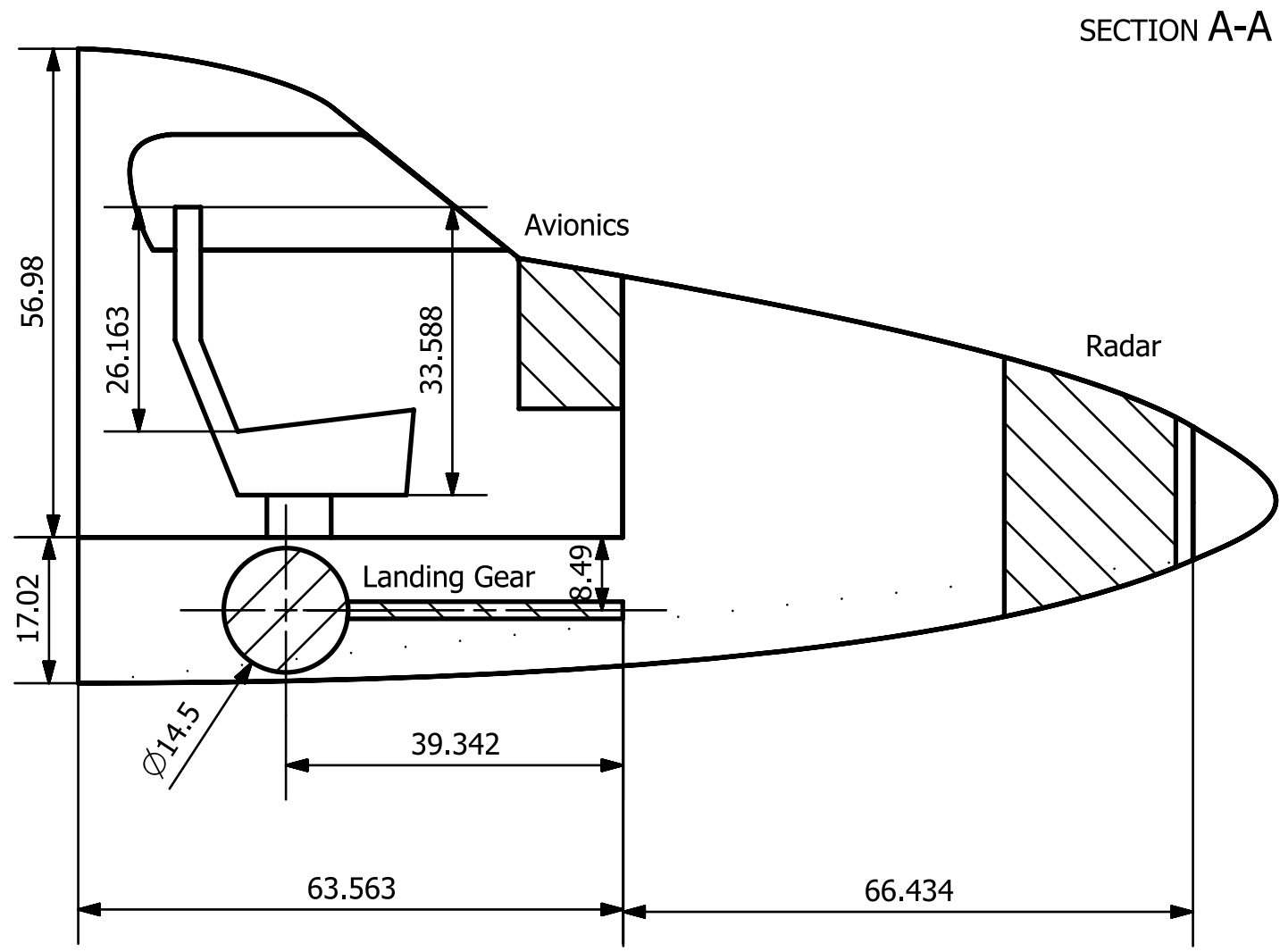


SECTION D-D

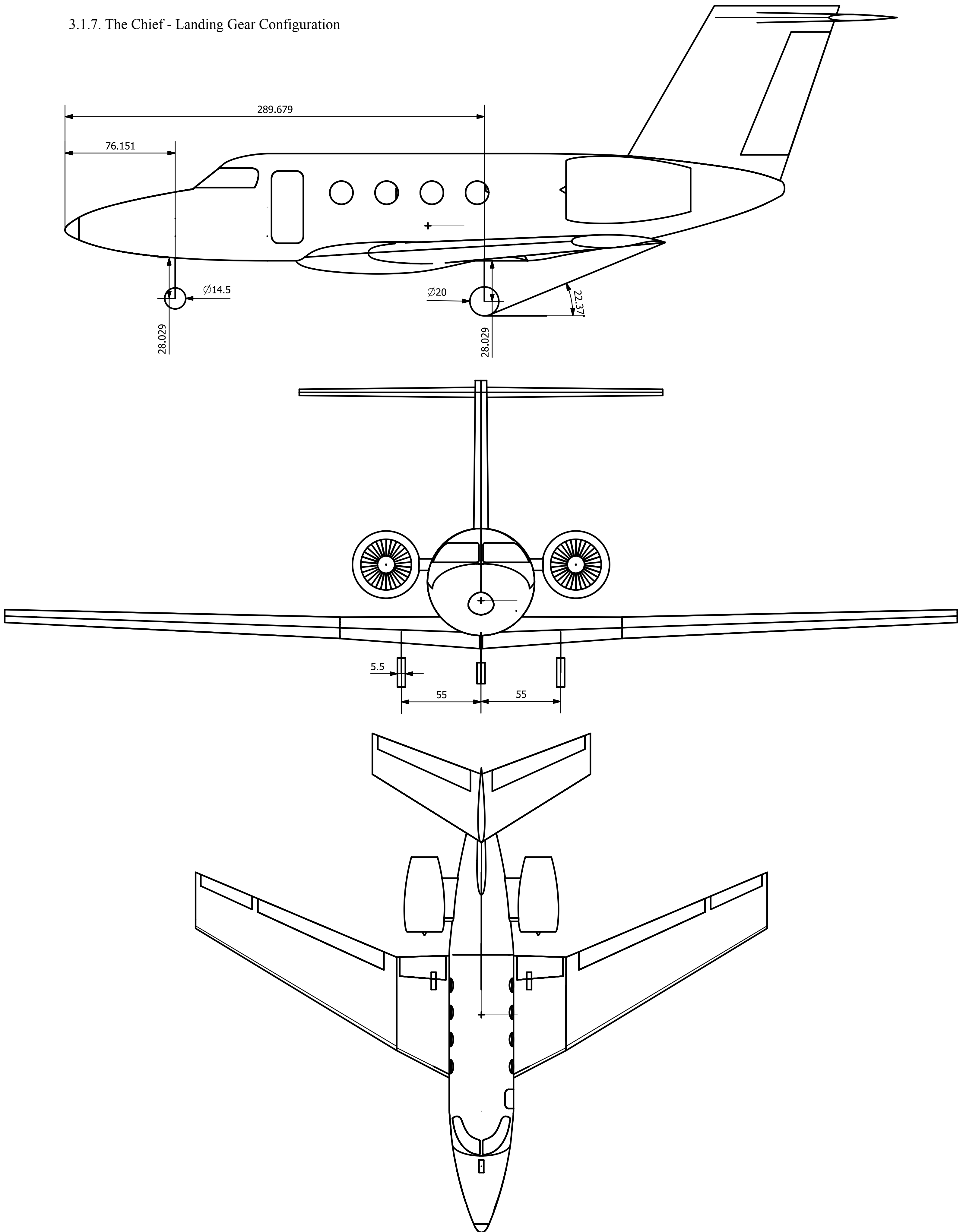




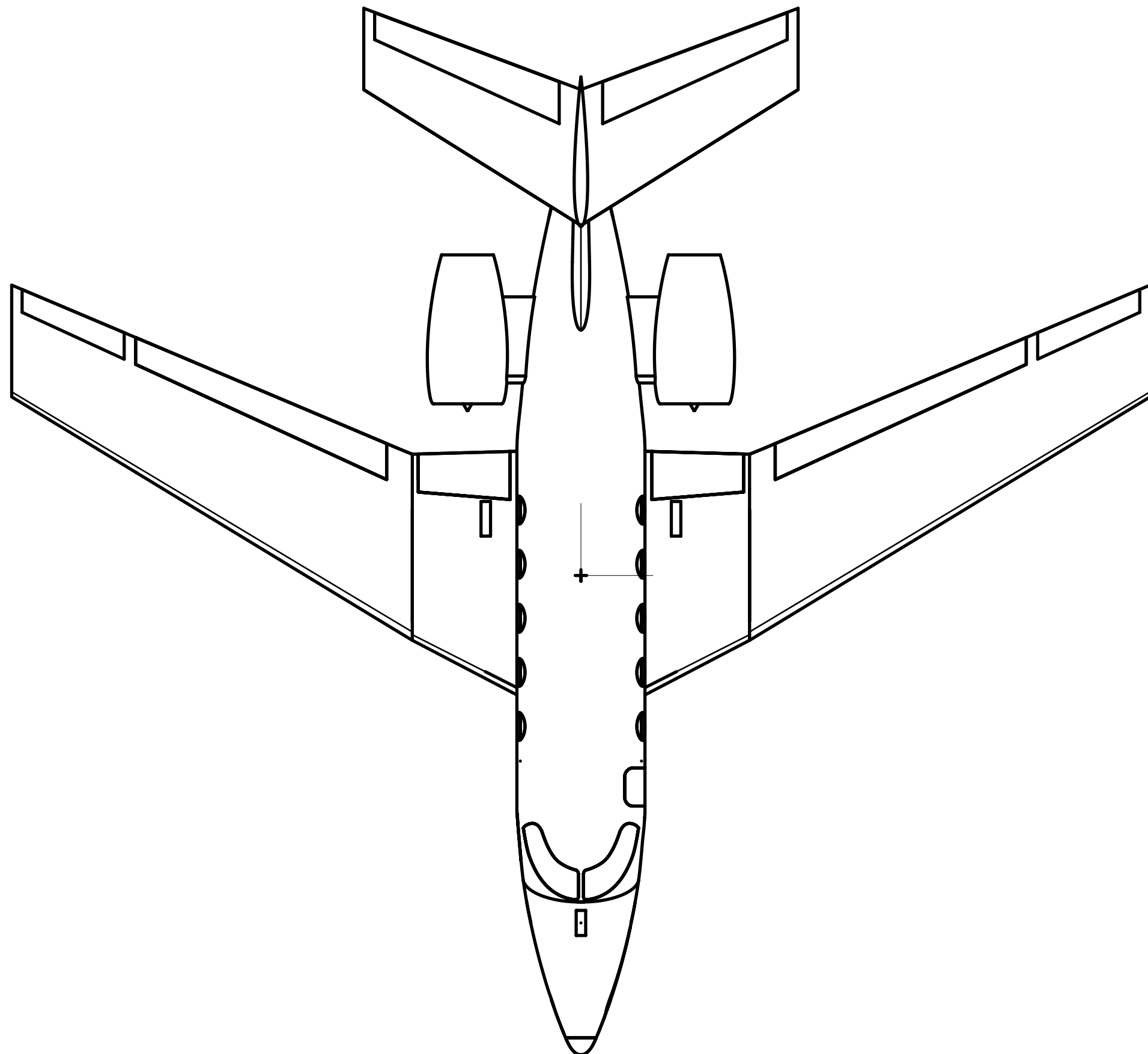
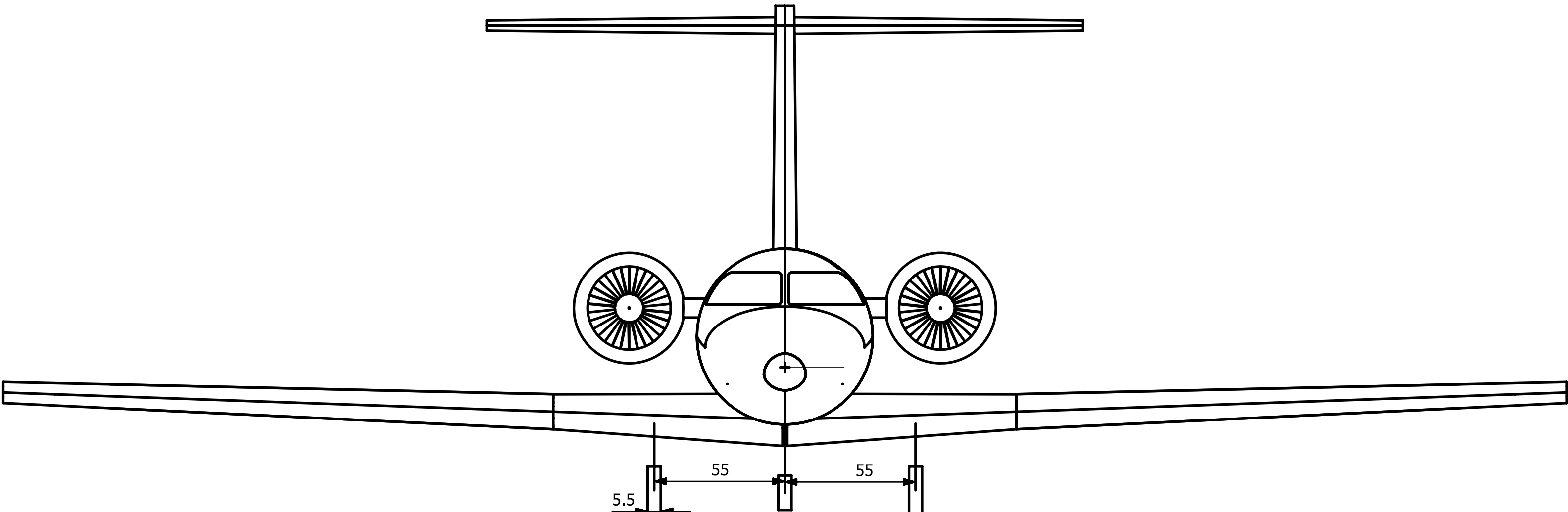
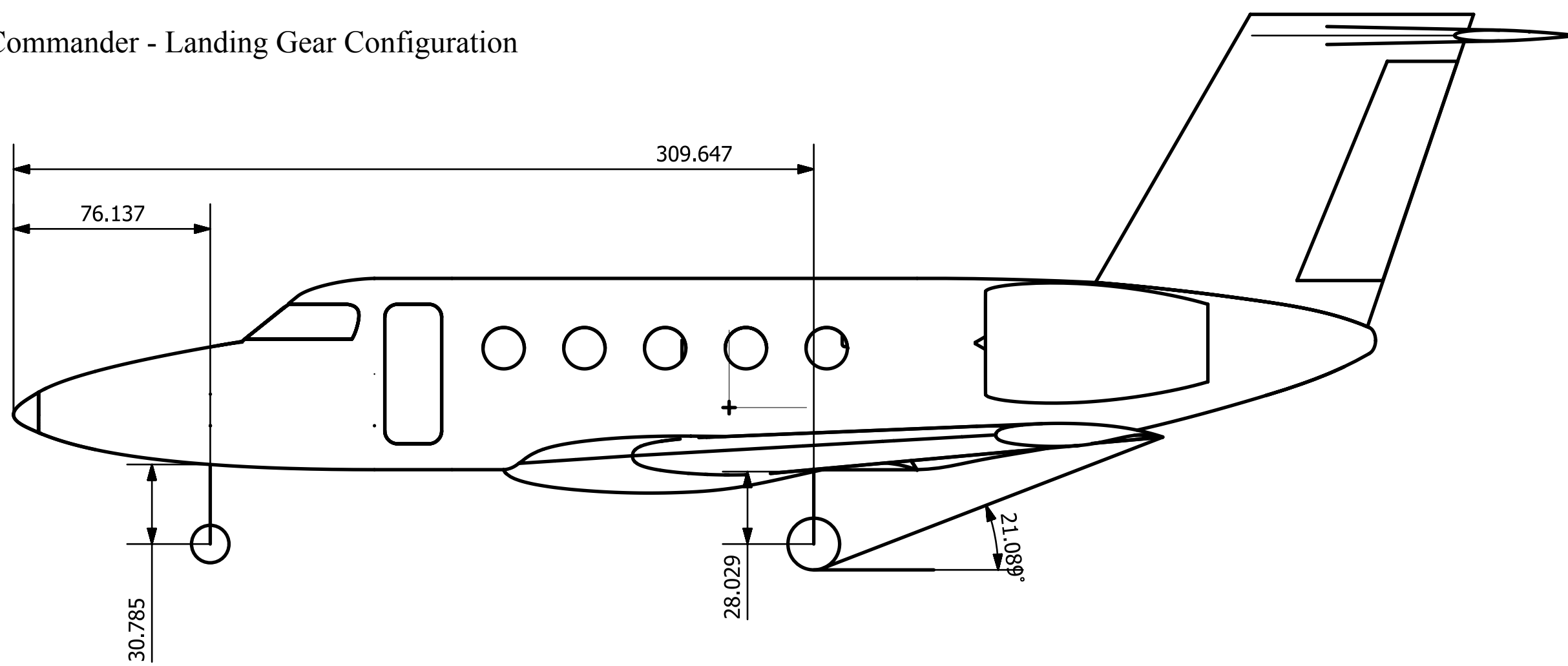
### 3.1.6. The Commander - Cockpit Configuration



3.1.7. The Chief - Landing Gear Configuration



3.1.8. The Commander - Landing Gear Configuration



## 3.2 Morphology

The final configuration of the aircraft was systematically determined by considering component configurations individually. Any component configuration unable to meet the specific requirements were systematically eliminated. All feasible configurations are then integrated and all possible design combinations are produced, before considering the feasibility of the integrated configuration. A final trade study was performed between two designs to produce a final configuration for the family of aircrafts.

### 3.2.1 Fuselage Configuration

The conventional fuselage was preferred over other choices due to multiple reasons. With a conventional fuselage, other members of the same family of planes can have a much greater part commonality. Other fuselage configurations such as the Blended or Flying Wing would have a much lower recycling of parts with most components being redesigned for a new aircraft.

In addition to the commonality of parts, the aerospace industry has been familiar with aircrafts with a conventional fuselage. Most airport ground equipment are tailed to support these types of aircrafts due to their prolonged usage in the aerospace industry. As most major component suppliers are familiar with integrating their components to a conventional fuselage, the conventional fuselage was ultimately picked over the remaining types.

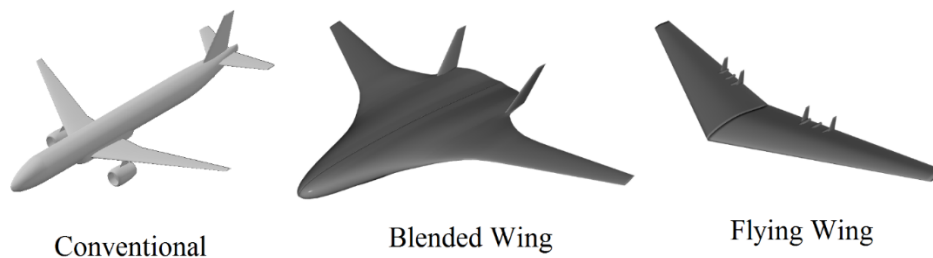


**Figure 3.1. Possible fuselage configurations considered.**

### **3.2.2 Engine Configuration**

After considering the 8 common engine placement configurations, buried engine configurations such as engines buried in the wings, tail or fuselage and a podded over the wing configuration were eliminated due to the difficulty in engine servicing required. The difficulty in servicing an engine could potentially increase the aircraft's operation cost. A more specialized equipment and crew will be required in servicing the aircraft due to the difficulty in accessing the engines.

In addition to that, with buried engine configurations, a much higher development cost is incurred due to a redesign required when accommodating different engines required in other family members or the upgrading of the aircraft. Should there be a change in engine dimensions or specifications, a complete structural design is required to integrate the engines into the aircraft. Engine configurations such as a podded under the fuselage were eliminated due to height clearance required and the greater potential for debris damage to the engine with such configuration. The potential damage to the engine could lead to a greater operational cost for the user.

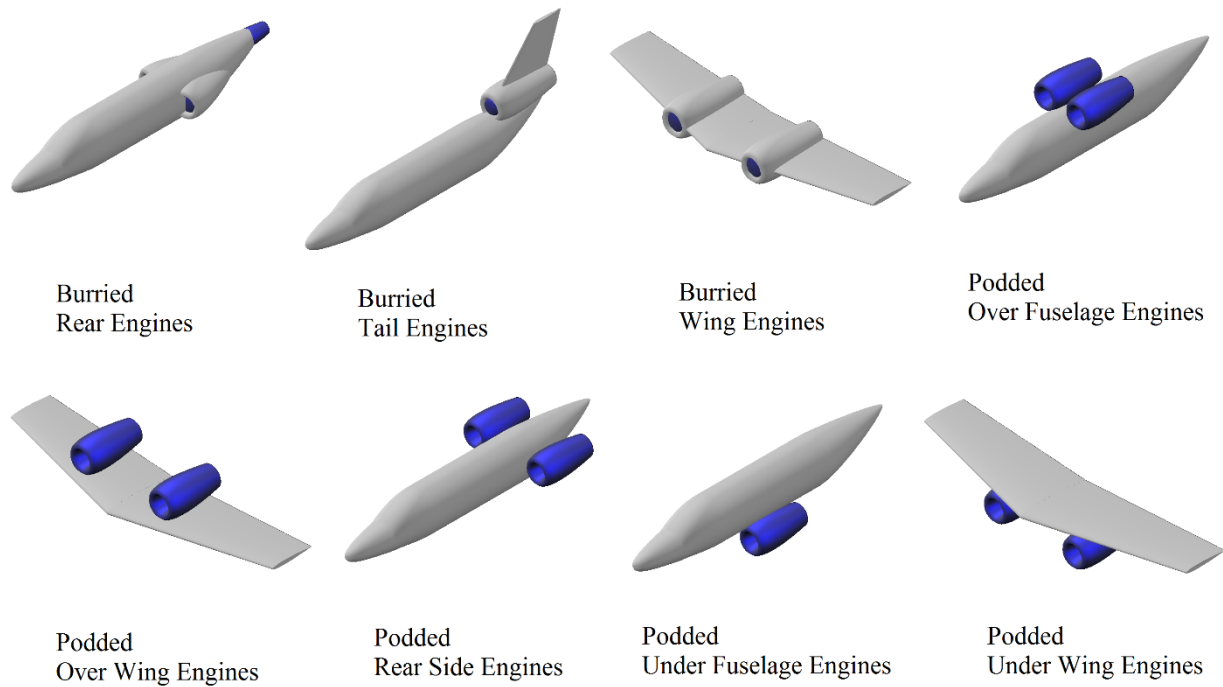


**Figure 3.2. Possible engine mount configurations.**

### 3.2.3 Wing Configuration

The details of wing type, high-lifting device, sweep and shape of the wing are considered in detail at the Aerodynamics Subsection. Only the wing location, type and structural configuration are considered in this section.

A cantilever wing was considered over a braced wing due to the clearance it gives inside the fuselage for cabin space.

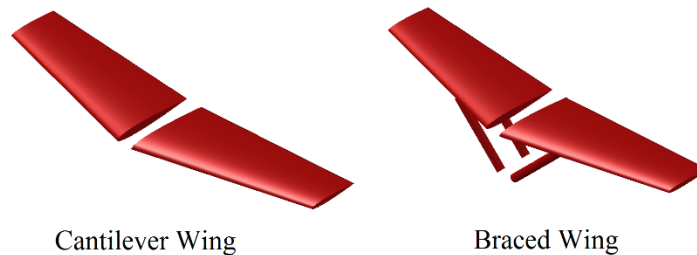


**Figure 3.3. Possible wing structure configurations.**

3 major wing locations are considered, being a high wing, mid wing and a low wing. Immediately, the mid wing configuration was eliminated due to multiple reasons. A Mid Wing requires a greater aircraft structure due to the reinforcement required at the interface between the wing and the fuselage. In addition to that, a Mid Wing at the fuselage reduces the vision available for passengers, as multiple window parts are replaced by structural components to support the wing.



**Figure 3.4. Possible wing locations.**

### **3.2.4 Empennage Configuration**

The empennage configuration chosen is the aft tail with one vertical aft tail. Twin vertical tails were eliminated as one tail is sufficient to provide yaw stability and the structural weight of two vertical tails will add more to combined weight and cost.

A canard configuration was eliminated entirely as the canard will take space reserved for passenger doors and subsequently makes the passenger loading more difficult. In addition to that structural integration of a canard could potentially take up cabin space. With a conventional aircraft chosen, a Tailless configuration was eliminated entirely.

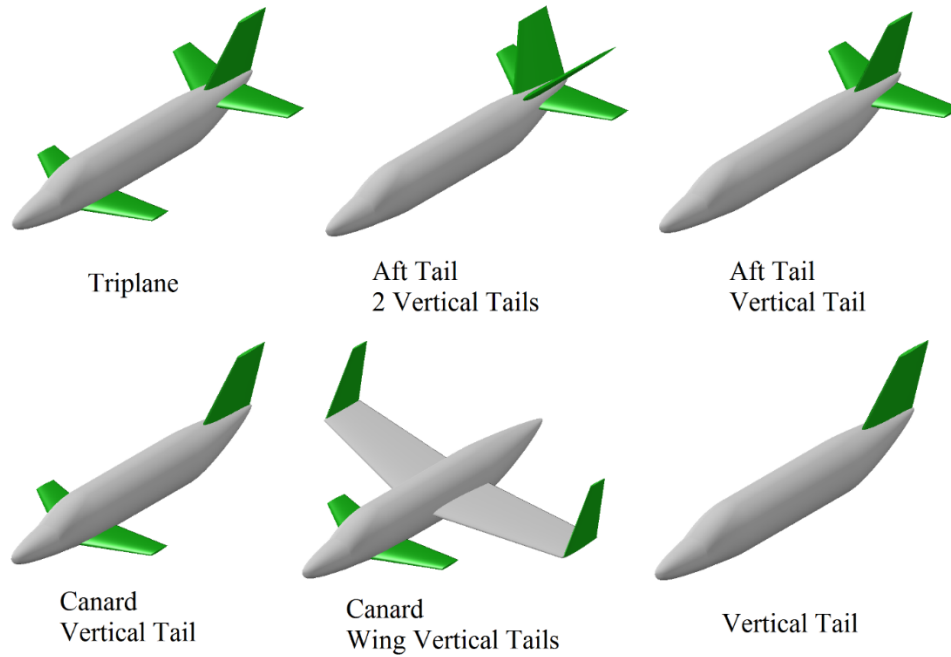


**Figure 3.5. Possible empennage configurations.**

With an aft-tail with one vertical tail chosen, two configurations of tails considered were the fuselage mounted tail or the T-tail. No configuration was eliminated until integrated with the rest of the configurations.

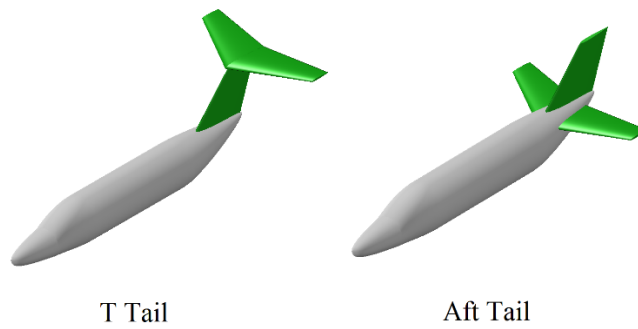


**Figure 3.6. Possible tail configurations.**



### **3.2.5 Landing Gear Configuration**

A tricycle landing gear configuration was selected due to multiple reasons entailed in Section 9.7 of the report.

### **3.2.6 Integrated Configuration Possibilities**

With the selected configuration, the following figure shows 8 possibilities in total. As we can see, a low wing with under wing engines (f. and h.) can be eliminated as the engines would not have sufficient ground clearance to operate. The rear mounted engines with an aft tail (a. and e.) was immediately eliminated as a rear mounted podded engine would be conflicting for space with an aft mounted tail. A high wing with under wing engines and an aft tail (b.) was eliminated due to the aft tail being directly affected by the downwash from the engines. A high wing with rear engines (c.) was also eliminated as the wing downwash could affect the engine inlet resulting in poor performance.

With all possible configurations eliminated except for only two configurations being a low wing with rear mounted engines and a T-tail (g.) and finally a high wing with under wing engines and a T-tail, a trade study was performed to determine the ultimate configuration for the family of aircrafts.

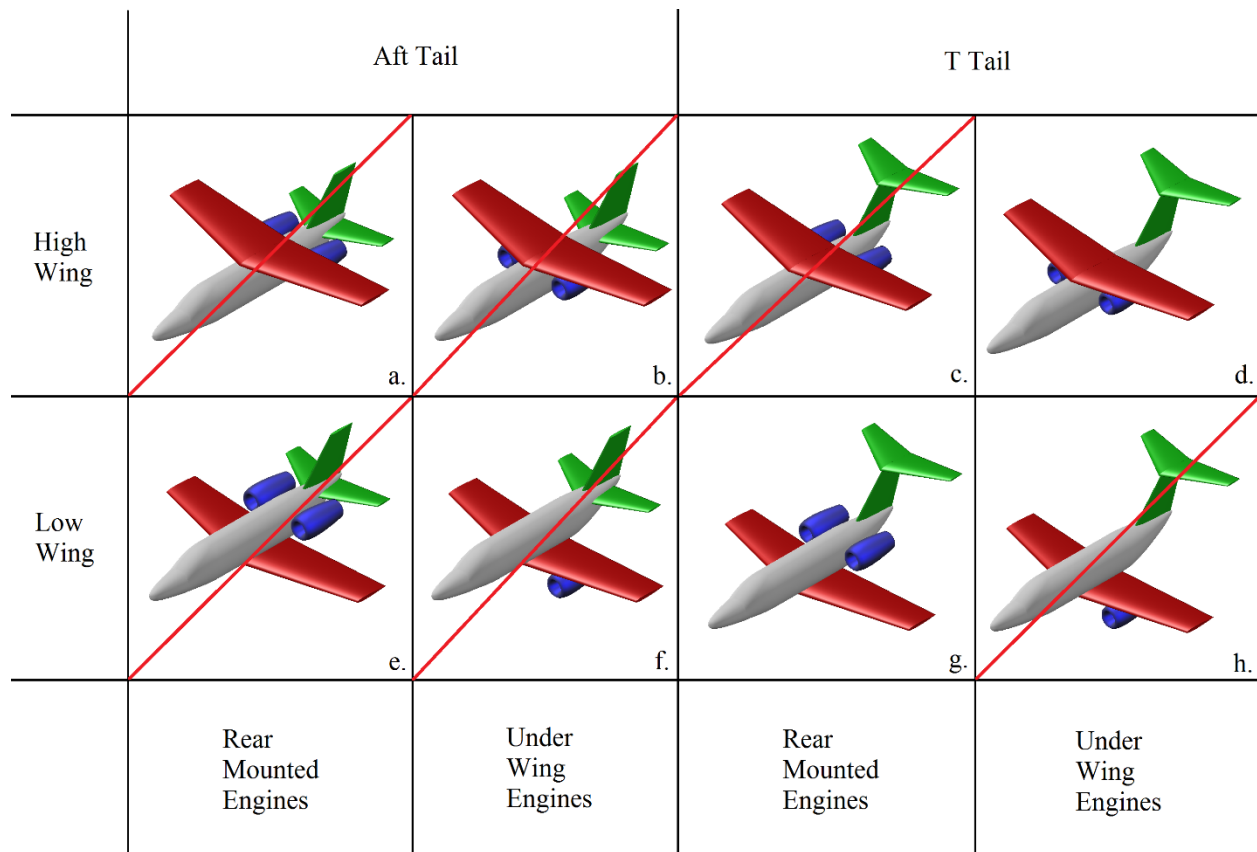


**Figure 3.7. Combinations of all possible configurations before integration.**

### 3.3 Internal Configuration

#### 3.3.1 Seat Selection

One of the primary goals for this aircraft series is to provide passengers with a comfortable and connected cabin environment, a large component of achieving this goal is the passenger's seat. The size and positioning of seats depends on various inter-related spatial constraints including the fuselage structure and dimensions. Consultation was made with B/E Aerospace in order to determine how these constraints specifically relate to the design requirements of the Commander & Chief aircraft series and how they impact the configuration and final dimensions of seats. B/E Aerospace is an aircraft cabin interior products manufacturer with a product range including six different types of business jet seats. These seats do not have distinct dimensions but instead are

designed to have ranges of values for the dimensions of each component allowing a customer to customize their purchase to best meet their needs. Below is a list of the customizable components with their ranges in dimensions, as provided by the company:

- Upholstered width between arms = from 19 to 25.5 inches
- Upholstered armrest width = from 2 to 5 inches
- Upholstered width between arms = from 19 to 25.5 in
- Upholstered armrest width = from 2 to 5 in
- Upholstered largest width will match width between arms
- Overall height will depend on upholstery build up on structure = structure can be 36, 37, 39 or 40
- Headrest will usually be flush with the backrest upholstery, but structure-wise it is usually 2 inches above the backrest structure to 5 inches
- Bottom cushion height is usually around from 18 to 20 inches from the floor
- Maximum weight = 140 lbs

By iterating through various combinations of these component dimensions a seat was designed which not only fit into the cabin but optimized the space around it for the sake of passenger comfort.

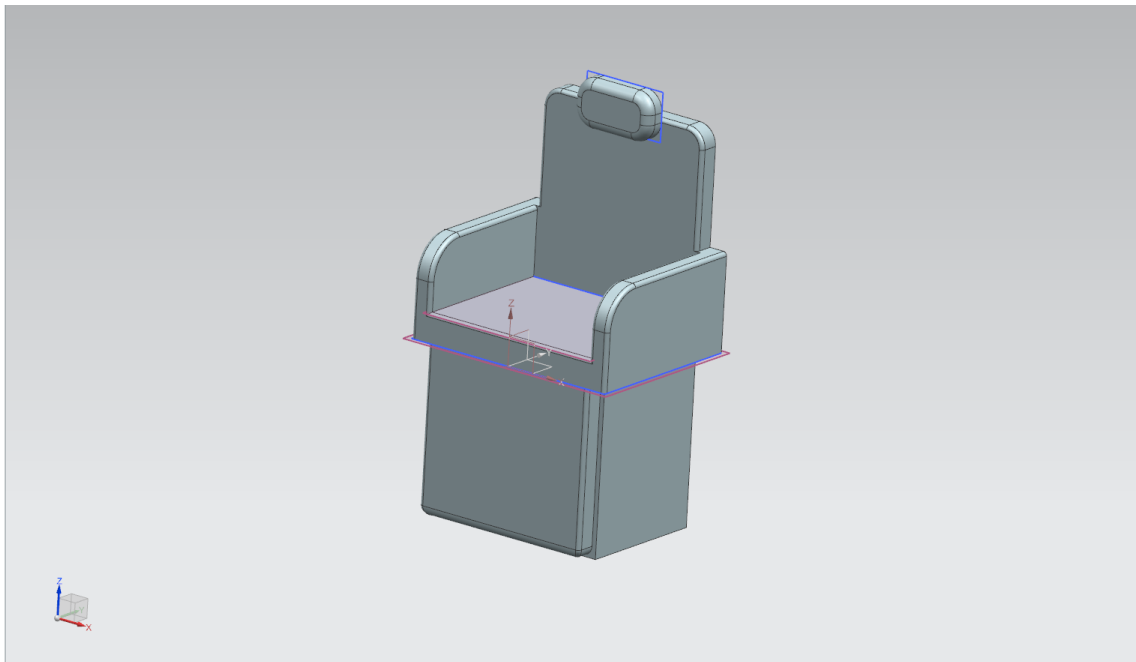


**Figure 3.8. CAD model of a seat.**

**Figure 3.9. Seat Dimensions**

Item	Provided by B/E Aerospace [in]	Chosen Dimensions [in]
Between Armrests	19 – 25.5	19
Armrest Width	2 – 5	2
Overall Height	36 – 40	42
Headrest	2 – 5 above the backrest	2.6 above the backrest
Bottom Cushion	18 - 20 from the floor	18
Legrest Width	19 – 25.5	19

Positioning these seats within the circular cross section of the fuselage required consideration of further constraints. By implementing a CAD model of a chair into the fuselage model, as shown in Figure 3.10, the shape of the seat was optimized and further modifications were made to the dimensions shown in Figure 3.9.

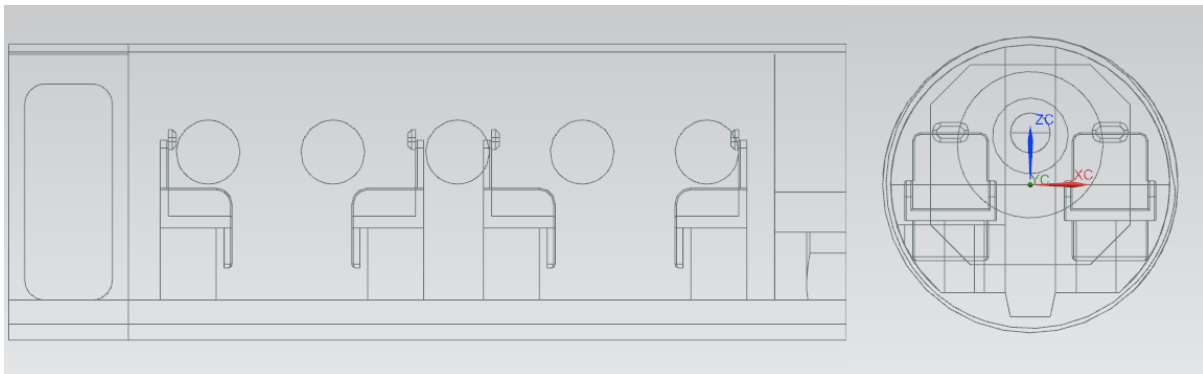


**Figure 3.10. Implementation of the seats in the fuselage.**

A further consideration in the design of the seating configurations was passage space through the fuselage. By limiting the total seat width to 23 in. it is possible to create 17 in. of passage space. Also, in the interest of maximizing leg room and the seat's range of motion, 7.5 in of empty space is placed behind the seat and 15 in of space at the front. This will allow passengers to recline the seat freely and further increase their comfort.

### 3.3.2 Fuselage for the Commander

The primary consideration in the design of a fuselage is providing enough space for passengers, luggage, and all other aircraft components and is determined by its shape, length, and

size. Determination of these properties was dictated by three main factors: the passengers, the fuselage shape, and the seat, galley, and lavatory placements. The first requirement was met by selecting a fuselage with sufficient standing room. The second was determined by selecting a circular cross section for its benefits to the structural stability. An outer diameter of 74 in and an inner diameter of 70 in were chosen to facilitate the necessary standing room and the fuselage's thickness of 2 in. Finally, seat displacement along with galley and a toilet is considered to determine overall length of the fuselage. As discussed in the previous section, seat dimensions and displacements are closely related to the overall length of the fuselage. Since an addition of a galley and a toilet to the fuselage is anticipated, 30 inches of length for both of them were allocated. This results in 60 additional inches to the length derived from the seat positioning. As such, the overall fuselage length becomes 210 inches with the galley and 180 inches without.

### **3.3.3 Empennage**

Empennage is a rear portion of the fuselage typically used as cargo space. Similar to the fuselage, a circular cross section for the empennage was chosen for the added structural stability. By selecting fineness ratio of 2.4 based on typical values for a business jet, the length of the empennage was calculated. The empennage was created by drawing guidelines along circular cross sections like the fuselage with varying diameters along the empennage. In order to avoid creating too much drag from the fuselage, the angle at which the empennage narrows down is determined so that there would not be a flow separation occurring from the surface of the empennage.

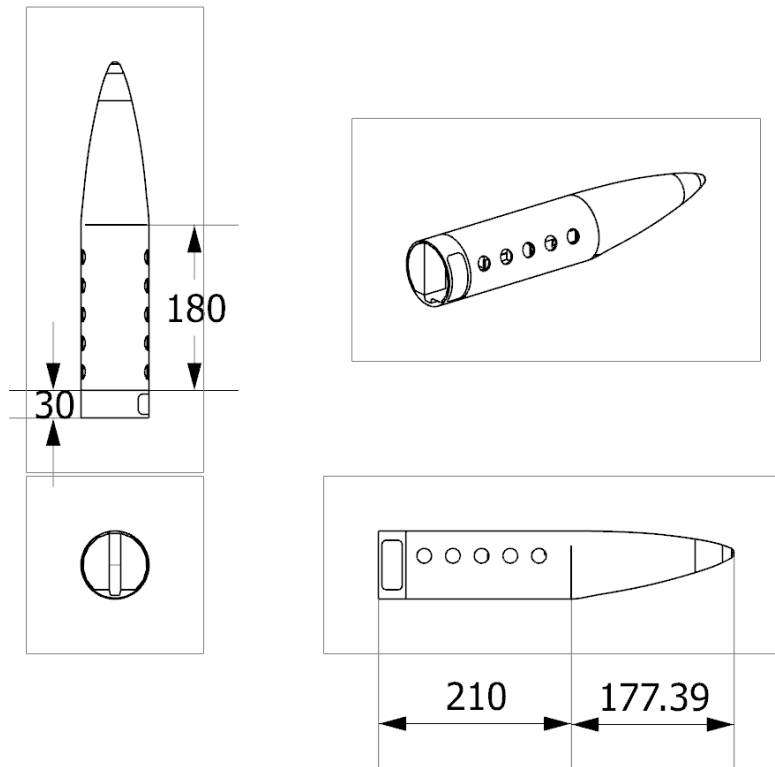


**Figure 3.11. Three views of the fuselage with empennage.**

### 3.3.4 Cockpit

The primary factors in designing the nose and cockpit of an aircraft are the pilot's visibility, the accessibility and ergonomics of the flight controls, and the aerodynamics of the nose. The first factor is dictated by FARs, the second by averaged data from anthropometry studies of pilots and the third by industry conventions. The configuration of the cockpit and nose must also allow room for avionics and the nose landing gear.

Given the complexity of the constraints related to visibility regulations and ergonomic considerations it is the standard convention to define all measurements in the cockpit from the eye level of the pilot. From this, the position of the pilots' seat, rudder pedal, and flight controls can be determined. This in turn allows for a constraint of the side-view positioning of the windows which must allow the pilot  $15^\circ$  of visibility below their eye level and  $20^\circ$  above it. The windows



all internal components of the nose now positioned, and further constraints provided by additional ergonomic factors such as head height, it is possible to design the exterior of the nose section. This is achieved by iterating through nose shapes with the primary design driver of optimizing aerodynamics. As such, the process first started off with circular cross sections for the cockpit with varying diameters and spline tool to draw guidelines and create surfaces to make the cockpit. However, in real manufactured systems, the cockpit is not circular. In order to make the cockpit more aerodynamic and additionally, to provide more space for avionics system and crews, additional guidelines were added to modify the shape of the cockpit.

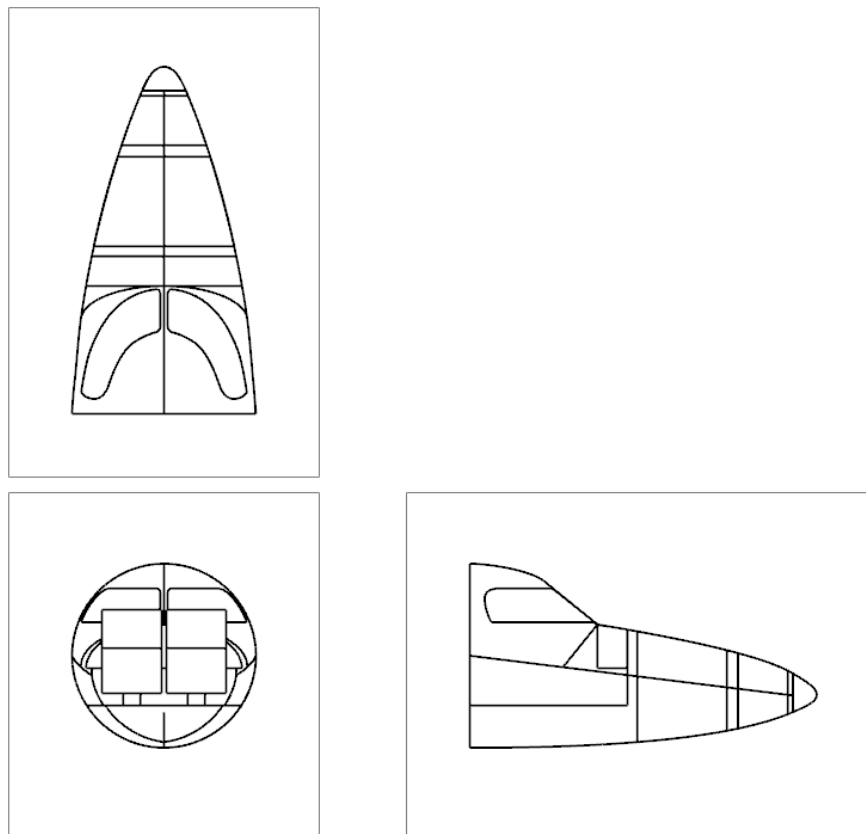


**Figure 3.14. CAD draft of the cockpit.**



The final FAR requirements to meet are those related to the radial distribution of the cockpit windows. These stipulate, using arcs of radial degrees in the top-view plane, window heights and where struts may be placed.

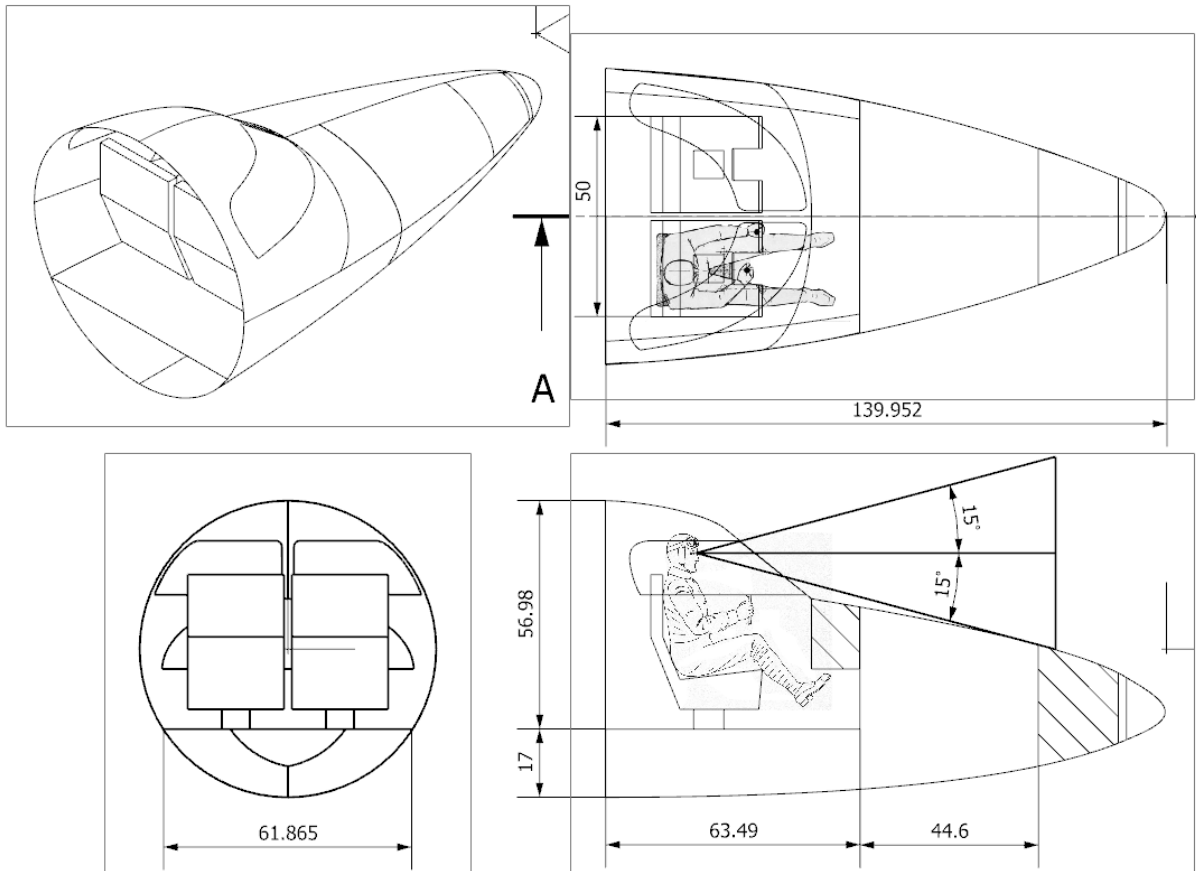


**Figure 3.15. Final CAD model draft of the cockpit.**

### 3.3.5 Fuselage for the Chief

For the Chief, two major changes were enacted: a reduction in two seats from the original eight seater iteration, and a decrease in the fuselage length from 180 in to 150 in to account for the loss of two seats. This reduction in length allows for an overall decrease in cabin space and luggage capacity. This translates into a lighter aircraft, with a lower thrust requirement but a similar fuel capacity requirement. As such, in terms of the interior, there is no drastic change in terms of the

seating layout; it remains the same, albeit with two fewer seats. The general shape of the cabin and cockpit stays the same, increasing the efficiency of production: there will not need to be a special configuration procedure for the Chief as compared to the Commander. This means that the interior production lines will be largely similar, with the six seater lines being more or less the same as the eight seater lines. In terms of the interior products and services, the Chief will offer the same level of comfort and connectivity as the Commander; its only difference is the number of seats and baggage capacity.

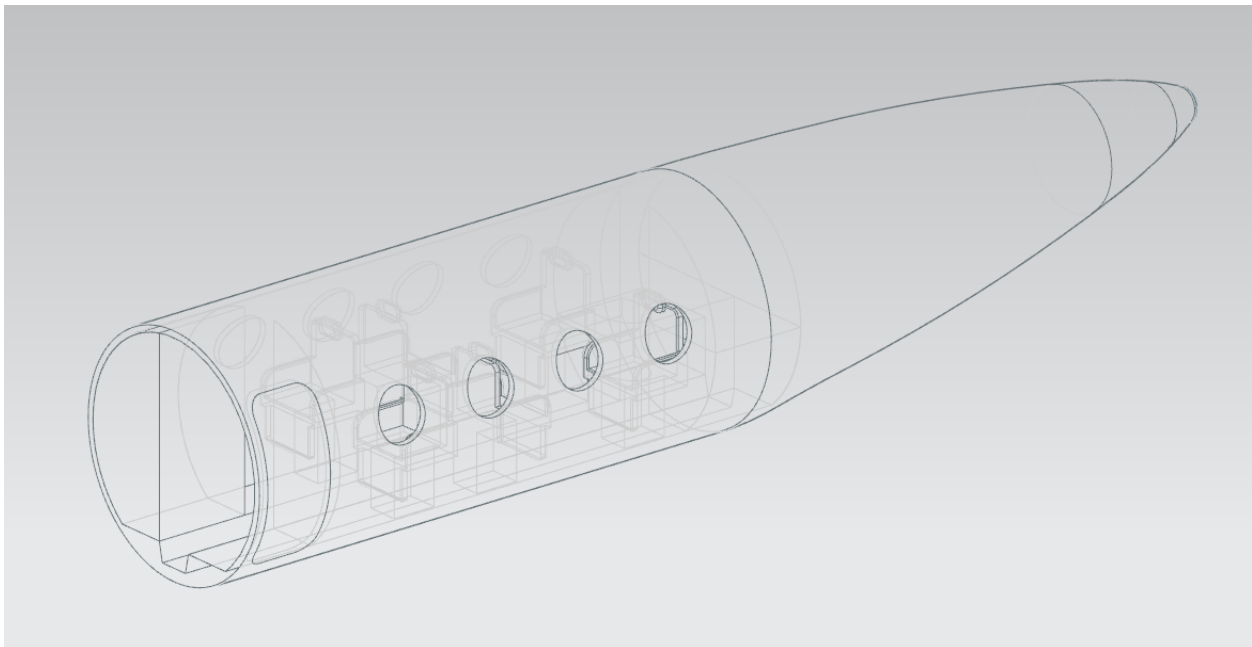


**Figure 3.16. The Chief's fuselage.**

### **3.4 Future Work**

There are two major changes in order to convert the Commander into the Chief– removing two seats and decreasing the fuselage length by 30 in. Just changing the length of the fuselage and keeping other factors constant leads to only slight changes to the calculations, leaving a small amount of reiteration that needs to be done. Any future study will be based on the resulting features from changing other factors as well as the fuselage length by changing fuselage diameter, length

of an empennage, resizing the cockpit, etc. This will allow for the analysis of the effectiveness of each factor in designing an aircraft and further optimize the design for the business jet.

## **4 Weights, Center of Gravity and Balance (Choakpichitchai & Dvorak)**

### **4.1 Component Weights and Location**

To systematically calculate the combined weight and center of gravity, the component weights of the aircraft are subdivided into 4 major components being, fixed equipment, structural, propulsion system and lastly operation components. The center of gravity of each component was determined through two ways. Should the component be distributed throughout the aircraft, an assumption is made that the component does not contribute to the center of gravity location. For the rest of the components, the center of gravity was calculated by measuring the mass properties of the solid body representing the component in the cad model. The weights of each individual component were measured as follows.

The weights of individual fixed equipment components were approximated by using Roskam's equations for fixed equipment [24]. Components such as Instrumentation, Avionics and Electronics are obtained using the weights of the selected systems described Section 11.2. Structural weight of components was obtained through structural estimation detailed in Section 9. The propulsion system weights were determined according to the selected engine for the aircraft. Lastly for operation weights, components such as fuel weight were approximated through fuel burn calculations detailed in Section 2.1 while components such as passenger, baggage and pilot weight were set to meet the requirements. The details of the weights and center of gravity for both the Chief and Commander are detailed in the tables below.

#### **Figure 4.1. Weights and Center of Gravity of the Chief**

<b>System</b>	<b>Subsystem</b>	<b>Weight [lb]</b>	<b>Horizontal Distance from tip of radome [in]</b>	<b>Vertical Distance from tip of radome [in]</b>	<b>Horizontal Moment [ft-lb]</b>	<b>Vertical Moment [ft-lb]</b>
<b><u>Fixed Equipment Weight</u></b>		3381.2			309596.336	-9290.768
Flight Control System		502.5	Distributed	Distributed	0	0
Hydraulic and/or Pneumatic System		154	Distributed	Distributed	0	0
Electrical System		637.6	Distributed	Distributed	0	0
Instrumentation, Avionics and Electronics		402.4			31185.416	219.872
	Honeywell Primus Radar	36.4	23.69	-14.17	862.316	-515.788
	Proline 21	366	82.85	2.01	30323.1	735.66
Air-conditioning and De-icing System		234.73	Distributed	Distributed	0	0
Auxiliary Power Unit		88	467.09	10.88	41103.92	957.44

Furnishings		1361.97			237307	-10468.08
	Passenger Seats	840	243.515	-10.642	204552.6	-8939.28
	Pilot Seats	280	116.98	-5.46	32754.4	-1528.8
	Lavatory, Galley and Furnishings	241.97	Distributed	Distributed	0	0
<b><u>Structural Components Weight</u></b>		4911.1568			1408607.52	-56640.208
<b>Wing</b>		2213.72938	160	-37	630780.05	-69931.7111
	Shell (Skin)	257.40288	124.94	5.41	73344.3766	-8131.35698
	Structural	1956.3265	124.94	5.41	557435.673	-61800.3541
<b>Tail</b>		595.749	377	19	283910.143	63232.79886
	Shell (Skin)	79.307	99.56	87.14	37794.5439	8417.64498
	Structural	516.442	99.56	87.14	246115.6	54815.15388
<b>Empennage</b>		239.688615			93775.7738	1234.396367
	Shell (Skin)	38.83	391.24	5.15	15191.8492	199.9745
	Structural	200.858615	391.24	5.15	78583.9246	1034.421867
<b>Fuselage</b>		550.6172			127761.117	-3676.21232

	Floor (Plate - no structure)	128.1522	236	-28.78	30243.919 2	- 3688.22032
	Walls (Plate - no structure)	8	273.781	1.501	2190.248	12.008
	External Barrel (Skin)	127.77	230	0	29387.1	0
	Structural	286.695	230	0	65939.85	0
<b>Cockpit</b>		336.2426			28496.560 4	- 3258.19079
	Structural	307.0936	84.75	-9.69	26026.182 6	- 2975.73698
	Skin	29.149	84.75	-9.69	2470.3777 5	-282.45381
<b>Landing Gear</b>		951		-102.153	234363.62 8	-48186.689
	Nose Landing Gear	194	76.462	-51.764	14833.628	-10042.216
	Main Landing Gear	757	290	-50.389	219530	-38144.473
<b>Engine Nacelles</b>		24.13			9520.2502	3945.4
	Skin	24.13	394.54	10	9520.2502	3945.4
<b><u>Propulsions Weight</u></b>		1888.18	160	-37	770335.80 5	8972.9756
Fuel System		244.18	136.47	6.42	72392.044 6	-7467.0244
Engines		1644	424.54	10	697943.76	16440

<b><u>Operational Weight</u></b>		7493.29	160	-37	1966304.69	-177354.808
Passengers	6 pax	1200	243.515	-10.62	292218	-12744
Flight Crew	2 pax	400	116.98	-5.46	46792	-2184
Fuel	Fuel Tanks	5393.29	136.47	6.42	1598948.69	-164926.808
Baggage	30 cubic feet	500	56.692	5	28346	2500
<b><u>Total</u></b>		17673.8268	252.058844	-13.257616	4454844.35	-234312.809

**Figure 4.2. Weights and Center of Gravity of the Commander**

<b>System</b>	<b>Subsystem</b>	<b>Weight [lb]</b>	<b>Horizontal Distance from tip of radome [in]</b>	<b>Vertical Distance from tip of radome [in]</b>	<b>Horizontal Moment [ft-lb]</b>	<b>Vertical Moment [ft-lb]</b>
<b><u>Fixed Equipment Weight</u></b>		3808.68			389363.736	-12268.288
Flight Control System		502.5	Distributed	Distributed	0	0
Hydraulic and/or Pneumatic System		154	Distributed	Distributed	0	0
Electrical System		699.3	Distributed	Distributed	0	0

Instrumentation, Avionics and Electronics		402.4			31185.416	219.872
	Honeywell Primus Radar	36.4	23.69	-14.17	862.316	-515.788
	Proline 21	366	82.85	2.01	30323.1	735.66
Air-conditioning and De-icing System		282.7	Distributed	Distributed	0	0
Auxiliary Power Unit		88	497.09	10.88	43743.92	957.44
Furnishings		1679.78			314434.4	-13445.6
	Passenger Seats	1120	251.5	-10.64	281680	-11916.8
	Pilot Seats	280	116.98	-5.46	32754.4	-1528.8
	Lavatory, Galley and Furnishings	279.78	Distributed	Distributed	0	0
<b><u>Structural Components Weight</u></b>		5000.2641			1546204.35	-56916.501
<b>Wing</b>		2213.72938	190	-37	697191.931	-69931.7111



	Shell (Skin)	257.40288	124.94	5.41	81066.463	- 8131.3569 8
	Structural	1956.3265	124.94	5.41	616125.46 8	- 61800.354 1
<b>Tail</b>		595.749	407	19	301782.61 3	63232.798 86
	Shell (Skin)	79.307	99.56	87.14	40173.753 9	8417.6449 8
	Structural	516.442	99.56	87.14	261608.86	54815.153 88
<b>Empennage</b>		239.68861 5			100966.43 2	1234.3963 67
	Shell (Skin)	38.83	421.24	5.15	16356.749 2	199.9745
	Structural	200.85861 5	421.24	5.15	84609.683	1034.4218 67
<b>Fuselage</b>		639.7245			158019.03 9	- 4252.5052 8
	Floor (Plate - no structure)	148.176	251	-28.78	37192.176	- 4264.5052 8
	Walls (Plate - no structure)	8	294.685	1.5	2357.48	12
	External Barrel (Skin)	149.07	245	0	36522.15	0
	Structural	334.4785	245	0	81947.232 5	0
<b>Cockpit</b>		336.2426			28496.560 4	- 3258.1907 9
	Structural	307.0936	84.75	-9.69	26026.182 6	- 2975.7369 8
	Skin	29.149	84.75	-9.69	2470.3777 5	-282.45381

<b>Landing Gear</b>		951			249503.628	-48186.689
	Nose Landing Gear	194	76.462	-51.764	14833.628	-10042.216
	Main Landing Gear	757	310	-50.389	234670	-38144.473
<b>Engine Nacelles</b>		24.13			10244.1502	4245.4
	Skin	24.13	424.54	10	10244.1502	4245.4
<b><u>Propulsions Weight</u></b>		1752.18	190	-37	719923.765	7612.9756
Fuel System		244.18	136.47	6.42	79717.4446	-7467.0244
Engines		1508	424.54	10	640206.32	15080
<b><u>Operational Weight</u></b>		8956.09	190	-37	2768176.7	-196345.232
Passengers	8 pax	1600	251.5	-10.64	402400	-17024
Flight Crew	2 pax	400	116.98	-5.46	46792	-2184
Fuel	Fuel Tanks	5956.09	136.47	6.42	1944484.7	-182137.232
Baggage	60 cubic feet	1000	374.5	5	374500	5000
<b><u>Total</u></b>		19517.2141	277.891534	-13.2148494	5423668.56	-257917.046

The Chief must weigh less than 19,000 lb to comply with FAR 23. As shown in table Figure 4.1 the maximum takeoff weight of the Chief is 17,673 lb. Subsequently the Commander also meets all weight requirements.

## 4.2 Weight and Balance

**Figure 4.3. The Commander Center of Gravity Travel**

Stage	Weight [lb]	C.G. Y-Position Aft of the Nose [in]	Fuel Burned this Stage [lb]	Total Fuel Burned [lb]
Engine Startup	19515.00	277.89	[-]	[-]
Taxi, Takeoff, Climb	18720.69	275.83	794.31	794.31
2500 nm Cruise	14766.20	262.27	3954.49	4748.80
30 min Loiter	14478.07	260.99	288.13	5036.93
Descent, Missed Landing, Climb	14030.85	258.91	447.22	5484.15
100 nm Divert	13898.24	258.26	132.61	5616.76
30 min Loiter	13627.12	256.91	271.12	5887.88
Descent, Landing, and Taxi	13558.98	256.56	68.14	5956.02

**Figure 4.4. The Chief Center of Gravity Travel**

Stage	Weight [lb]	CG Y-Position Aft of the Nose [in]	Fuel Burned this Stage [lb]	Total Fuel Burned [lb]
Engine Startup	17671.00	252.05	[-]	[-]
Taxi, Takeoff, Climb	16951.75	250.17	719.25	719.25
2500 nm Cruise	13370.93	237.77	3580.82	4300.07
30 min Loiter	13110.02	236.60	260.91	4560.98
Descent, Missed Landing, Climb	12705.06	234.69	404.96	4965.94
100 nm Divert	12584.98	234.10	120.08	5086.02
30 min Loiter	12339.41	232.86	245.57	5331.59
Descent, Landing, and Taxi	12277.71	232.55	61.70	5393.29

For these CG travel and fuel burn calculations, a MATLAB code was used to model the fuel burn over the cruise and loiter stages. Weight fractions were used for all other stage. The mission profile used for this stage contained a 2500 nm cruise and a 30 minute loiter, followed by a 100 nm diversion and an additional 30 minute loiter prior to landing. This was calculated with both full baggage and passengers for both the Chief and the Commander. This gave us a worst-

case scenario for loading and fuel burn. The code was run iteratively until the gross takeoff weight and fuel burn corresponded to the empty weight of the aircraft. The same method was used for both the Chief and the Commander. Once the fuel burn was known, the aircraft weight at each stage could be found by subtracting the cumulative fuel burned from the gross takeoff weight. Plugging these weights into our system weight spreadsheet gave the CG throughout the mission profile.

It should be noted that these calculations result in burning all of the fuel onboard the aircraft. This is not realistic, as reserves are always kept and there is fuel trapped in the tanks and fuel lines. The extra passenger and baggage weight will help account for the trapped fuel and reserves. In addition, the wings of our aircraft family were found to have storage for up to 130 ft<sup>3</sup> of fuel, which is approximately 6600 lb of fuel. This provides space for a fuel reserve, which makes it increasingly unlikely that incidents occur due to fuel exhaustion.

## **5 Aerodynamics (MacDuff)**

### **5.1 Airfoil Selection**

The selection of the airfoil is a vital first step in the design of a wing planform. Choosing the airfoil that performs well at each leg of the design mission is crucial to the success of the entire wing. At transonic speeds, minimizing drag becomes a bigger issue than generating lift, and the design mission calls for a Mach number at cruise of 0.85, which falls into the transonic regime. Two types of airfoils that accomplish this are natural laminar flow (NLF) and supercritical airfoils, but they minimize different types of drag.

Natural laminar flow airfoils are designed to reduce skin friction drag by forestalling the transition of laminar flow in the boundary layer to turbulent flow. Turbulent flow along a wing creates large amounts of drag relative to laminar flow, even on the order of double the drag created

by laminar boundary layers in many cases [18]. The skin friction drag is a major portion of drag on an airplane which makes NLF airfoils very enticing; however, it is important to consider that maintaining laminar flow at very high velocities is difficult, and that other types of drag become more prominent at transonic conditions.

Supercritical airfoils work differently. First, one must understand that although the entire aircraft may be traveling at a subsonic Mach number, the Mach number locally at points on the aircraft can reach sonic conditions. For example, flow over the upper surface of an airfoil is usually faster to generate a pressure difference and create lift, so many times even if the flow an airfoil is in is at a subsonic speed close to Mach 1, somewhere locally on the upper surface of the airfoil a Mach number greater than one will be achieved. Reaching the sonic condition forms a shock which creates what is known as wave drag. Supercritical airfoils are designed to deter the formation of these strong shocks wave drag, is a typical issue in the design of transonic aircraft.

After comparing several airfoils, which is discussed later in the trade studies section, a supercritical airfoil was selected. The NASA SC(2)-0714 airfoil was selected as it created good amounts of lift while creating much less drag than other airfoils, especially at cruise conditions. Below are the lift curve and drag polar of the airfoil. The data was acquired using XFOIL direct analysis within XFLR5, and then the data was exported to a \*.txt file and imported into MATLAB and plotted. The Reynolds number was set to 1,000,000 to get data that better represents the true performance of the airfoil compared to a very high Reynolds number.

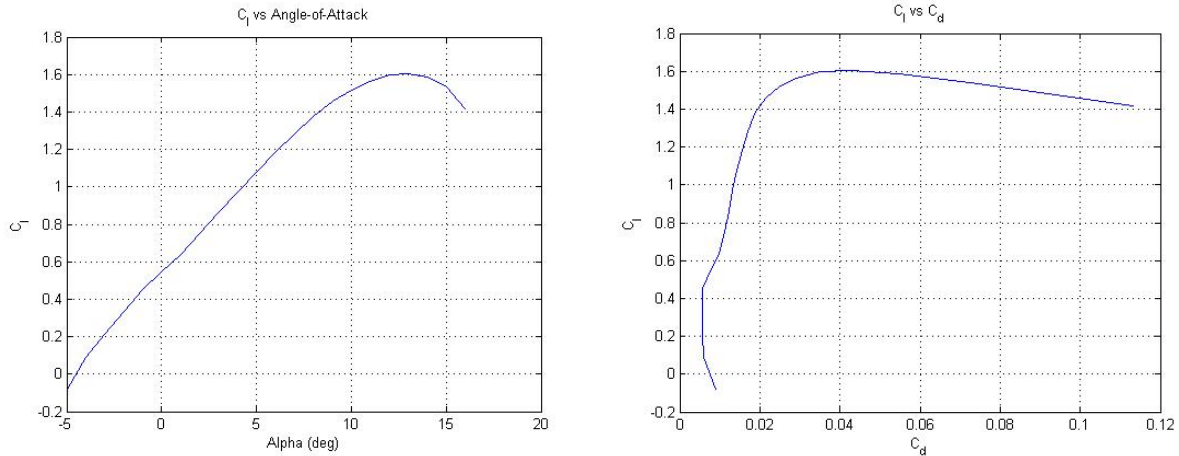


**Figure 5.1. Airfoil lift curve and drag polar.**

## 5.2 Wing Selection and Shape

Once the airfoil is selected, the overall shape of the 3D wing is the next step in the aerodynamic design process. The original constraint analysis generated a wing loading of 40 lb per ft<sup>2</sup>. Planes with similar design missions had a span near the range of 50 to 55 ft. Initial sizing produced a takeoff gross weight of 20006 lb. This information gives a general idea of the size of the wing by giving a first estimate of span and area. Now with a general idea of the size, the next step is to choose the shape. The two main geometries seen in the industry are straight, trapezoidal tapered and swept wings. Both geometries have pros and cons. A tapered wing is lighter because it requires less structure and has favorable stall conditions. A swept wing decreases a lot of induced drag, but requires more structural weight and tends to stall at the tips. After weighing the pros and cons a swept wing with some taper was selected. It was selected to reduce drag, but still not require too much structural weight.

## 5.3 Aircraft Drag Buildup

The drag buildup on The Commander, the 8 passenger jet, and The Chief, the 6 passenger jet, are shown in the tables that follow. The Component Buildup Method was implemented in a MATLAB code and used to calculate the parasite drags of the fuselage and the nacelles [18].

XFLR5 was used to calculate the drag on the main wing, horizontal tail, and vertical tail. XFLR5 works by first using XFOIL to calculate airfoil data. Then XFLR5 extrapolates this sectional data onto a 3D geometry you define. An approximation based on historical values was used for the drag from the flaps and landing gear for takeoff and landing [20]. Flap sizing was done by implementing a method from the second book of Roskam's Airplane design series into MATLAB code [21]. Originally, the flap chord ratio, the amount of the chord taken up by the flap, was 0.3, but this conflicted with the landing gear placement. To solve this conflict, the flap chord ratio was decreased to 0.2, and the span of the flaps was increased to increase the wetted flap area, which increases the change in lift created by the high lift system. Diagrams for the high lift systems can be seen in the figure below.

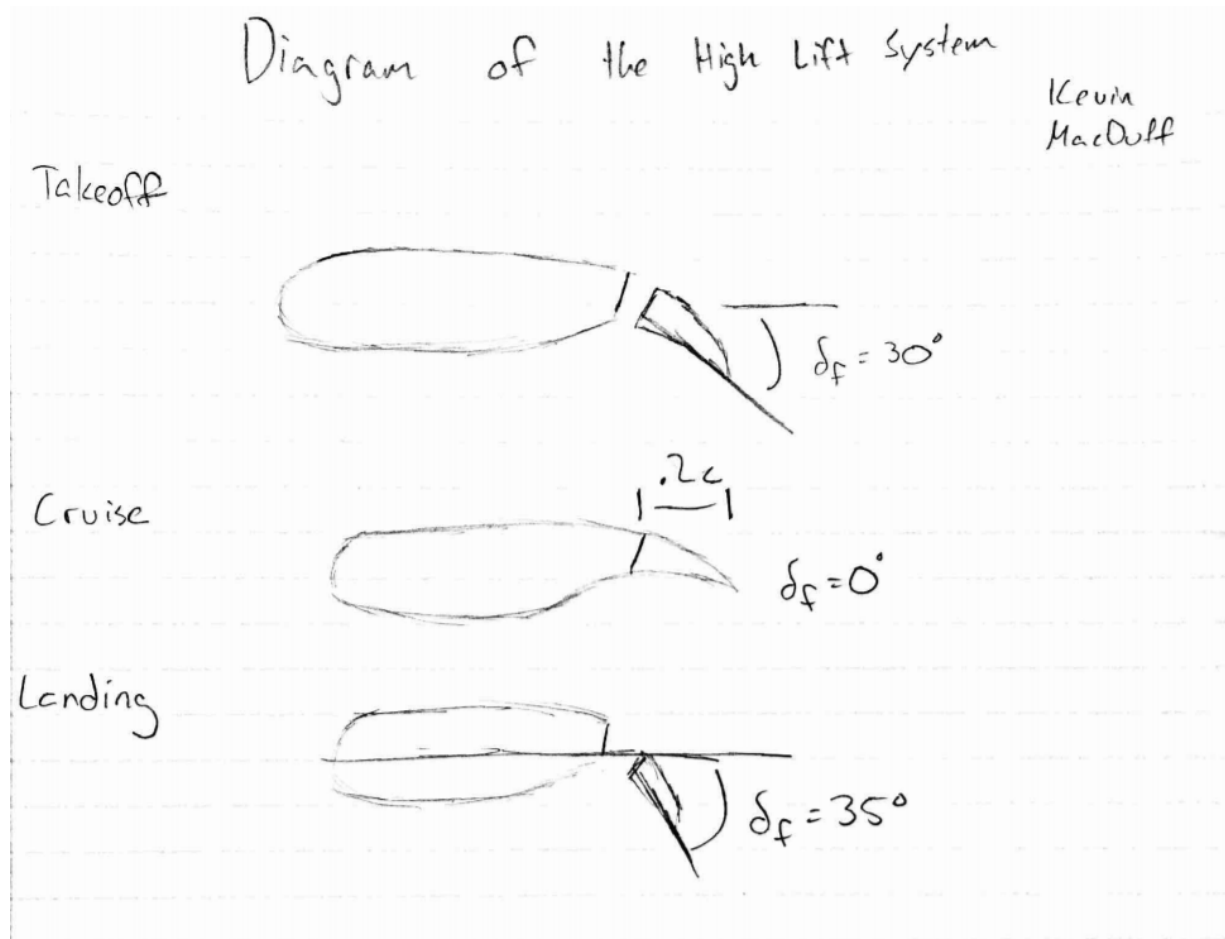


**Figure 5.2. Diagram of the high lift system.**

**Figure 5.3. Drag Coefficient Values for Takeoff, Cruise, and Landing for The Commander**

<b>Component</b>	<b>C<sub>D</sub> (Takeoff)</b>	<b>C<sub>D</sub> (Cruise)</b>	<b>C<sub>D</sub> (Landing)</b>
Wing	0.149	0.013	0.149
Horizontal Tail	0.00342	0.00567	0.0033
Vertical Tail	0.005	0.005	0.005
Fuselage	0.0098	0.0093	0.0098
Nacelles (x2)	0.002	0.0019	0.00203
Landing Gear Interference	0.017	N/A	0.017
Flaps	0.015	N/A	0.060

Since the wing, tail, and nacelles are the same on the Chief as they are on the Commander, only the drag on the fuselage changes, so one only needs to calculate the different drag on the fuselage. This is shown in the table below.

**Figure 5.4. Drag Coefficient Value for The Chief Fuselage for Takeoff, Cruise, and Landing**

<b>Component</b>	<b>C<sub>D</sub> (Takeoff)</b>	<b>C<sub>D</sub> (Cruise)</b>	<b>C<sub>D</sub> (Landing)</b>
Fuselage	0.010	0.0096	0.010

It is important to note that the takeoff velocity is 178 ft/s at an angle of attack of 15 degrees, and that the landing velocity is 193 ft/s at the same angle of attack. Both models cruise at an altitude of 35,000 ft and a Mach number of 0.85, but The Commander cruises at an angle of attack of -0.5°, while The Chief cruises at an angle of attack of 0°.

#### **5.4 Aircraft Lift Curves and Drag Polars**

Calculations for the aircraft lift curves and drag polars were done in XFLR5 once again. The data was then exported from XFLR5 and imported into MATLAB. The data was plotted using a MATLAB script that also adjusted  $C_L$  and  $C_D$  for when the flaps are deployed at takeoff and landing.



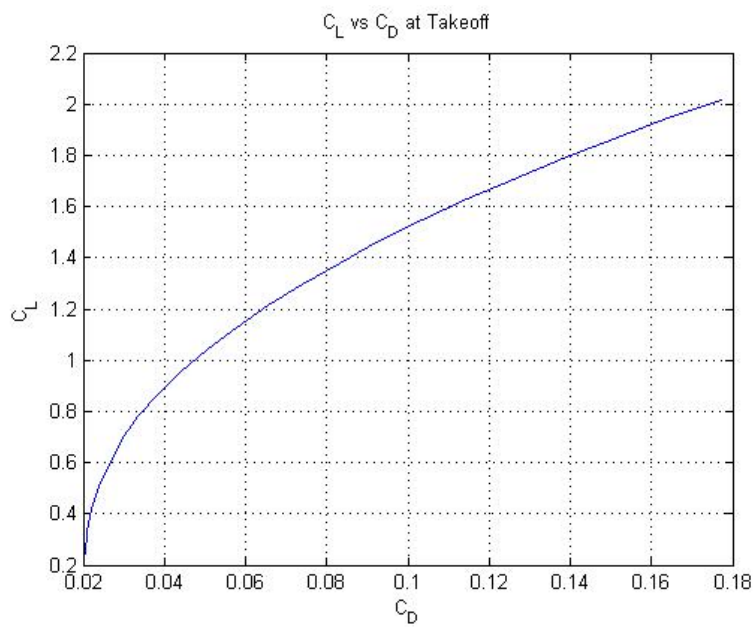
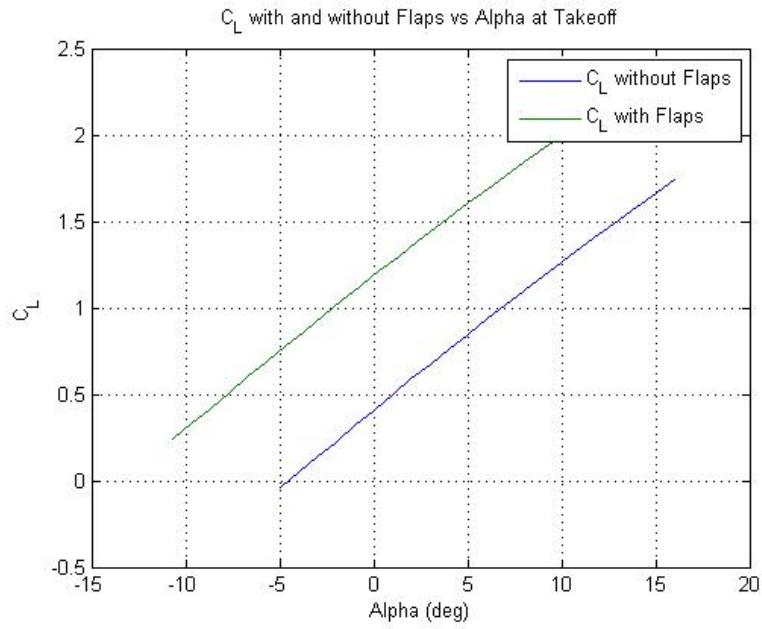


**Figure 5.5. Aircraft lift curve and drag polar at takeoff.**

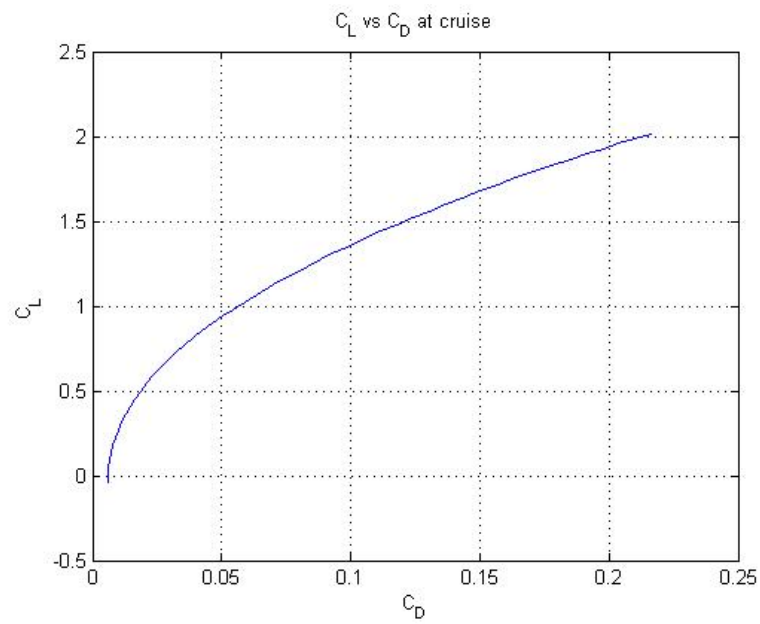
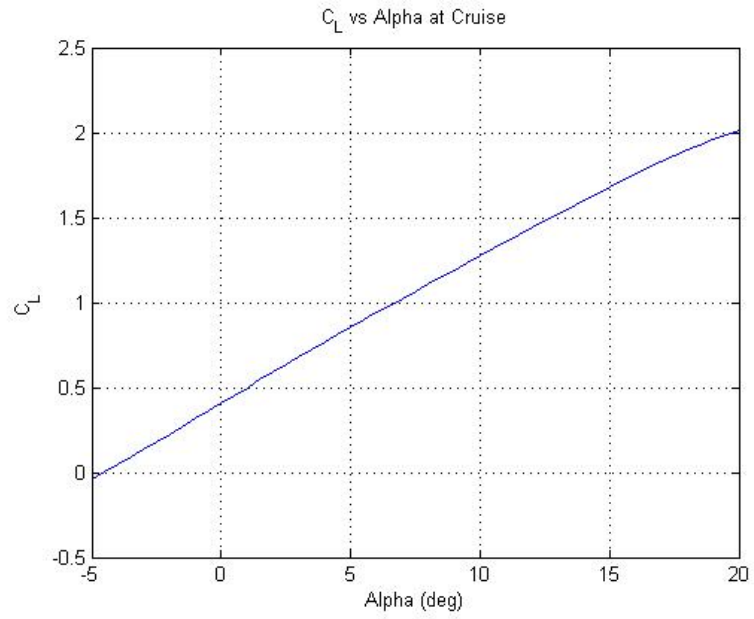


**Figure 5.6. Aircraft lift curve and drag polar at cruise.**

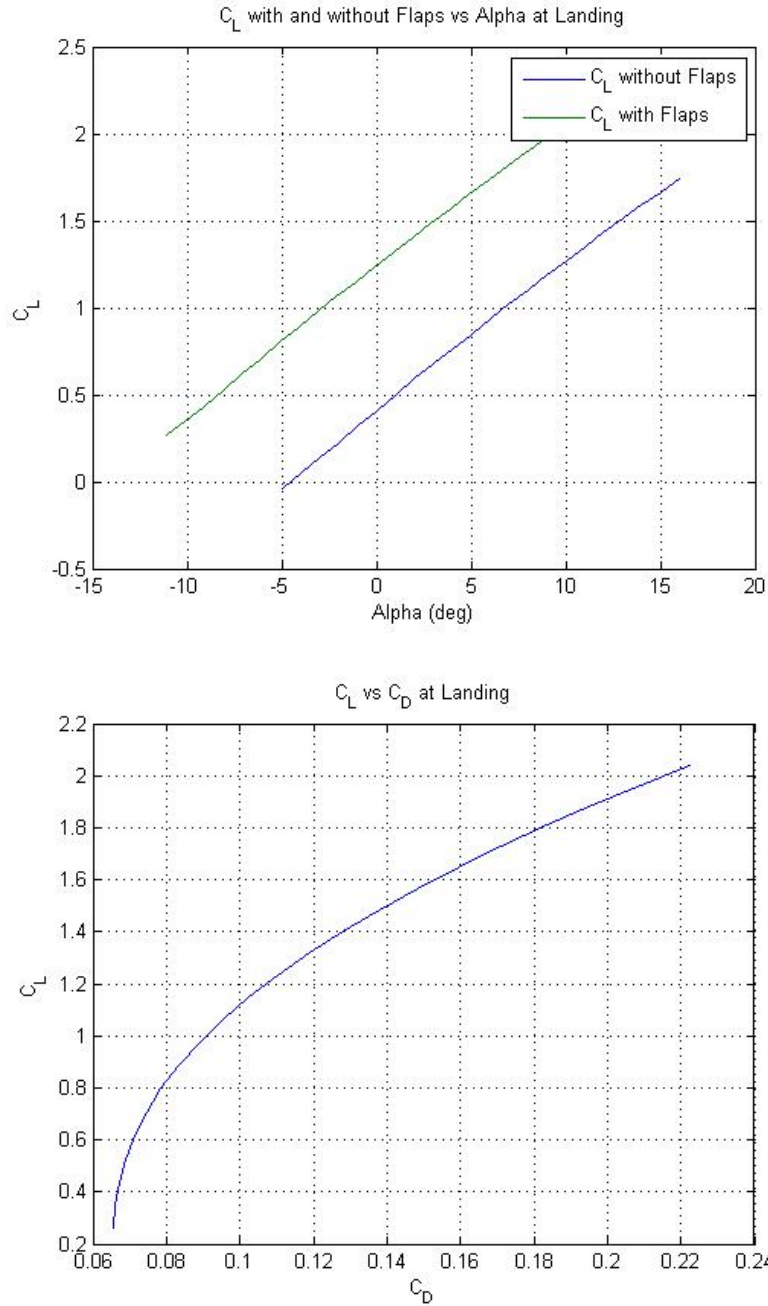


**Figure 5.7. Aircraft lift curve and drag polar at landing.**

## 5.5 Trade Studies

One trade study that was conducted was the selection of the airfoil. There were several aerodynamic characteristics that had to be weighed against each other. The final two airfoils that had to be chosen between were the NASA SC(2)-0714 and the NASA/Langley NLF(1)-0215F.

The airfoil aerodynamic properties can be seen plotted in Figure 4.6 below. The aerodynamic properties were calculated in XFLR5 at a Reynolds number of 1000000 and a Mach number of 0.2.

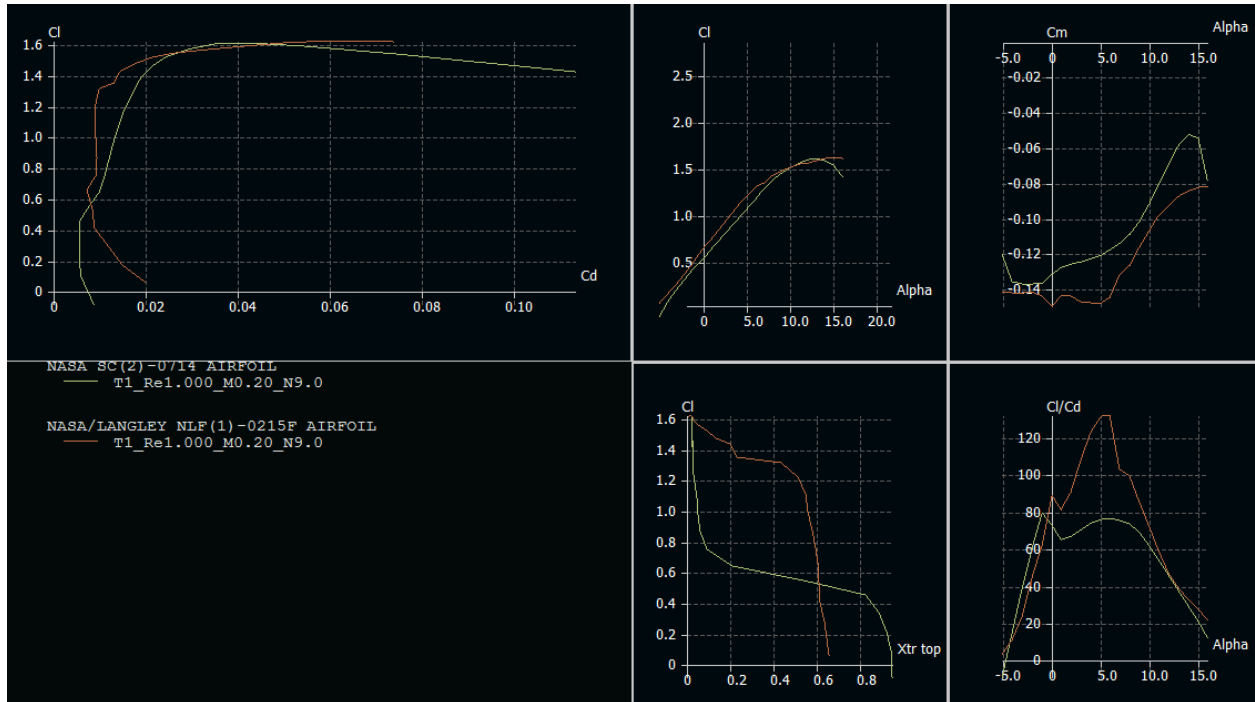


**Figure 5.8. Comparing the Aerodynamic Properties of the Airfoils.**

After weighing the different properties against each other, it was decided that the  $C_L$  and  $C_D$  were similar enough, while the moment of the NLF airfoil appeared to make it much more unstable.

## 5.6 Future Work

Much of the future work that needs to be done is optimization. For, example the wing needs to be modified to decrease both lift and drag. A possible solution to this is downsizing the wing. Also, it would be useful to decrease the moment created by the wing, so that the tail would possibly not have to be as large or generate such great negative lift. This would also decrease drag, as the tail is creating more drag than is preferred. Both of these issues could also be addressed on a

smaller scale by modifying the airfoil. In all, future work is needed for the optimization of aerodynamic properties to better aid in performance and stability and control.

## **6 Performance (Dvorak & Vasiliauskas)**

The request for proposal for the family of business jets has a few general design requirements that are performance related. These design requirements are a maximum cruise speed of Mach 0.85 at 35000 ft, rate of climb of 3500 ft/min, service ceiling of 45000 ft, maximum sea level takeoff balanced field length of 4000 ft at maximum take gross weight with dry pavement, and maximum landing field length of 3600 ft at typical landing weight [8].

The Chief must meet FAA FAR Part 23 Airworthiness Standards for certification and have a minimum range of 2500 nm at LRC assuming NBAA IFR range with 100 nm alternate with a pilot and three passengers at 200 lb each [8].

The Commander must meet FAR Part 23 Standards for certification and have a minimum range of 2500 nm at LRC assuming NBAA IFR range with 100 nm alternate with two pilots and three passengers at 200 lb each [8].

Performance ensured that these requirements were met by conducting initial sizing, constraint analysis, calculating the balanced field length, landing field length, climb rate and then breaking down drag and fuel consumed for all segments. Performance worked closely with propulsion and aerodynamics to confirm that the engines and main wing generated enough thrust and lift to achieve the requirements given in the RFP.

### **6.1 Initial Sizing**

To begin the design process, the design team decided to work on the Commander and assume a worst-case scenario mission profile for the initial sizing. This mission profile is shown below in Figure 6.1. The design team believed that creating a worst case scenario for the larger of

the two business jets was the best plan of attack to size a business jet that would definitely accomplish the requirements listed in the RFP. Furthermore, a worst-case scenario was used to size the jets because most of the values that are used to complete the initial sizing are just historical numbers that vary between sources. More often than not, these values are underestimations, such as the thrust specific fuel consumption for the cruise and loiter legs when using a high bypass turbofan. Extending the mission profile into a worst-case scenario compensates for the inherent underestimation involved with initial sizing. This allowed propulsion and aerodynamics teams to start their respective component design with a more realistic estimate of size in mind.

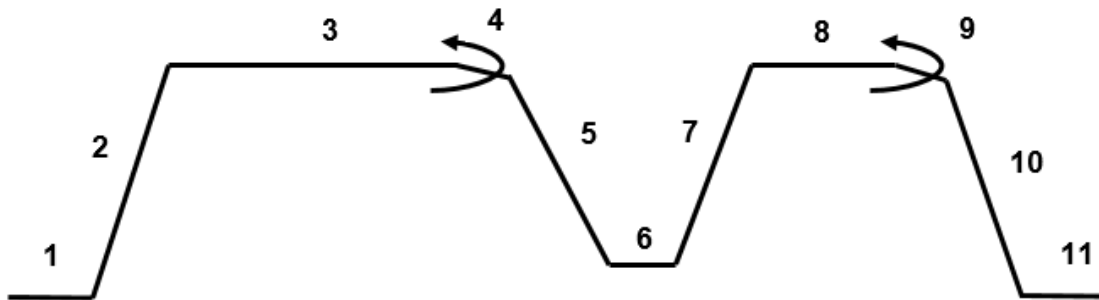


**Figure 6.1. Worst-case scenario mission profile.**

A breakdown of this mission profile is that the Commander with two pilots, eight passengers, and full baggage cruises 2500 nm, loiters for an hour, goes in for a landing which it then aborts, climbs back to cruise altitude for a 100 nm alternate to another airport, loiters for half an hour, and then lands. A more in-depth breakdown of this mission profile is shown in Figure 6.1.

With this mission profile in mind, the process and values for initial sizing were obtained from Section 1.2 [25]. A custom MATLAB script was employed to efficiently run through the initial sizing calculations. After running the script with a payload of 3000 lb for the two pilots, eight passengers, and full baggage, the takeoff gross weight for the worst case scenario was 22100 lb. To quickly size the six passenger business jet with the same mission profile, the payload weight

was changed to 2100 lb for the two pilots, six passengers, and full baggage. This resulted in a takeoff total gross weight of 16650 lb.

**Figure 6.2. Mission Profile Performance Summary**

Leg	Segment	M	Height (10 <sup>3</sup> ft.)	Range (nm)	L/D	Assume	$\frac{W_i}{W_{i-1}}$	$\frac{W_i}{W_0}$
1	Engine Start-Up Taxi, and Takeoff	-	0	-	-	Business Jet has high bypass turbofan engines Payload = 3000 lb	0.980	0.980
2	Climb	-	-	-	-	-	0.980	0.960
3	Main Cruise	0.8 5	35	2500	13	Mach 0.85 at 35,000 ft is 823.8 ft/s; (L/D) <sub>cruise</sub> =0.866*(L/D) <sup>max</sup> c=0.5 (lb/hr)/lb for high bypass turbofan in cruise	0.821	0.788
4	Loiter	0.6 3	35	-	15	Max L/D during loiter; Loiter for 60 minutes; c=0.4 (lb/hr)/lb for high bypass turbofan in loiter	0.974	0.768
5	Descend	-	-	-	-	Descend remaining altitude	0.99	0.760
6	Aborted Landing	-	5	-	-	-	0.99	0.752
7	Climb	-	-	-	-	-	0.98	0.738
8	Alternate	0.8 5	35	100	14.7 2	Same as Leg 3	0.992	0.732
9	Loiter	0.6 3	35	-	17	Same as Leg 4 except loiter for 30 minutes	0.987	0.722
10	Descend	-	-	-	-	-	0.99	0.715
11	Land	-	-	-	-	-	0.992	0.709

## 6.2 Constraint Analysis

The constraint analysis was first done for the Commander. Following the three Constraint Analysis lecture slides presented by Professor D'Urso [5] [6] [7], Chapter 5 of Raymer [18], and Chapter 4 of Sadraey [26], the equations for the constraints were coded into a custom MATLAB script. Much like for the initial sizing, many values had to be estimated in the beginning of the

design process to even obtain a design space from the constraint analysis. The design team researched many similar business jets, mostly newer in-service jets, to acquire the best estimate for the values that were publicly available. For example, the Oswald efficiency factor, zero lift drag coefficient, and coefficient of lift were all best guesses in the initial stage. The design point chose was a  $T/W$  of 0.42 and a  $W/S$  of 55.

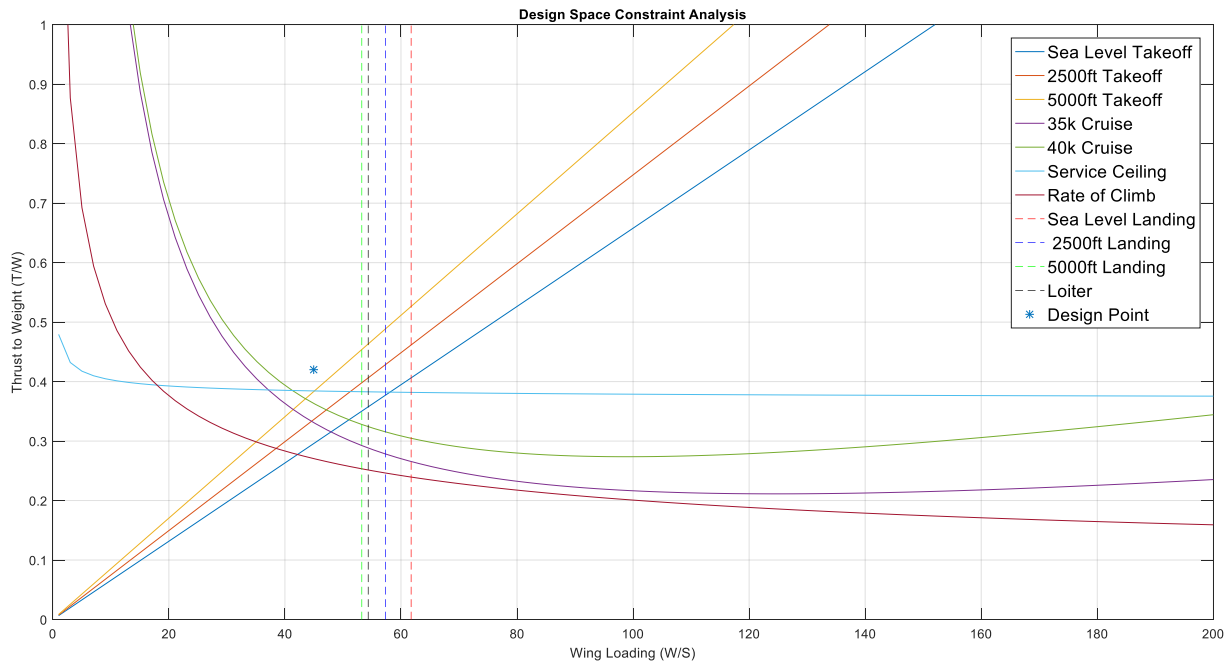


**Figure 6.3. The Commander constraint analysis and design space.**

While aerodynamics progressed on the design of the wing and high lift system, these values were updated and iterated to create a more accurate constraint analysis. The reasoning behind doing the larger of the two jets was because the equations wouldn't change much since the requirements were the same for each jet, besides the varying payloads. Further along in the design process, when the decision was reached that the two jets would share the same wing and tails, even less parameters would change for the constraint analysis. The only values that changed were the  $C_{D0}$  from 0.015 to 0.013 and the loiter Mach number because of the different engines. The new



design space can be seen in Figure 6.4 below. The design point for the Chief is the same as for the Commander at  $T/W$  of 0.42 and a  $W/S$  of 55.

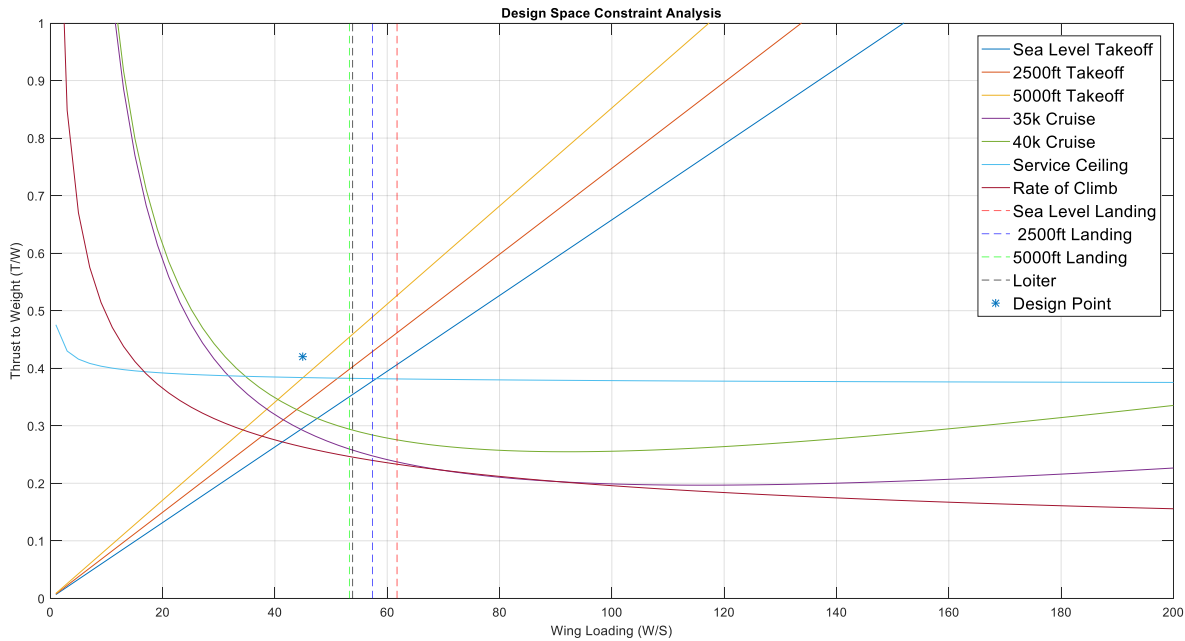


**Figure 6.4. The Chief constraint and analysis and design space.**

### 6.3 Mission Performance

As per the RFP, the maximum cruise speed is Mach 0.85 at 35000 ft. Therefore, the design cruise speed was set to Mach 0.85. Business jets are mainly used by men and women who have limited time. Therefore, designing the business jets to cruise at maximum allowable speed make them more attractive to prospective customers. The engines chosen for both variants of the business jet produce the required thrust to weight ratio to allow for a cruise speed of Mach 0.85 at 35000 ft.

Although the constraint analysis shows that the rest of the necessary requirements are met, the actual values for each requirement for the Commander and the Chief were calculated.

An equation from Section 5.2 of Roskam was used for the balanced field length requirement of 4000 ft at sea level [25]. A MATLAB tool was created to quickly solve the

equations with the different inputs of each of the jets. The key values for the Commander were a ground roll friction of 0.3 for dry pavement,  $C_{D0}$  of 0.32 for the take-off with flaps configuration, and an average thrust of 7675 lbf. The value for  $C_{D0}$  was estimated using a method from Section 3.2 of Roskam [20]. The Chief had a  $C_{D0}$  of 0.3 and an average thrust of 7020 lbf. These values generated a BFL of 3390 ft for the Commander and 3455 ft for the Chief. The margin between the value calculated and the requirement is reassuring since more conservative values were chosen.

Another MATLAB code was written to solve for the landing field length of each of the jets to ensure they were beneath the requirement of 3600 ft. The equations came from Section 5.9 in Roskam [25]. Since, the Commander and Chief have the exact same wing, many of the values are the same except for the typical landing weight, which were 15000 lb and 13000 lb, respectively. The value for the landing field length for the Commander was 3190 ft and for the Chief was 2880 ft.

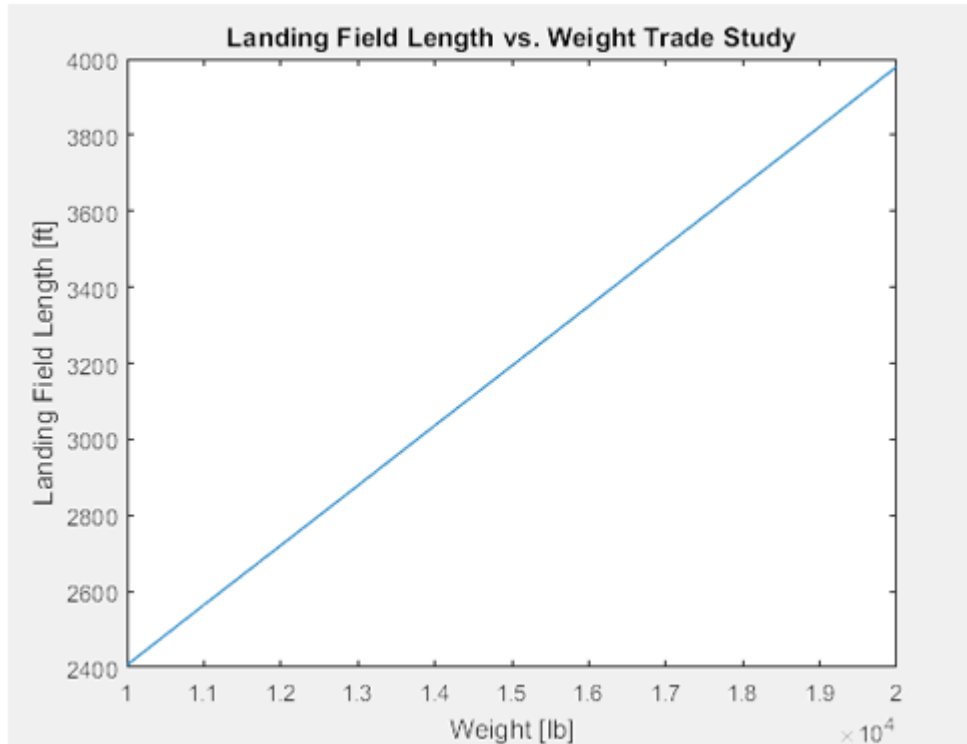


**Figure 6.5. Landing field length vs. weight.**

A basic trade study was done to find how the landing weight affects the landing length. The weight affected many terms in the equation used from Roskam [21], however, the result in Figure 6.5 was a very linear trend. The one important thing that is seen is that at a landing weight of 17950 lb or above does not meet the 3600 ft landing field length requirement given in the RFP. This will limit the short range trips of the Commander if it has close to 2000 lb of fuel in the tank during landing. Design alterations can be attempted to accommodate scenarios like the one mentioned, and if it cannot be fixed, the consumer and pilot of the aircraft must be informed.

Lastly, the climb was calculated following Section 5.3 from Roskam, specifically Equation 5.2 [25]. The  $T/W$  was equal to 0.42 and the  $L/D$  was estimated as 15 at climb for the Commander and the Chief. However, the values of steady state speed of climb differed between the two jets. For the larger Commander with a static thrust of 9000 lbf at sea level, the climb speed was

calculated to be around 200 ft/s. The smaller Chief was able to achieve a climb speed of 180 ft/s since the thrust is significantly less while the drag is close to the Commander. The rate of climb calculated for the Commander and the Chief was 4240 ft/min and 3815 ft/min respectively.

Another important part of the mission performance is the drag of all the segments through the flight. Aerodynamics completed a drag buildup chart that lists the coefficient of drag contributions of the main components during takeoff, cruise, and landing. Adding these drag coefficients together and multiplying it by the dynamic pressure of the segment and the wetted area will calculate the drag of each segment. The wetted area of both jets were estimated using the CAD models. They were calculated to be 707.5 ft<sup>2</sup> and 683.3 ft<sup>2</sup> for the Commander and the Chief, respectively. The drag per segment is shown in Figure 6.6 below.

**Figure 6.6. Drag per Segment**

Aircraft Variant	Takeoff (lbf)	Cruise (lbf)	Landing (lbf)
The Commander	5421	6511	7783
The Chief	5241	6340	7522

#### 6.4 Passenger Sensitivity Trade Study

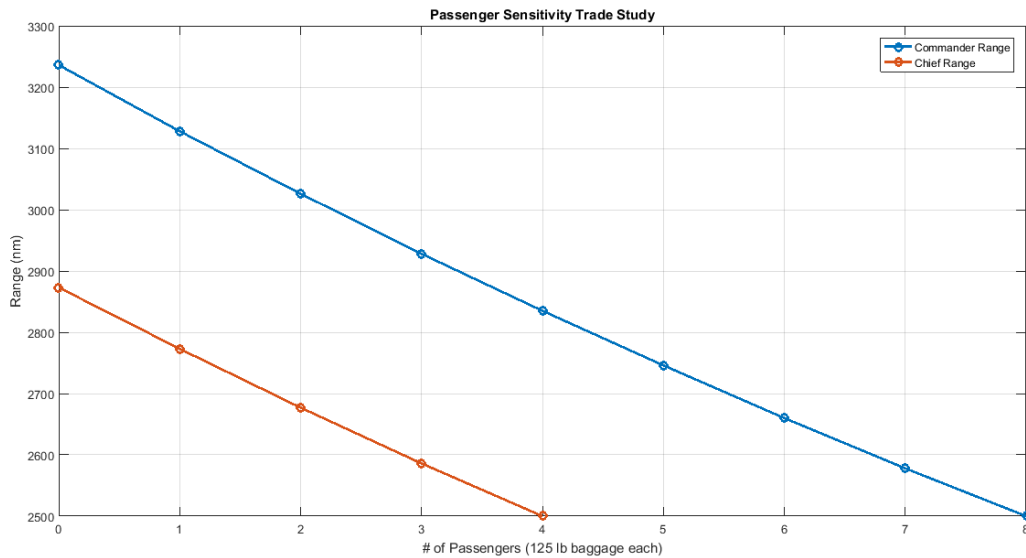


**Figure 6.7. Aircraft range vs. passenger load.**

Owners and operators of the Chief and the Commander may wish to fly their aircraft further than the 2500 nm cruise range dictated by the RFP during ferry or repositioning flights. By varying the passenger and luggage weight for a constant fuel load, the aircraft cruise range could be found by altering the cruise range and iterating using the MATLAB fuel burn code until the fuel requirement equaled the fuel load. This analysis was performed using constant fuel loads of 5393 lb for the Chief, and 5969 lb for the Commander. These fuel quantities are the bare minimum required to fly the mission profile without any reserves, and it was desired to find out how far each aircraft could cruise with a variable number of passengers. It was assumed that each passenger weighed 200 lb and brought a constant baggage weight of 125 lb, so each passenger removed from the flight reduced the gross takeoff weight by 325 lb. With no passenger or baggage weight, the Chief maximum cruise range increased to 2873 nm, and the Commander maximum cruise range increased to 3236 nm.

**Figure 6.8. Commander Maximum Cruise Range.**

<b>Passengers and Payload</b>	<b>Maximum Range</b>
8 passengers, 1000 lb baggage	2500 nm
7 passengers, 875 lb baggage	2578 nm
6 passengers, 750 lb baggage	2660 nm
5 passengers, 625 lb baggage	2746 nm
4 passengers, 500 lb baggage	2835 nm
3 passengers, 375 lb baggage	2928 nm
2 passengers, 250 lb baggage	3026 nm
1 passenger, 125 lb baggage	3128 nm
0 passengers, 0 lb baggage	3236 nm

**Figure 6.9. Chief Maximum Cruise Range.**

<b>Passengers and Payload</b>	<b>Maximum Range</b>
4 passengers, 500 lb baggage	2500 nm
3 passengers, 375 lb baggage	2586 nm
2 passengers, 250 lb baggage	2677 nm
1 passenger, 125 lb baggage	2773 nm
0 passengers, 0 lb baggage	2873 nm

## 6.5 Fuel Burn

**Figure 6.10. The Commander Stage Fuel Burn**

Stage	Weight [lb]	Fuel Burned this Stage [lb]	Total Fuel Burned [lb]
Engine Startup	19515.00	[-]	[-]
Taxi, Takeoff, Climb	18720.69	794.31	794.31
2500 nm Cruise	14766.20	3954.49	4748.80
30 min Loiter	14478.07	288.13	5036.93
Descent, Missed Landing, Climb	14030.85	447.22	5484.15
100 nm Divert	13898.24	132.61	5616.76
30 min Loiter	13627.12	271.12	5887.88
Descent, Landing, and Taxi	13558.98	68.14	5956.02

**Figure 6.11. The Chief Stage Fuel Burn**

Stage	Weight [lb]	Fuel Burned this Stage [lb]	Total Fuel Burned [lb]
Engine Startup	17,671.00	[-]	[-]
Taxi, Takeoff, Climb	16,951.75	719.25	719.25
2500 nm Cruise	13,370.93	3580.82	4300.07
30 min Loiter	13,110.02	260.91	4560.98
Descent, Missed Landing, Climb	12,705.06	404.96	4965.94
100 nm Divert	12,584.98	120.08	5086.02
30 min Loiter	12,339.41	245.57	5331.59
Descent, Landing, and Taxi	12,277.71	61.70	5393.29

When calculating the fuel burn during each mission leg, the engine TSFC and aircraft  $L/D$  were needed. Under steady level flight, the thrust of the engines is equal to the drag of the aircraft, and the lift produced by the wings is equal to the aircraft weight. For the first stage of the flight, the engines are started and the aircraft taxis to the runway and takes off. From Raymer [18], this stage burns approximately 3% of the TOGW in fuel, so the weight fraction for this stage is 0.97.

After taking off, the aircraft climbs and accelerates to its cruise speed. The weight fraction for this stage is given by Equation 6.9 [18].

The aircraft cruises at Mach 0.85, which gives a weight fraction of 0.979 for the takeoff and climb stage. Once at the cruising altitude of 35,000 ft above sea level, the aircraft enters the cruise stage. During this stage, the aircraft cruises for a distance of 2500 nm, and the aircraft weight decreases as fuel is burned. This decrease in aircraft weight changes the required wing lift and engine thrust, so the fuel burn changes over the duration of the cruise stage. The total fuel burn for this stage was solved using a MATLAB script, which used the aircraft  $L/D$  at cruise conditions,  $L/D$  at loiter conditions, TOGW, and TSFC under cruise and loiter conditions to iteratively step forward in time and solve for fuel burn. This mission profile also included a 30 minute loiter before the aborted landing and an additional 30 minute loiter after diverting 100 nms to an alternate airport. This script was used to solve for fuel burn from engine start through engine shut-down at the final destination. The fuel burn for the descent, aborted landing, and climb back to cruise altitude was calculated using the weight fractions for a standard descent (0.995), attempted landing (0.995), and climb back to 35,000 ft above sea level and a divert speed of Mach = 0.85 (0.979) [18].

As in the CG Travel calculations, these calculations result in all of the fuel onboard the aircraft being consumed. This is not realistic, as reserves are always kept and there is fuel trapped in the tanks and fuel lines. The extra passenger and baggage weight help account for the trapped fuel and reserves. In addition, the wings used in the aircraft family were found to have storage for up to 130 ft<sup>3</sup> of fuel, which is approximately 6600 lb of fuel. This provides space for a significant fuel reserve, which makes it increasingly unlikely that incidents would occur due to fuel exhaustion.

## **6.6 Future Work**

Performance will definitely be optimized going forward. The methods used to obtain most values were very crude, first class estimations. Many more variables will be taken into account for the upcoming design process. The fuel consumption per segment will increase as more accurate fuel burn methods are used, therefore the lift and drag must be optimized continually to create an efficient and air worthy jet.

## **7 Stability and Control (Vasiliauskas)**

Stability and control for this PCR is based on historical aircraft designs and guidelines that change depending on the source. Therefore, the main purpose of this first pass of tail sizing, control surface sizing, and static stability discussion is to decide on an appropriate empennage configuration and approximate size. With the basic empennage in place, structures, configurations, and weights and balances can get a rough estimate for the structures required to reinforce the tail and move the control surfaces, locate the center of gravity of the preferred concept, and calculate weight contribution of the empennage.

With center of gravity in place, a preliminary static stability analysis can be done. For each flight condition, the static margin can be calculated and the longitudinal stability can be checked. Stability and control worked closely with aerodynamics to iterate on wing and tail design to achieve the stability and lift requirements necessary. Once the static margin was within an acceptable range, and the business jets were statically longitudinally stable, the final requirement was to size the control surfaces.

### **7.1 Tail Configuration Selection**

The first argument in designing this family of aircraft was to decide the tail configuration. After researching business jets of similar size, passenger capacity, and range, an aft tail design was



found to be the most popular choice of tail configuration. An aft tail could be configured in a variety of ways, such as a conventional, t-tail, cruciform, h-tail, and v-tail. From the prior research, the remaining candidates for this business jet family tail configuration are conventional, t-tail, and cruciform. The other configurations were more complicated than need be and/or rarely used on business jets, leading to less empirical data of their advantages and disadvantages with regard to flight performance. These three candidates were analyzed in more detail to choose the best configuration.

Conventional tails, or an inverted t-shape configuration, are used on about 60% aircraft in service today [26]. The advantages of a conventional tail are simplicity in structure and convenience in performing the main tail functions of trim, stability, and control. Furthermore, the control surfaces are located close to the fuselage and require the least amount of structure and linkages.

T-tails main advantage is that the horizontal tail, located atop the vertical tail, is out of the region of wing wake, wing downwash, wing vortices, and engine exit flow during level flight [26]. This allows the horizontal tail to be more efficient in its performance of stability and control, leading to a smaller horizontal tail size. Also, the structure is safer and less prone to fatigue wear since it interacts with less body structure flow and engine exit flow. However, this configuration requires more structure to reinforce the vertical tail and to connect the control surfaces, and can also be subject to deep stall [26]. T-tails are used on about 25% of aircraft in service today [26].

Cruciform tails are a combination of a conventional tail and t-tail, where the horizontal tail is located about halfway up the vertical tail, creating a cross like shape [26]. The height of the horizontal tail can be raised to better avoid the engine exit flow. The structure weight is less than that of a t-tail since the control surfaces are closer to the fuselage. This configuration takes the

advantages of both the conventional tail and t-tail, while minimizing the disadvantages of both. The cruciform configuration seems to be the best choice, but the configuration of the rest of the plane must be considered.

Prior to choosing the tail configuration, the wing design and engine placement were chosen for this family of business jets. The wing configuration was chosen to be a low wing, therefore the wing downwash, vortices, and wake would hardly affect any of the three tail configurations. However, the engine configuration was decided to be a high, rear-fuselage placement. For this reason, the cruciform and t-tail design are the better choices of the three.

For the reasons stated above and from the research of business jets, the preliminary design was a high cruciform tail. The horizontal tail will be located approximately 90% up the vertical tail to ensure it avoids the engine exit flow while lowering the structure weight and linkage length for the control surfaces. For the intents of this preliminary analysis, the high cruciform tail will be considered a t-tail since the horizontal tail is closer to the top of the vertical tail than the middle.

## **7.2 Tail Airfoil Selection**

Selecting the horizontal tail airfoil comes down to having an airfoil that is able to generate the required lift for stability and control with minimum drag and minimum pitching moment [26]. In the preliminary design of the tail, the lift required to truly satisfy the longitudinal stability, also known as pitch stability, is not yet known. Therefore, choosing an airfoil with a lift curve slope as large as possible with a wide usable angle of attack is the best route. Furthermore, assuming the center of gravity moves throughout the flight and in different mission profiles, having an airfoil that can create positive and negative lift is required. A symmetric airfoil is utilized most often for the horizontal tail so that the tail behaves similarly in negative and positive angle of attacks [26].

Another requirement of the horizontal tail is that it must be clean of compressibility effects. To make sure this is enforced the lift coefficient of the horizontal tail should be less than that of the wing lift coefficient. This requirement is met by selecting a thinner airfoil for the horizontal tail than the main wing [26]. Since, the main wing airfoil is a NASA SC(2)-0714 with a maximum thickness to chord ratio of 0.15, a NACA 0009 meets all the requirements for the horizontal tail. It is a symmetric airfoil with a large lift curve slope that acts similarly across a large range of angle of attacks in both the negative and positive regime as can be seen in Figure 7.1. Furthermore, the  $(t/c)_{max}$  is 0.09, which will ensure the tail is clean of compressibility effects.

The main function of the vertical tail is to satisfy directional stability, also known as yaw stability, maintain directional control, and for directional trim [26]. Since the aircraft is arranged in such a way that it is symmetric along the  $x$ - $z$  plane, the vertical tail must not create a pitching moment to ensure directional stability. Also, the rudder, the control surface on the vertical tail, is used to maintain directional control and trim, therefore rendering these functions out of the discussion for airfoil selection.

As a result, the only factors that need to be taken into account for the vertical tail airfoil selection is that it must not create a pitching moment and it must be clean of compressibility effects. These requirements are met by using a symmetric airfoil with a thickness less than that of the wing. That being said, the NACA 0009 with no angle of incidence will also work for the vertical tail.

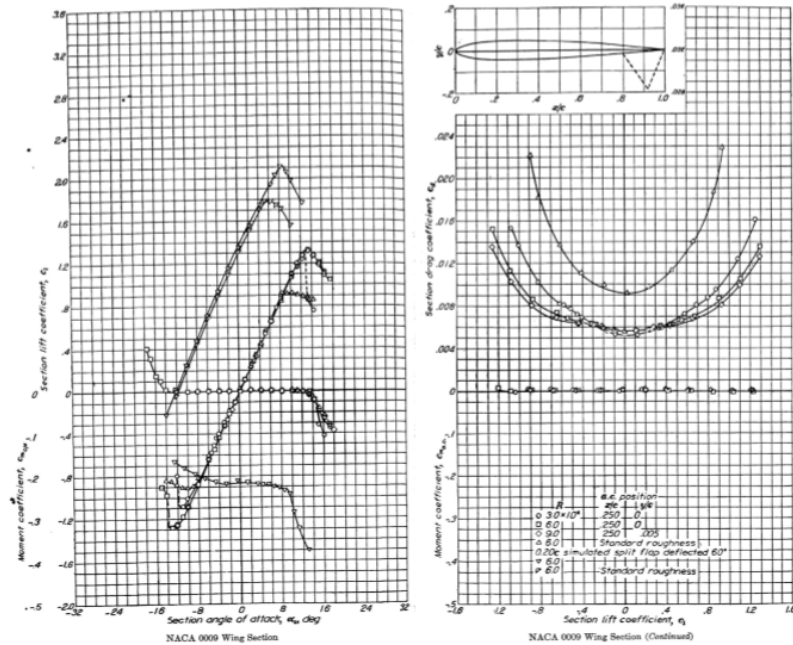


**Figure 7.1. NACA 0009 section lift coefficient plotted against angle of attack and section drag coefficient [25].**

### 7.3 Horizontal Tail Sizing

The initial design for the horizontal tail of the Commander followed the process outlined by Section 6.9 in Sadraey [26]. A  $V_h$  of 1.1 was selected to match other jet transport aircraft. The  $l_{opt}$  between the wing aerodynamic center and tail aerodynamic center was calculated to be 44.26 ft, but this was determined to be excessive given the length of the aircraft. A moment arm of 25 ft was chosen for initial tail sizing based on initial aircraft sketches. From Sadraey, Equation (1) was used to find the horizontal tail planform area with known  $\bar{C}$  and  $S_{wing}$ .

$$S_h = \frac{V_h * \bar{C} * S_{wing}}{l_{opt}} \quad (1)$$

The horizontal tail planform area was calculated to be 109.4 ft<sup>2</sup> using this method. The horizontal tail sweep angle was set to 32°, which is 5° greater than the wing sweep angle. This horizontal tail sweep angle was chosen to prevent shock formations at high airspeeds. At high enough airspeeds, the wing could form shocks and stall. By sweeping the horizontal tail more than

the wing, the horizontal tail will not suffer from shocks and stall under these conditions, which maintains longitudinal control [26]. A taper ratio of 0.6 was chosen based on similar business and commercial aircraft.

The design of the horizontal tail for the Chief was optimized when calculating the longitudinal stability. This process was chosen because keeping the same empennage and wing between the two jets would greatly help the 70% commonality requirement given in the RFP.

#### 7.4 Vertical Tail Sizing

The preliminary design process of the vertical tail begins with choosing a  $V_v$ . From Table 6.4 [26], the vertical tail volume coefficient for a jet transport is 0.09. Furthermore, since the tail is a t-tail  $V_v$  can be reduced by approximately 5% due to the end plate effect [18]. With the  $V_v$  value in place at 0.086, and assuming the  $l_v$  is the same as  $l$  at 25 ft. The following equation [26] can be used to calculate the vertical tail planform area:

$$S_V = \frac{b * S * V_V}{l_v} \quad (2)$$

For the Commander,  $S$  is equal to 460 ft<sup>2</sup> and  $b$  is equal to 55 ft. The planform area of the vertical tail was calculated to be 87 ft<sup>2</sup>.

With the preliminary planform area in place, the rest of the parameters governing the shape of the prototype vertical tail such as aspect ratio, span, taper ratio, and sweep angle were chosen after looking at values for similar aircraft.

According to Sadraey, a good starting value for the aspect ratio of the vertical tail is between one and two. The AR was chosen to be 1.2 after considering the effects of AR on stability and control from Section 6.8 in Sadraey [26].

Sadraey goes on to say that a good first choice for the sweep angle of the vertical tail is an angle similar to the sweep angle of the main wing. However, an increase in the sweep angle of the

vertical tail increased the horizontal tail moment arm which in turn improves the aircraft's longitudinal stability and control [26]. With these two suggestions taken into considerations the sweep angle for the vertical wing was chosen to be 30°.

The taper ratio of most business jets from preliminary research was in between a half and one, so the chosen value for taper ratio was 0.75.

The sizing of the vertical tail for this preliminary design is a very rough estimation and will have to be improved upon as the design of the business jet continues. These numbers do give a good first pass estimate that structures used in considering the weight of the tail and configuration used in sizing the aircraft and locating the center of gravity.

## **7.5 Control Surface Sizing**

Preliminary sizing of the control surfaces is based on historical guidelines and from seeing what works on current business jets of similar mission profile, size, and requirements. That being said following Section 6.6 [18], a good estimate at the size of the elevator, rudder, and ailerons can be determined.

For the tail, it is very common to see the elevator and rudder to extend close to 90% of the horizontal and vertical tail span [18]. With the T-tail, the elevator will begin close to the external wall of the vertical tail and extend close to the tip of the horizontal tail on both sides of the vertical tail. Likewise, the rudder will begin close to the fuselage and extend close to the intersecting location of the horizontal tail and vertical tail. The length of the elevator and rudder as a percentage of horizontal and vertical tail chord length is given in Table 6.5 of Raymer. For a business jet, the chord ratio for the elevator is 0.32 and for the rudder is 0.3.

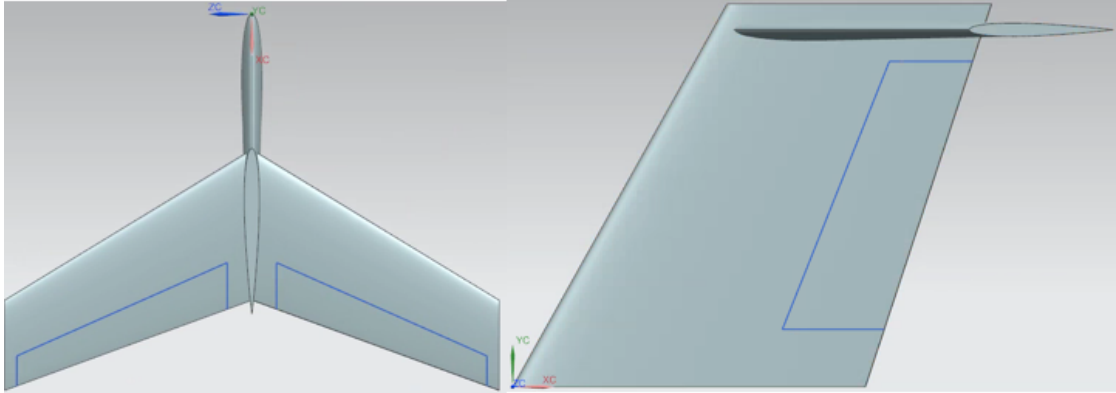


**Figure 7.2. Elevator and rudder diagram.**

As can be seen in Figure 7.2 the control surfaces are tapered in chord by the same ratio as the tail surfaces. The control surface maintains a constant chord percentage and allows the spars to be straight-tapered rather than curved [18].

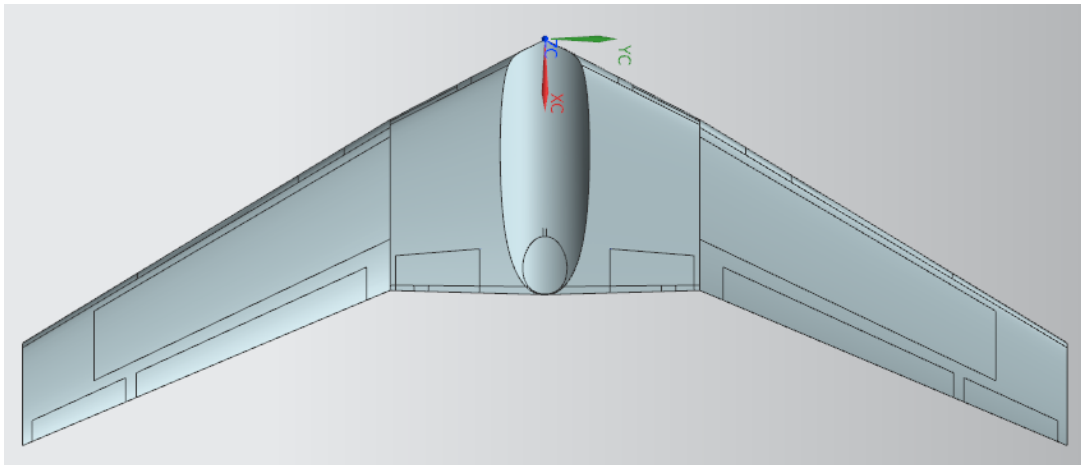


**Figure 7.3. Main wing ailerons and flaps diagram.**

For the main wing, the sizing of the aileron was very similar to the elevator and rudder. As a first pass, the size of the ailerons was found as a percentage of the chord length and span based on historical guidelines. The data from Figure 7.3 in Raymer pointed lead to an aileron chord size of 20 percent wing chord length and an aileron span of 40 percent wing span [18]. However, the size of the ailerons was decreased as a design choice because of the need for more flap area. Also,

the wing span is relatively large compared to similar sized business jets, therefore the moment arm associated with the ailerons is higher than normal, justifying a smaller aileron area.

Figure 7.3 above shows the flaps on the inner and outer portion of the wing, along with the ailerons near the end by the wingtips. The elliptical circle in the center is the area covered by the fuselage when the wing is attached. The size of the flaps had to be determined by aerodynamics and performance to ensure the high lift system could produce the necessary lift to meet the requirements. Therefore, the reasoning behind the sizing of the flaps and more in-depth diagrams of the high lift system is covered in the aerodynamics section.

## **7.6 Pitching Moment and Trim**

Many different parts of the aircraft contribute to the overall pitching moment about the center of gravity. For the Commander and Chief the location of the aerodynamic chord of the main wing is aft of the center of gravity and the direction of lift of the tail is in the opposite direction of the main wing lift. Therefore, the horizontal tail is the main component to ensure stability and trim is possible. A tool was created in MATLAB to ensure the horizontal tail designed in the previous section creates enough lift to satisfy pitch trim during cruise. This MATLAB function was used following the direction of Section 16.4 from Raymer [18].

Some contributions were not considered in this class 1 stability and control analysis. For example, the pitching moment created from the drag of the tail and wing are considered negligibly small, the fuselage and nacelle pitching moments are difficult to estimate without wind tunnel data, and the vertical force produced at the engine inlet from the turning freestream flow. Also, the flaps are not in use during steady level flight, making those terms zero.

Conducting the trim at cruise calculation on the Commander with the relevant contributions for a first pass estimate resulted in a  $-0.35 \text{ rad}^{-1}$  moment about the center of gravity. This moment



could not be brought down to zero by changing the variable parameters in the code, such as angle of incidence of the horizontal tail or main wing. A remedy to the problem was to increase the amount of negative lift the tail was creating to counteract the negative moment about the center of gravity. A trade study was done with several different airfoils to discover an airfoil that would create the necessary lift without changing the size of the horizontal tail.

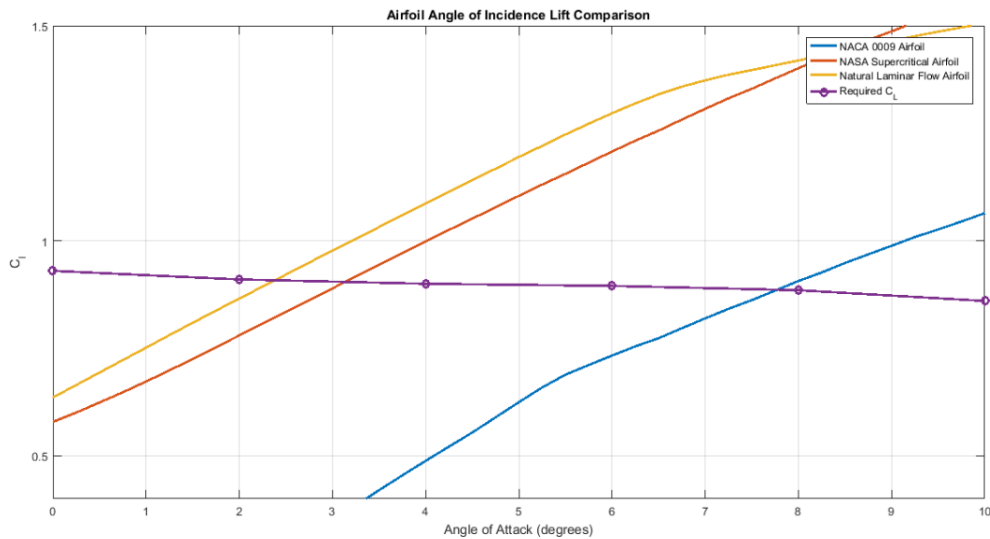


**Figure 7.4. Horizontal tail airfoil trade study.**

Using the code, the necessary coefficient of lift produced by the horizontal tail required to counteract the negative moment was calculated at a range of angle of attacks spanning from 0° to 10°. Then a trade study was done to compare a few cambered airfoils to see if they could generate the required lift. As can be seen in Figure 7.4. Horizontal tail airfoil trade study., the NASA supercritical airfoil that was used for the main wing, NASA SC(2)-0714, and the natural laminar flow airfoil, NASA/Langley NLF(1)-0215F were compared with the NACA 0009. Since the coefficient of lift of the tail will decrease from the sectional lift data, the natural laminar flow airfoil was chosen and tested in XFLR by the aerodynamic team to ensure the required lift could be generated. The tail created the necessary lift with a -6° incidence angle.

## **7.7 Static Margin**

Ensuring the Commander & Chief have longitudinal stability is a key responsibility of the stability and control team. Longitudinal static stability is the stability of the aircraft in the pitching plane while in steady level flight. The most important term in longitudinal stability of an aircraft is the static margin [18]. The static margin was calculated using Section 16.3.2 from Raymer, specifically the subtraction of the location of the center of gravity from the neutral point [18]. The aerodynamics team used XFLR5 to run an analysis on the main wing and horizontal tail to find the neutral point. This method did not take into account the fuselage moment coefficient or the inlet normal force, therefore a 5% fore correction was placed on the neutral point. The neutral point was found at takeoff, cruise, and landing, and the CG flight envelope was found by performance. Using the method mentioned above static margin can be found at takeoff and landing and a range could be found at cruise which is caused by the fuel burn. This data is compiled in the table below.

## **7.8 Future Work**

Many of the values used in the sizing of the empennage and control surfaces were estimated or extrapolated from historical guidelines of business jets in service. Also, calculating the static margin took only the relevant contributions into consideration, because some of the contributions such as pitching moment due to the fuselage drag could not be calculated without wind tunnel data. Therefore, future work will include updating, iterating, and optimizing the empennage size, geometry, and aerodynamic characteristics. This will lead to a more realistic calculation of static stability and control of the entire aircraft.

Furthermore, dynamic stability will have to be explored and tools will have to be made to ensure dynamic phenomena such as flutter will not plague the aircraft within the range of the

mission profile. The aircraft will have to remain statically and dynamically stable in yaw, pitch, and roll. A major focus for future work will be ensuring that the Commander and Chief are both statically and dynamically stable, or modifying the designs until they are, will.

Finally, making sure the jets have control surfaces large enough for the necessary trim and maneuverability to complete the mission given by the RFP will have to be optimized and tested. Also, increasing the flexibility to modify the desired mission and requirements to attract potential buyers will have to be explored. Trade studies will have to be conducted to find the limits of the aircraft so that dangerous scenarios can be safely avoided.

Lastly, the tail airfoil required to stabilize the aircraft is creating excess drag. Optimization of the tail and wing will have to take place to ensure the stability and aerodynamic properties meet requirements while being efficient.

## **8 Propulsion (Balsu)**

### **8.1 Introduction**

An engine is a critical mission component of any aircraft; most importantly, it generates thrust that propels the aircraft forward, but it also performs the crucial job of providing electricity that are utilized for other services onboard. As such, an exhaustive evaluation of engines based on performance, cost, and maintainability must be carried out in order to select one that best fits the needs of the aircraft, which in this case is a light business jet. In keeping with the design philosophy of economizing cost and providing customers with the best product value, engines which have lengthy service lifespans and low-cost maintenance will be prioritized.

### **8.2 Engine Selection**

Keeping in mind the requirements of a light business jet capable of coast-to-coast travel, a high bypass turbofan engine will satisfy the needs put forward by the RFP. Since fuel economy is

also an important part of the design philosophy, turbofan engines (which have a good thrust to fuel consumption ratio) are excellent propulsion choices. Yet another design philosophy tenet is the consideration of passenger appreciation and comfort. Since turbofan engines have internally housed engines and fans, their noise output is quite low, increasing passenger comfort.

Given that this is a light business jet, the weight and number of the engines is also important to consider. In this case, multiple engines were favored over a single-engine approach due to redundancy being factored in; in the case of a catastrophic engine failure, there will still be another engine(s) available in the former case, while the latter will not be able to make use of any propulsive power whatsoever. In the case of light business jets moreover, the presence of a very small APU means that the engine is also responsible for generating the majority electricity used by the aircraft. A failure therefore would mean that the avionics and electronics of the aircraft would be rendered useless due to a lack of electric power in the case of a single-engine aircraft. This redundancy factor therefore makes the multi-engine approach decidedly more attractive. As such, two different approaches were considered: one with two engines and the other with a three engine configuration. The latter was seen as prohibitive in terms of cost and weight parameters, although providing a good amount of trust. However, the comparison of thrusts between the two engine and three engine configuration led to a thrust margin that did not warrant the implementation of a three engine configuration, i.e., the costs outweighed the advantages garnered. As such, a two engine approach was decided to be the best option for the aircraft.

Another design principle that must be taken into account is the location of the engines; in this case, the configurations sub-team determined that the location of the engines would be optimized on the sides of the fuselage.

### 8.2.1 Trade Study: Engine Selection Process for the Commander

Using the low-cost design philosophy, and adding the time-constraint of being able to go into production by 2020, designing an entirely new engine was deemed unfeasible by the systems engineering team. As such, existing propulsion systems which have been tried and tested will be used for this aircraft. Shown below in **Error! Reference source not found.** are various engine types used in different business jet configurations and their technical parameters. This will be useful to help judge which propulsion system will be used for the aircraft based on the required parameters.

**Figure 8.1. Comparing Various Engine Candidates**

Engine	BPR	Dry Weight (lb)	Takeoff Thrust (lb)	T/W	Type	Installed on
2 X TFE731-5R	3.33	1790	9000	0.410	Medium-bypass, two spool, geared front fan turbofan engine	Dassault Falcon 900A/B/C
2 X TFE731-40	2.9	1790	8500	0.386	Medium-bypass, two spool, geared front fan turbofan engine	Bombardier Learjet 40/45
2 X TFE731-4R	2.8	1740	8160	0.371	Medium-bypass, two spool, geared front fan turbofan engine	Cessna Citation VII
2 X PW545C	4.12	1660	8200	0.373	High-bypass, single stage fan, turbofan engine	Cessna Citation II
2 X PW305A	4.24	2302	9360	0.425	High-bypass, single stage fan, turbofan engine	Bombardier Learjet 60
2 X FJ44-4	-	1300	7200	0.327	High-bypass, two-spool, front fan, turbofan engine	Cessna CJ4

Based on the requirements of the T/W being in the range of 0.38 – 0.43 (calculated in the constraint analysis), the candidates can be narrowed down; right away, three engines, TFE731-4R,

PW545C, and FJ44-4, can be eliminated from consideration. This leaves three other engine choices in the running: the TFE731-5R, PW305A, and the TFE731-40. Within these options, the PW305A, which produces 9360 lb of thrust is quite excessive. Given that the expected thrust requirement is around 8800 lb to 9150 lb, this is far more thrust than is required by the jet. Adding to the unfeasibility of implementing this engine is its weight: at 2302 lb, it is the heaviest engine measured, making it an unattractive choice for a light business jet. This then leaves two other engines, the TFE731-5R, and the TFE731-40. Comparing the two, the TFE 731-5R has a higher bypass ratio and a much higher takeoff thrust as compared to the TFE731-40, and is only 20 lbs heavier. Since a high bypass ratio is preferable due to benefits of improved fuel economy and noise reduction, both of which are defining characteristics of the team's design philosophy, and the tradeoff in thrust for weight is extremely favorable, the choice is obvious. Realistically, the actual T/W will most likely be around 0.40, leaving a small amount of excess thrust, which is good in terms of design constraint analysis. As such, this leaves the TFE731-5R as the sole contender for the desired propulsion system choice.

### 8.3 Engine Description for the Commander



Figure 8.2. TFE731-5R engine.

Figure 8.3. Specifications of TFE731-5R.

Length [in]	Diameter [in]
65.6	40.5

The TFE731-5R is manufactured by Honeywell Aerospace and consists of one stage geared fan, four stage axial flow pressure compressor, a one stage HP compressor, three stage LP compressor, and is two-spooled. As such, it is an engine that has ease-of-maintenance, further decreasing the cost-of-ownership for the customer. Additionally, at a length of 65.6 in, it is a very compact engine, further improving its modularity and ease of placement on the aircraft, ensuring that the configuration team has more freedom to place the engine in an optimal location on the aircraft.

## **8.4 Engine Performance for the Commander**

### **8.4.1 Thrust**

It is extremely important to conduct engine thrust performance analysis at various conditions, which in this case will be multiple Mach values. This will accurately simulate the preparedness of the engine to operate at different conditions, which are not always what it was designed for, and will be a good measure of the robustness of the propulsion setup. Using the thrust lapse equation:

$$T_{Altitude} = T_{Sea Level} * \left(\frac{\rho}{\rho_0}\right)^{0.9} \quad (3)$$

where for both engines combined,  $T_{Sea Level} = 9000 \text{ lbs}$ , and  $\rho_0 = 1.225 \frac{\text{kg}}{\text{m}^3}$ , the following set of thrust lapse curves can be obtained for the uninstalled thrust:

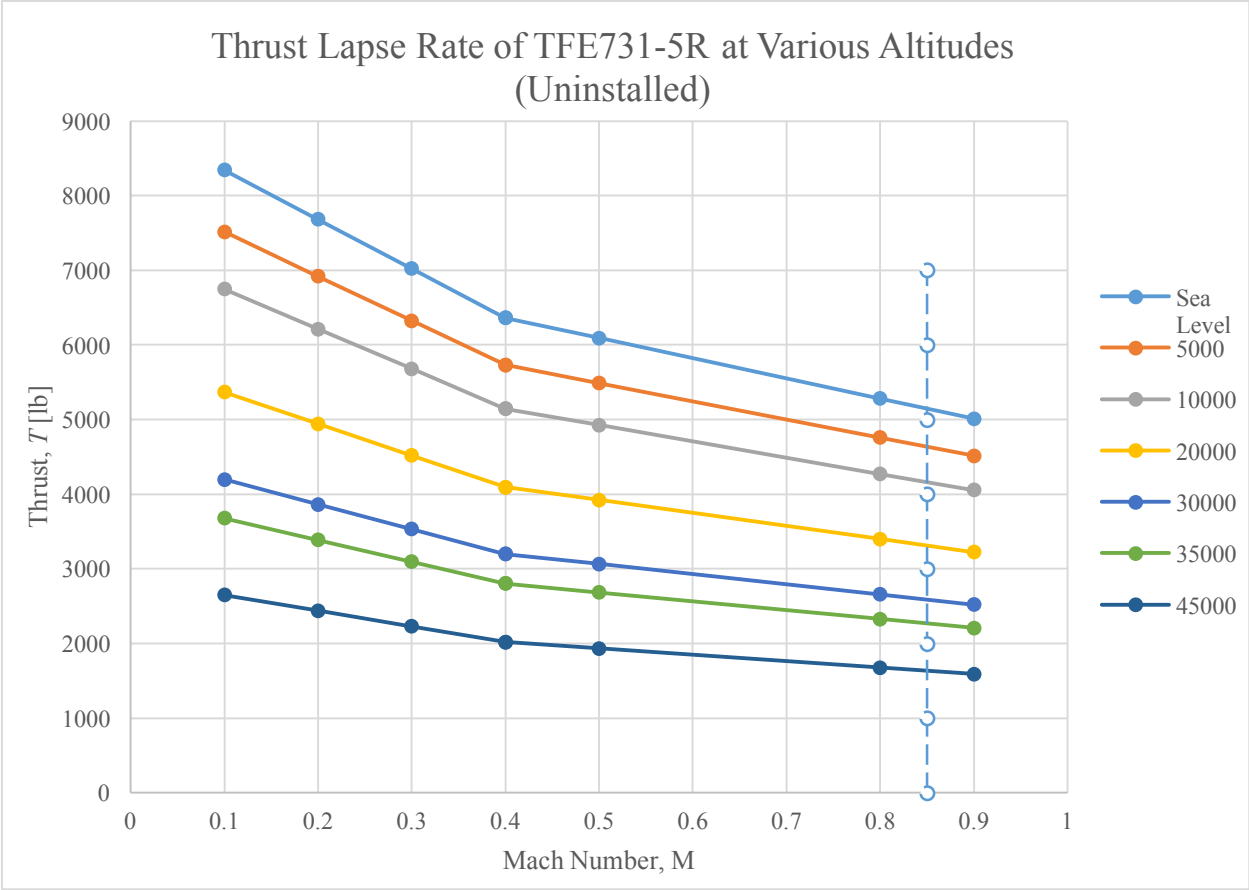


**Figure 8.4. Uninstalled thrust vs. Mach number at varying altitudes from sea level (0 ft) to service ceiling (45,000 ft).**

However, it is unrealistic to expect these values following the installation of the propulsion system on the aircraft. As a conservative estimate, the installed thrust values will be roughly 10% of the uninstalled thrust, leading to a new  $T_{Sea\ Level} = 8100\ lbs$ . As such, the following thrust lapse curves can be obtained for the installed thrust:



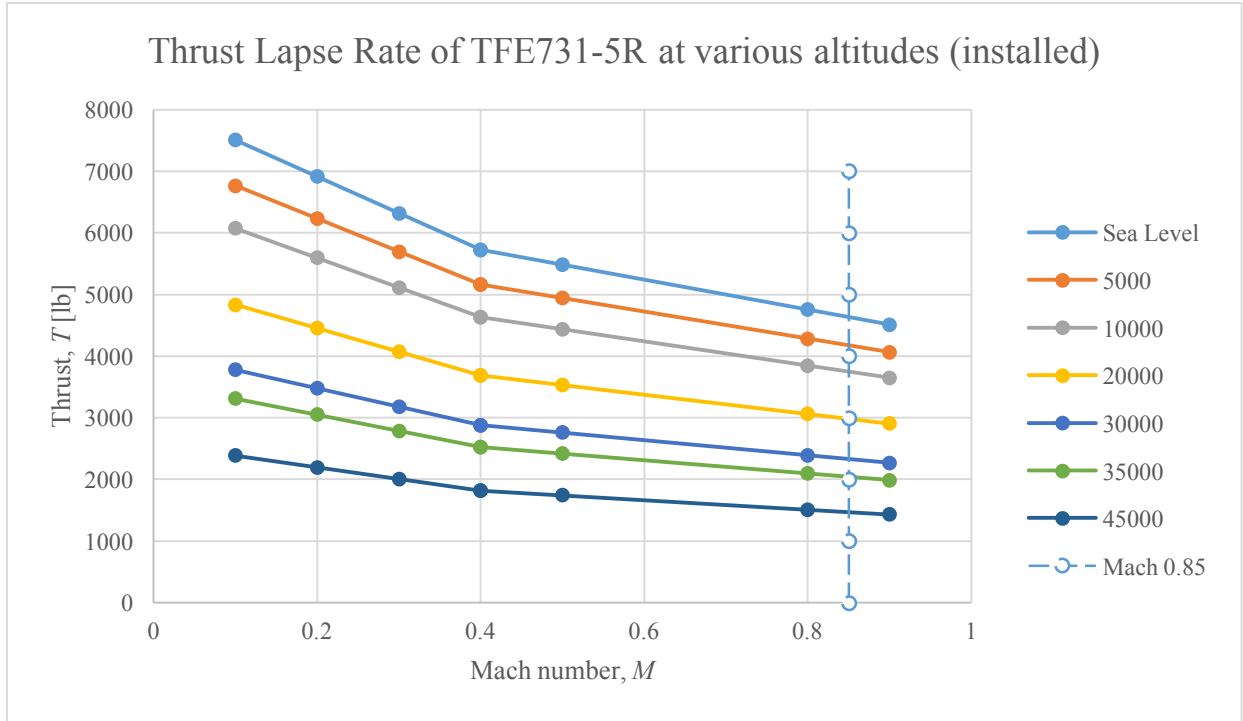


**Figure 8.5. Installed thrust vs. Mach number at varying altitudes from sea level (0 ft) to service ceiling (45,000 ft).**

### 8.4.2 Thrust Specific Fuel Consumption for the Commander

The TSFC of an engine is crucial towards understanding its overall fuel efficiency. Fuel efficiency is important because it helps determine the lifetime cost of the plane for the customer. In order to calculate this parameter, the following Equation 1.36, obtained from Mattingly’s textbook, *Elements of Propulsion*, [11] was used:

$$(0.4 + 0.45 * M_0) * \sqrt{\theta} \tag{4}$$

$\theta$  is a dimensionless temperature constant that varies with altitude. However, this constant has three different variants for standard, hot, and cold days. Given how variable temperatures are on the coastlines of the United States of America, and the breadth of travel destinations that the clientele of this aircraft might fly to, it is especially important to consider the TSFC at these different temperature conditions.

The TSFC estimation models are as follows:

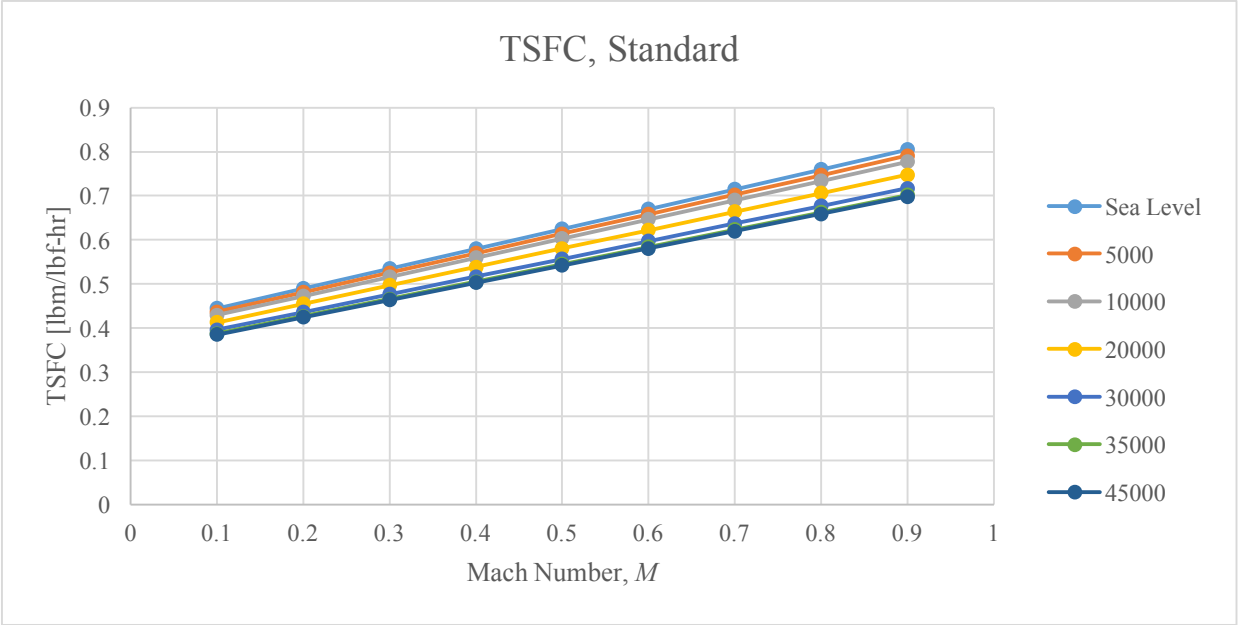


Figure 8.6. TSFC vs. Mach number at standard temperature.

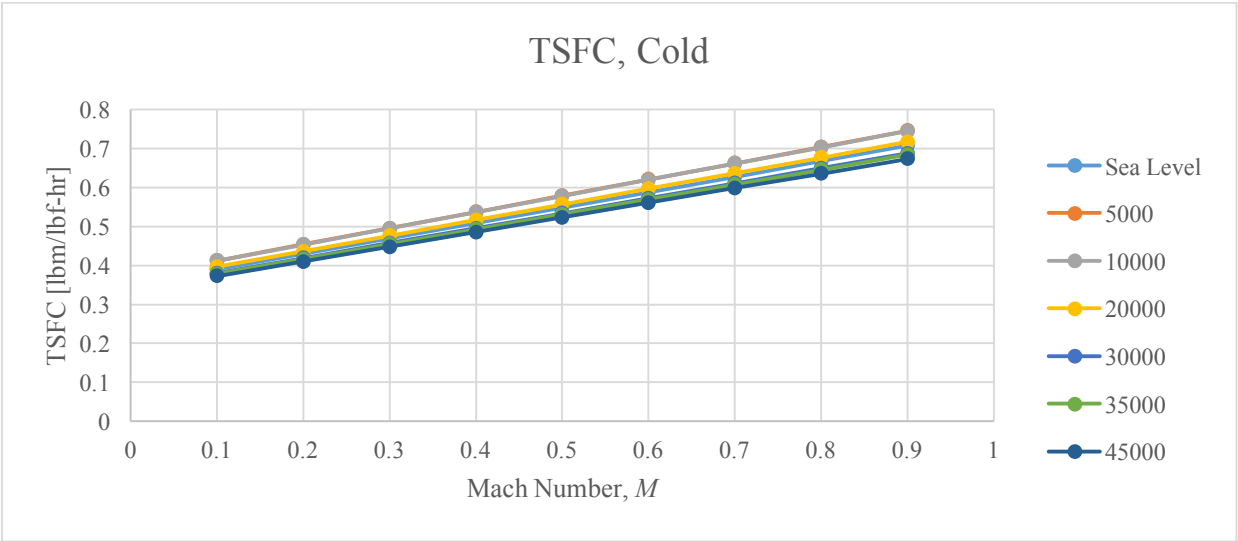
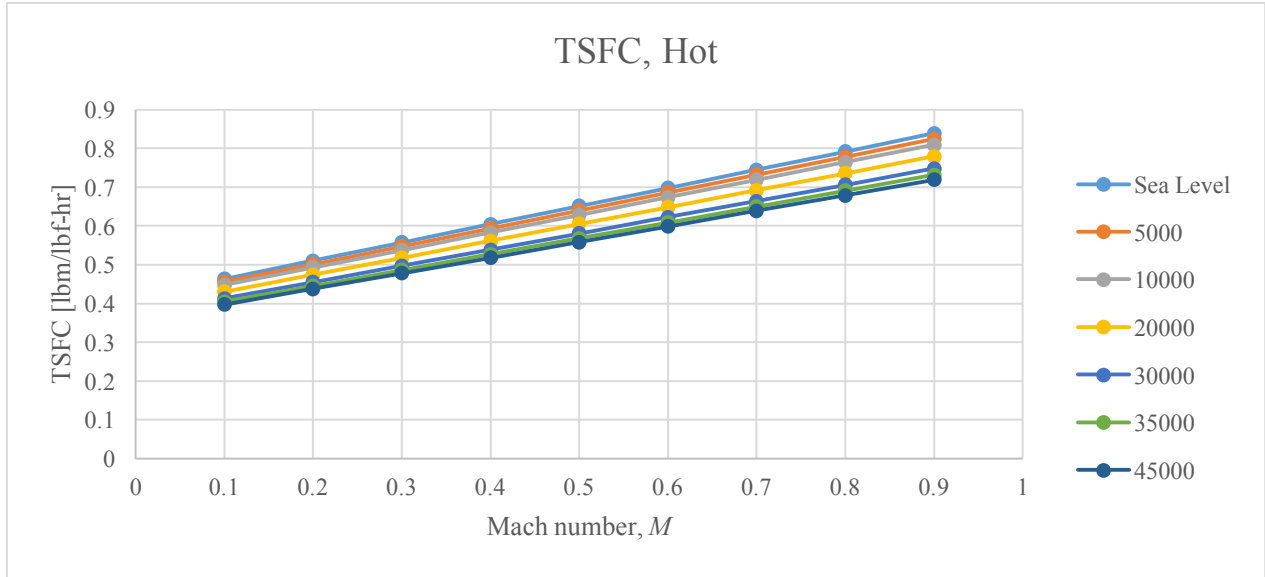


Figure 8.7. TSFC vs. Mach number at cold temperature.



**Figure 8.8. TSFC vs. Mach number at hot temperature.**

### 8.5 Trade Study: Engine Selection Process for the Chief

A propulsion system for the Chief can be obtained by following a similar selection process as was used for the Commander, albeit accounting for the decrease in the thrust and weight requirements. As before, the underlying design philosophy of optimal customer value will be a priority in the selection process.

**Figure 8.9. Comparing Various Engine Candidates for the Chief**

Engine	BPR	Dry Weight (lb)	Takeoff Thrust (lb)	T/W	Type	Installed on
2x TFE731-2	2.66	1486	7000	0.389	Medium-bypass, two spool, geared front fan turbofan engine	Dassault Falcon 10
2x TFE731-3	2.8	1508	7400	0.411	Medium-bypass, two spool, geared front fan turbofan engine	Learjet 55
2 x TFE731-4R	2.8	1644	8160	0.453	Medium-bypass, two spool, geared front fan turbofan engine	Cessna Citation VII

2 x PW 545C	4.12	1660	8200	0.455	High-bypass, single stage fan, turbofan engine	Cessna Citation XLS+
2 x PW 535A	2.55	1232	6800	0.377	Medium-bypass, single stage fan, three stage turbine, turbofan engine	Cessna Citation Encore
2 x PW 545A	4.12	1630	7242	0.402	High-bypass, turbofan engine	Cessna Citation Excel

Working with the performance sub team, the max TOGW was determined to be around 16650 lb, assuming worst case scenario. However, a safe estimate to consider a propulsion system for is roughly 18000 lb, in order to account for unexpected changes with the progression of the design morphology. Additionally, the T/W ratio will be similar, if not the same as the iteration of the Commander, and is roughly in the range of 0.39 to 0.43. However, a ratio that is higher to the upper limit of 0.42 is also favorable, to maximize the thrust capacity of the overall aircraft.

From the engines selected, the TFE731-2 and PW 545A choices can be eliminated immediately, because their T/W ratios are outside the desired range. This leaves four other engines to be considered. From these engines, the PW 545C system seems like an attractive choice; however, its weight is the highest amongst all the others being considered. Adding to its unattractiveness is the fact that the TFE731-4R produces almost comparable levels of thrust at a lower dry weight. As such, it can be eliminated from consideration. Now, out of the three engines remaining, two belong to the same family (Honeywell) and the other is a Pratt & Whitney product. Analyzing the Honeywell engines first, the TFE731-4R seems like the better option: it has the same bypass ratio, a higher weight (by 136 lbs) for a thrust increase of 760 lbs, which is an acceptable tradeoff. The increase in thrust (while not needed) is still useful because of the uncertain nature of the weight, i.e., in order to be prepared for a scenario in which the weight increases. As

such, this leaves the TFE731-4R and the PW 545A as the final contenders. Analyzing both engines, while the the PW 545A is lighter, it also produces significantly less thrust. In fact, with a T/W ratio of 0.402, it is close to the lower limit of the range of acceptable ratios. As such, in the scenario that weight increases, the PW 545A might not be able to sustain the new weight of the aircraft. The TFE731-4R is a simpler system, decreasing its maintenance costs, which subsequently translates into decreased cost of ownership for the customer. Given that the Commander’s configuration uses the TFE731-5R engines, Honeywell Aerospace might be inclined to offer the manufacturers a favorable price. This also dovetails well with the overall design philosophy of best value for the customers; if the manufacturer is able to produce the planes at a lower cost, the customer might be able to purchase the aircraft at a lower unit cost. Therefore, after comparing all of the possible engine choices, the TFE731-4R has been chosen as the preferred propulsion system for the Chief.

### 8.6 Engine Description for the Chief

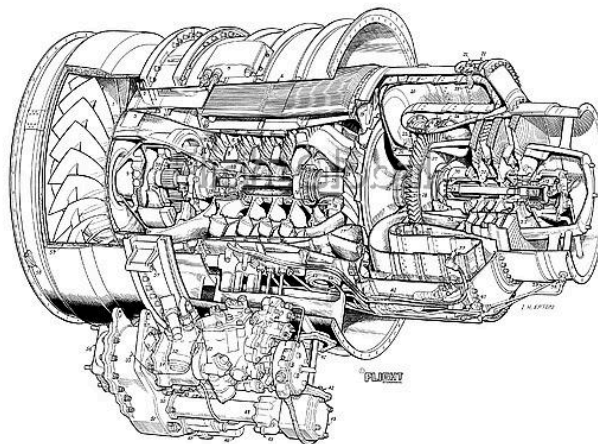


**Figure 8.10. Cutaway of TFE731-4R engine.**

**Figure 8.11. Specifications of TFE731-4R**

Length [in]	Diameter [in]
60.2	39.4

The TFE731-4R is manufactured by Honeywell Aerospace and consists of one stage geared fan, four stage axial flow pressure compressor, a one stage HP compressor, three stage LP compressor, and is two-spooled. As such, like the TFE731-5R, it is an engine that has ease-of-maintenance, further decreasing the cost-of-ownership for the customer. At a length of 60.2 in, it is also a very compact engine, further improving its modularity and ease of placement on the aircraft, ensuring that the configuration team has more freedom to place the engine in an optimal location on the aircraft.

### 8.7 Engine Performance for the Chief

This process will be undertaken using the same processes that were used earlier for the Commander.

#### 8.7.1 Thrust

Using the Equation (3), but where for both engines combined,  $T_{Sea\ Level} = 8160\ lbs$ , and  $\rho_0 = 1.225 \frac{kg}{m^3}$ , the following set of thrust lapse curves can be obtained for the uninstalled thrust:

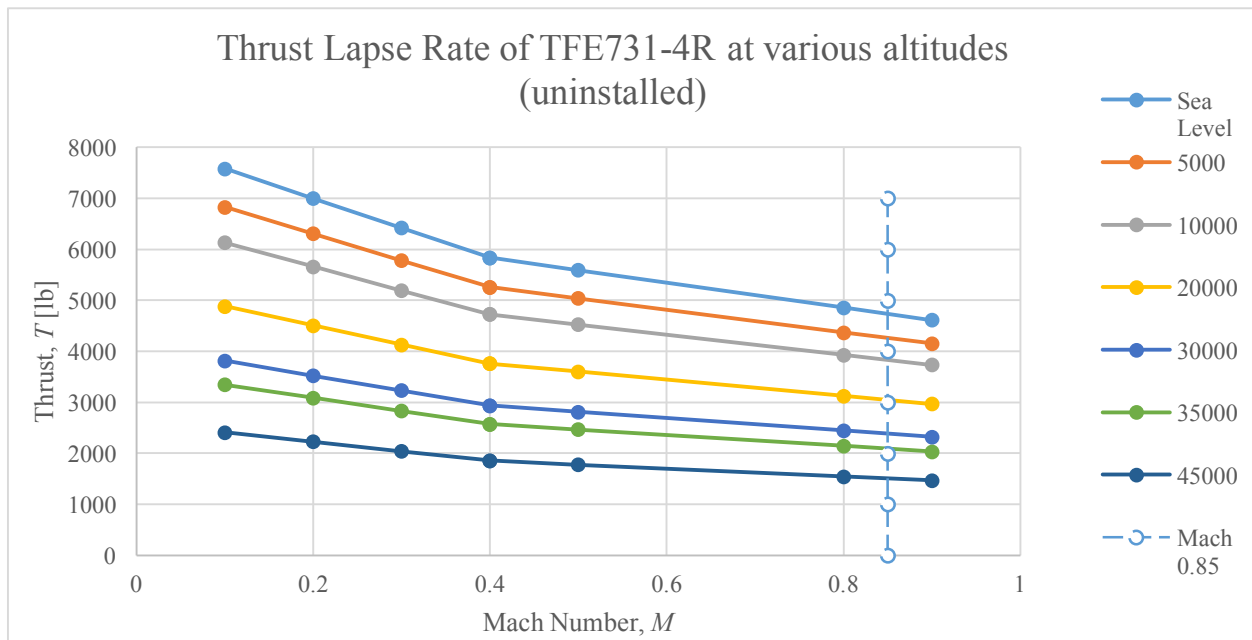


**Figure 8.12. Uninstalled Thrust vs. Mach Number at varying altitudes from Sea Level (0 ft) to Service Ceiling (45,000 ft)**

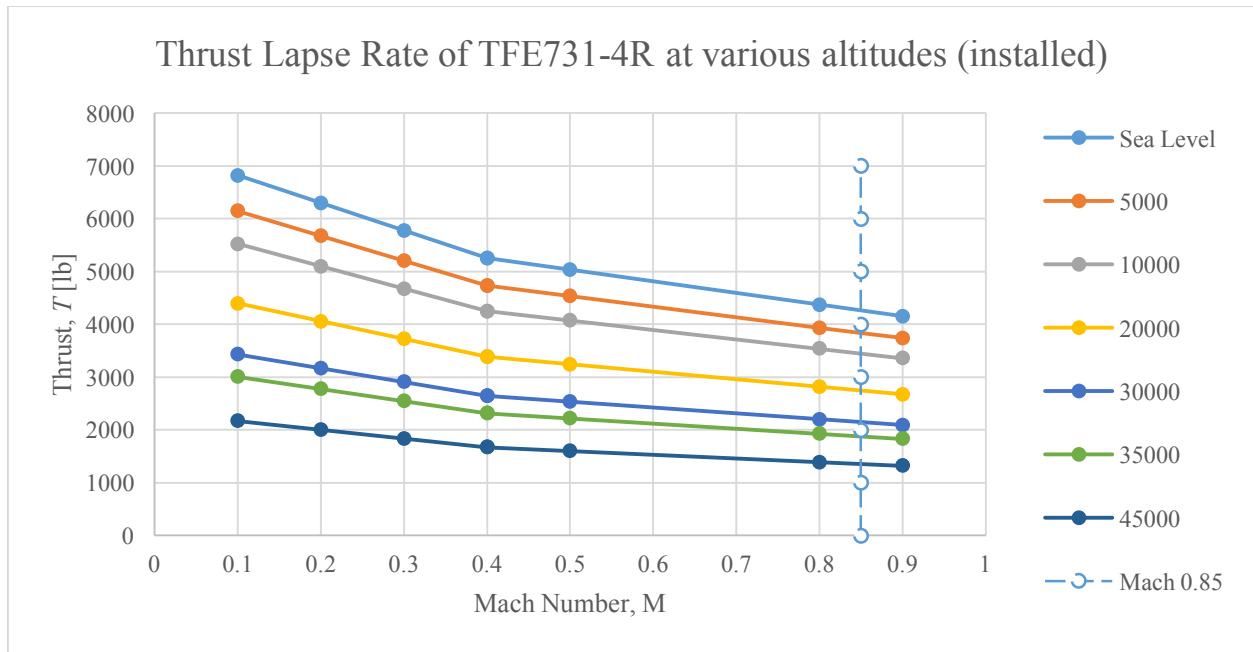


**Figure 8.13. Installed thrust vs. Mach number at varying altitudes from sea level (0 ft) to service ceiling (45,000 ft).**

### 8.7.2 Thrust Specific Fuel Consumption for the Chief

Since the TFE731-4R belongs to the same family of engines as the TFE731-5R, and is a medium bypass engine, Equation (4) can be used, which will yield the same results as in Figure 8.6, Figure 8.7 and Figure 8.8.

### 8.8 Future Work

The propulsion systems for both the Commander and the Chief were determined based on the factors of cost, reliability, ease of maintenance, and overall efficiency. Following a somewhat exhaustive series of steps in the trade studies, these systems were determined. However, since the trade study requirements were based on approximations and rough estimates, these systems are subject to change. Following a concrete tabulation of unchanged data, the aircraft may be outfitted with propulsion systems that are more fuel efficient, lighter, or easier to maintain. Since the trade

study process accounted for changes to the aircraft where it would become heavier as the design morphology progressed, the only areas where the engines can be improved is if the weight (and subsequently thrust) requirements decrease.

In regards to the nacelle specifications, Honeywell Aerospace fits all of its engines with a preconfigured nacelle. This reduced the ability of the configuration team to place the engine; originally, it was decided that an engine blended into the fuselage of the plane would be chosen. However, following the selection of the engine, the next step in the design morphology was to place the engine on the rear end of the fuselage, and higher up. This was done to avoid downwash from the wings, and to ensure that clean, smooth flowing air will be entering the inlet of the engine. More details about this design choice are discussed in the configuration section of the report.

As such, the propulsion system for both aircraft were chosen with the following design principles in mind: cost-of-ownership, reliability, and efficiency. Adhering to this common theme throughout the report allowed for a consistent selection process throughout the trade studies.

## **9 Structures (Klepacki & Qiu)**



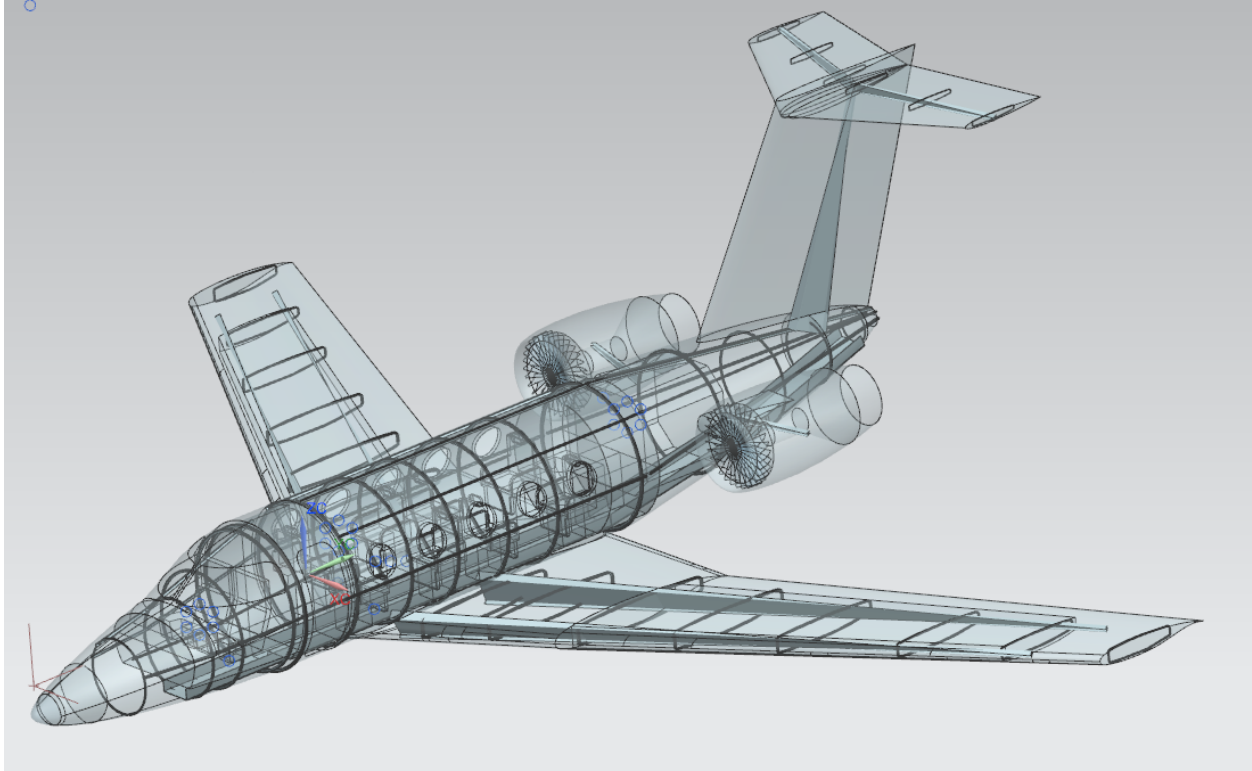


**Figure 9.1. Complete structures CAD assembly.**

## **9.1 Introduction**

The primary structures for the family of small business aircraft that we are designing compose all the major and critical load bearing structures located throughout the plane. These included all the wing primary and secondary structures, the fuselage skin, longerons and stringers, as well as any associated structures for the forward and aft cockpit and empennage. A common methodology was employed for sizing, designing and analyzing each of these structures with three primary constraints. The first major constraint employed was that aircrafts being designed were part of a family of planes, and thus, it was necessitated that a minimum of 70 percent commonality between the two planes was achieved. The second primary constraint was weight consciousness. This was realized through proper sizing of components to the required safety margin specified by FAR 21 standards. The third primary constraint was that the first aircraft in the family was required

to be in production and flight within four years. This necessitated a DFM oriented design process in which components and materials were chosen such that new methods of manufacturing and assembly were not need with the expedited schedule.

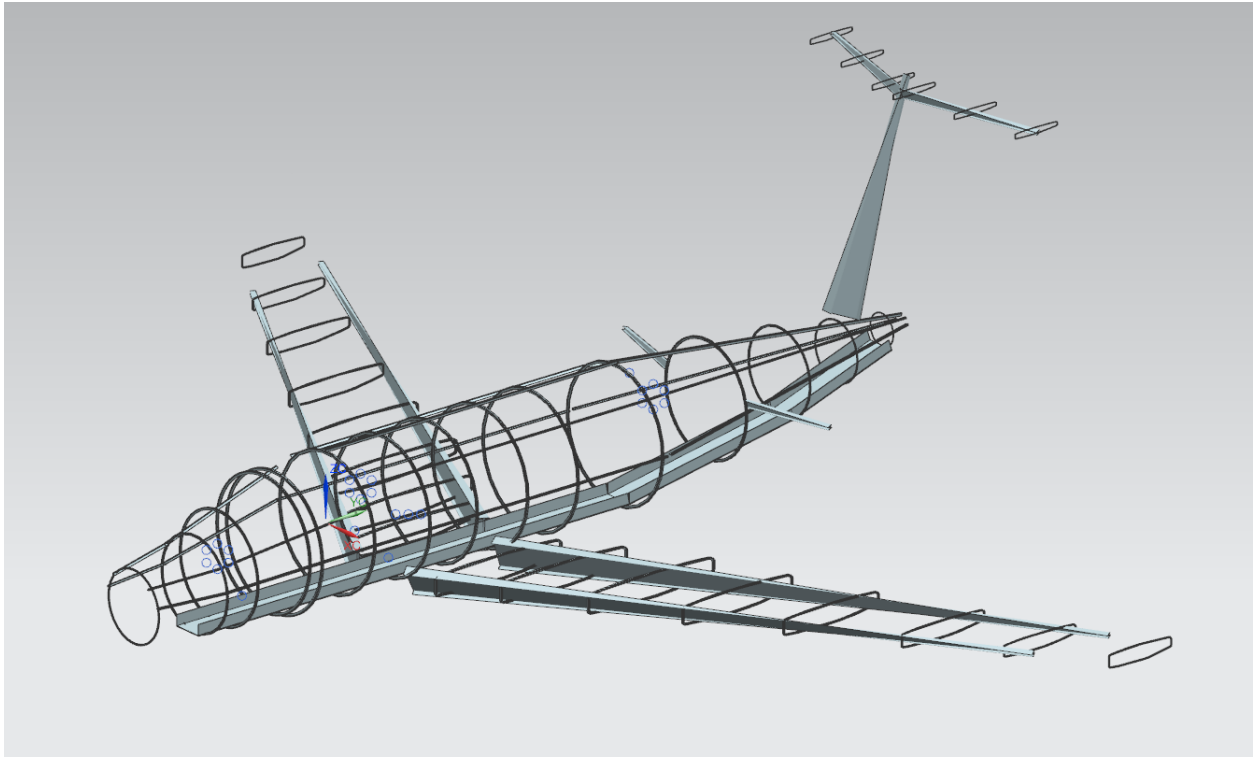


**Figure 9.2. Isometric view of all primary structures.**

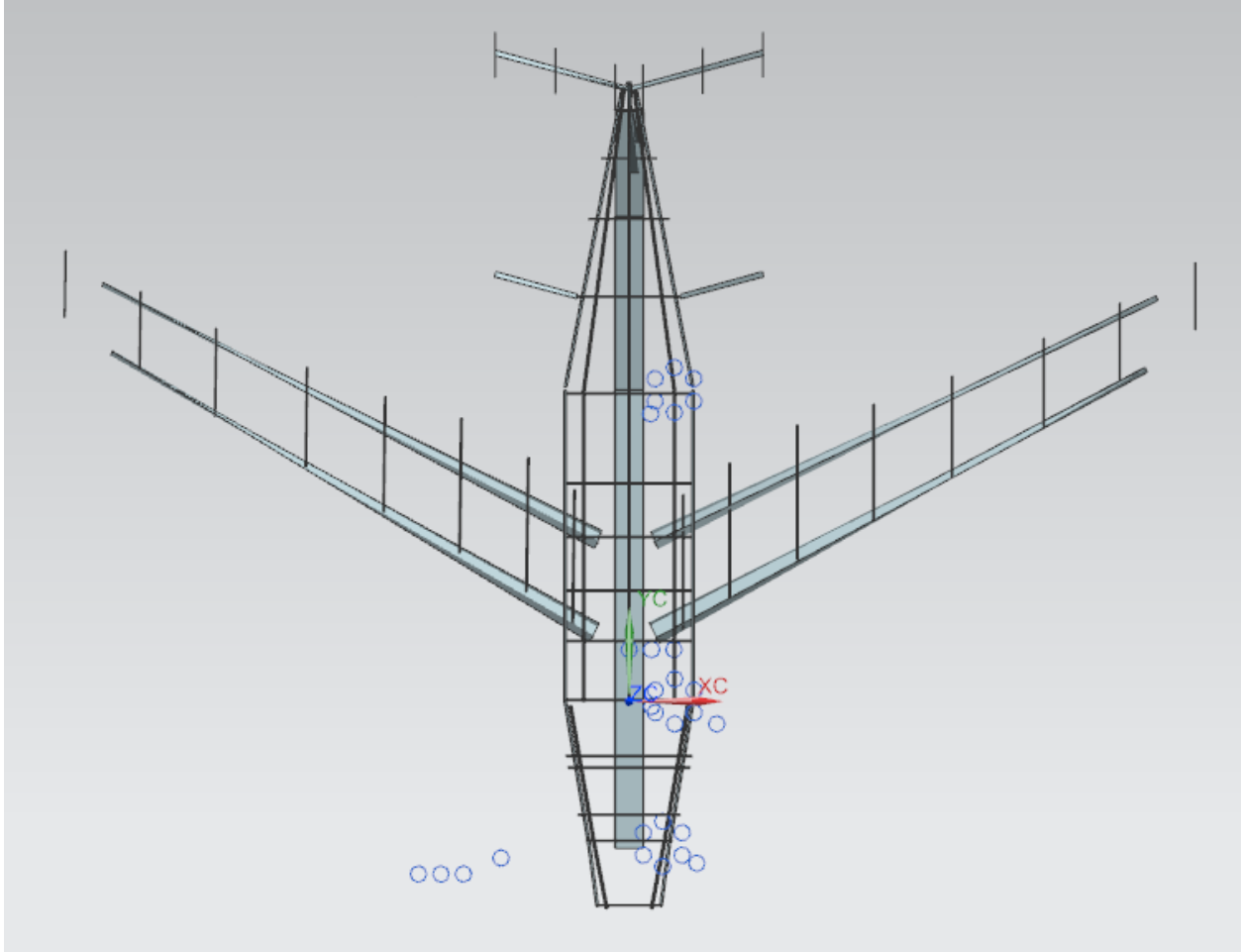


**Figure 9.3. Top view of all primary structures.**

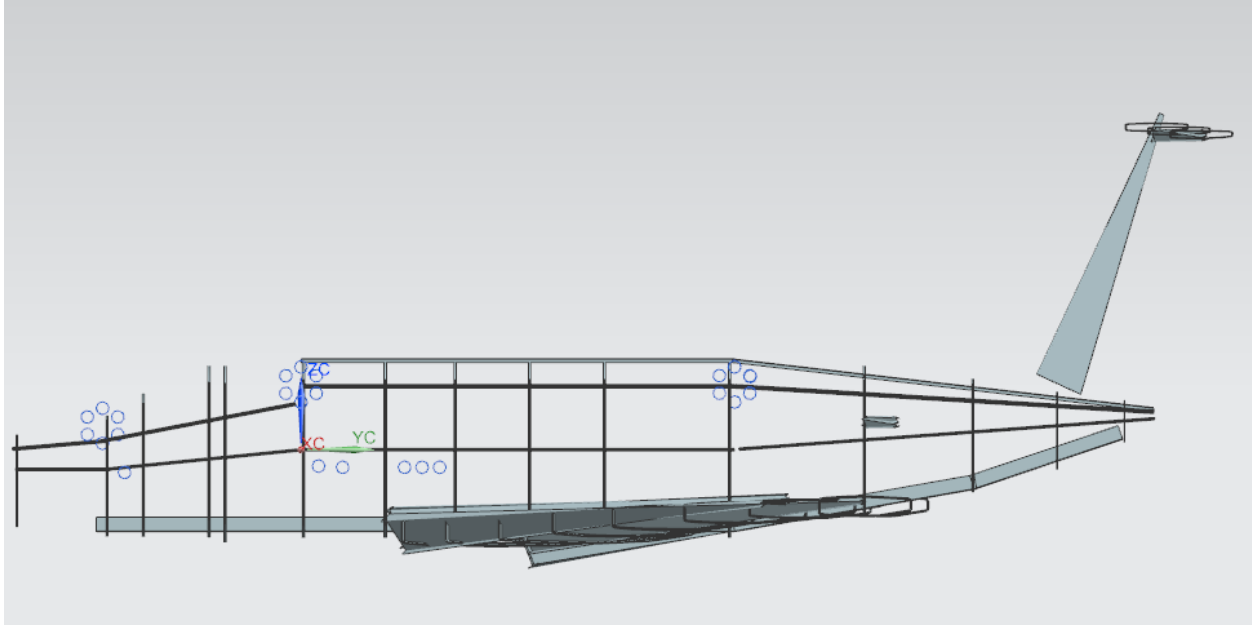


**Figure 9.4. Side view of all primary structures.**

The primary material chosen for the structures of this aircraft was an aerospace-certified alloy, Aluminum 7075-T6. The specific alloy and temper gives extremely high material properties in both strength and stiffness, while providing a high specific strength [12]. Another advantage of this material is that the processing, machinability and manufacturing of this material has been widely used in the aerospace industry and thus is easy to source and implement.

Physical Properties	Metric	English	Comments
Density	2.81 g/cc	0.102 lb/in <sup>3</sup>	AA, Typical
<b>Mechanical Properties</b>			
Hardness, Brinell	150	150	AA, Typical; 500 g load; 10 mm ball
Hardness, Knoop	191	191	Converted from Brinell Hardness Value
Hardness, Rockwell A	53.5	53.5	Converted from Brinell Hardness Value
Hardness, Rockwell B	87	87	Converted from Brinell Hardness Value
Hardness, Vickers	175	175	Converted from Brinell Hardness Value
Ultimate Tensile Strength	572 MPa	83000 psi	AA, Typical
Tensile Yield Strength	503 MPa	73000 psi	AA, Typical
Elongation at Break	11 %	11 %	AA, Typical; 1/16 in. (1.6 mm) Thickness
Elongation at Break	11 %	11 %	AA, Typical; 1/2 in. (12.7 mm) Diameter
Modulus of Elasticity	71.7 GPa	10400 ksi	AA, Typical. Average of tension and compression. Compression modulus is about 2% greater than tensile modulus.
Poisson's Ratio	0.33	0.33	
Fatigue Strength	159 MPa	23000 psi	AA; 500,000,000 cycles completely reversed stress; RR Moore machine/specimen

**Figure 9.5. Aerospace certified material properties and allowables for AL 7075-T6.**

The goal and constraint of being weight conscious was achieved by identifying the major loading scenario for each of the primary structures on the aircraft, choosing the optimal geometry and ultimately sizing the part for the minimum allowable MOS as specified by the FAR 21 document, which for all primary structures is  $MOS = 1.5$ . Common load bearing geometries such as I-beams and C-channels were widely used throughout the aircraft structures due to their exceptional strength and stiffness.

## 9.2 Wing Structures

### 9.2.1 Wing Primary Structures

The primary structures for the main wing of the aircraft are the two beams at the forward and aft part of wing. The major loading cases that the beams are sized to correspond to lift and drag loading, and the maximum values for the entire mission profile are chosen to be the limiting case, as shown in **Error! Reference source not found.** below.

**Table 9.1. Limited Load Cases for Wing Primary Structures**

<b>Wing Primary Structures Limited Load Cases</b>	
Lift	34882 lbf at landing
Drag	3505 lbf at landing

An I-beam geometry was chosen for both the forward and aft beams running along the leading and trailing edges of the wing. The reasons for choosing this geometry is three-fold. The first reason is that the I-beam is designed to take large bending loadings in the direction of the main web. Bending is the critical failure mode of the wings at the root of the wing-fuselage interface due to the moment induced by the lift force. The beam can also take bending loads in the perpendicular direction though the top and bottom skins, which will take the bending loads induced by drag of the aircraft. The second reason is that the beams have a high degree of optimal sizing. This is due to the various variable dimensions, as shown in Figure 9.6, that can all be independently changed so that the smallest amount of material is used while maintaining

adequate strength and stiffness. The final reason for the chosen geometry is that it is relatively uniform, allows for ease of manufacturing through extrusion or forging, and can easily be made of the aluminum alloy chosen.

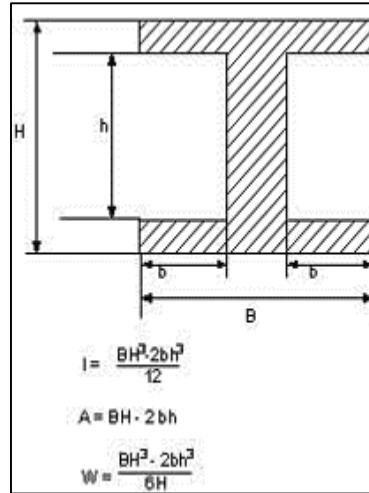


**Figure 9.6. Primary I-beam dimensions [19].**

The I-beam was sized for maximum bending induced at the wing root using the fundamental bending stress formula derived from solid mechanics:

$$\sigma_{bending} = \frac{M \cdot h}{I} = \frac{Lift * \left( \frac{Wing\ Thickness}{2} \right)}{I_{I-beam}} \quad (5)$$

The moment is idealized as a point load at the span-wise CP, with a moment arm from the CP to the wing root. Using the linearity of bending stress span-wise down the wing, it is tapered linearly to the wing-tip with a ratio identical to the aerodynamic taper ratio. This allows for optimal sizing as compared to a uniformly dimensioned wing beam. The final and dimensionally sized geometry is shown below in Figure 9.8. The dimensions were chosen using an automated and iterative solver in Microsoft Excel using the ‘Goal Seek’ and ‘Solver’ features, where the variables were the four critical beam dimensions (see Figure 9.6), and the mass was minimized while always keeping a  $MOS \geq 0.5$ . Due to the maximum drag value being an order of magnitude lower than the

maximum lift force, the moment induced by lift was always the stress limiting loading scenario, and thus the beam has a relatively large aspect ratio in the vertical  $z$ -direction.

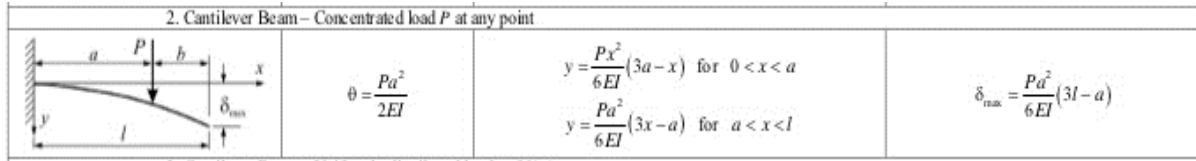


**Figure 9.7. Stresses and deflections of a cantilevered beam with a point load.**

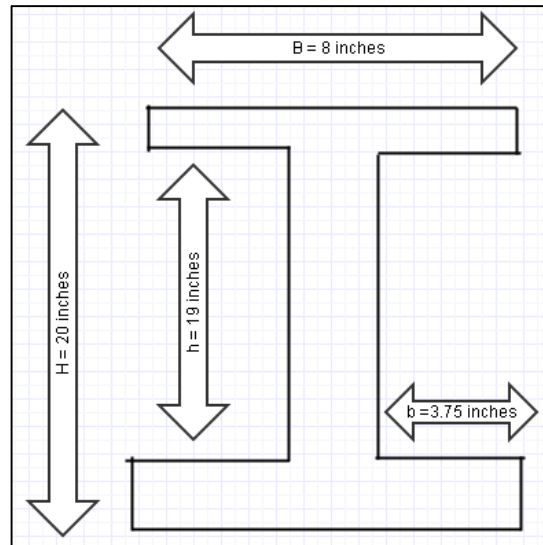


**Figure 9.8. Final primary wing beam dimensions.**

### 9.2.2 Wing Secondary Structures

The secondary structures of the wing are composed of the outer skin and the internal ribs placed span-wise along the wing. These provide span-wise stiffness for the wing and enough strength to prevent any pressure induced deflection and failure created by the fuel in the wings. The major loading cases for the secondary structures are the hoop stresses induced the pressure differential created between maximum fuel pressure and ambient atmospheric conditions at service ceiling flight. The skin thickness is to be chosen to match the skin thickness of the fuselage to

homologate manufacturing processes across the aircraft, and due to the max pressure differential being less than that of the fuselage to atmosphere at equivalent conditions.

The second component of the secondary structures are the wing ribs and these aid in increasing stiffness in the span-wise direction, holding the two primary beams in place, supporting the wing skins, and providing an area where fuel could be stored. Eight ribs are chosen to be implemented per wing, which provides an inter-rib space of about 38 in. The cross section for the perimeter of the rib, is chosen to be a T-beam so that the flat face can lie flat with the skin while still being stiffened by the web of the beam. A CAD model of this is shown below in Figure 9.9.

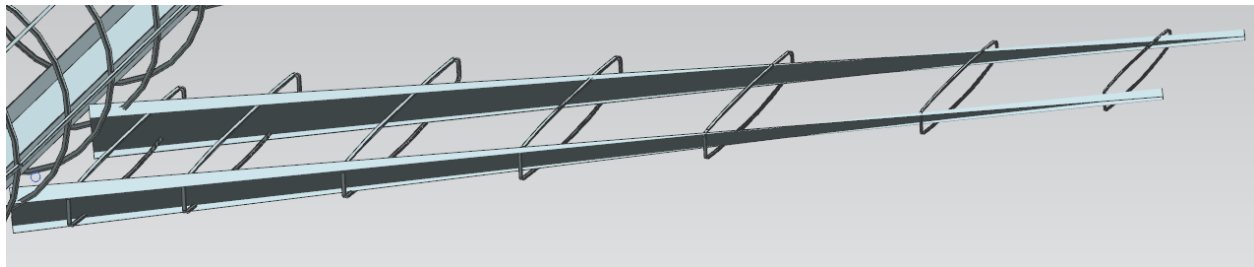


**Figure 9.9. Detailed view of wing primary and secondary structures.**

## **9.3 Fuselage Structures**

### **9.3.1 Longerons and Floor**

The main components of the fuselage structure are the floor beam and the longerons that run along the length of the entire plane. The main load bearing section is the fuselage section, while has a set of five uniform T-beams along the top half of the fuselage as shown in Figure 9.10 below, and a larger single C-channel running along the floor of the entire plane, from the cockpit, all the way through to the empennage.



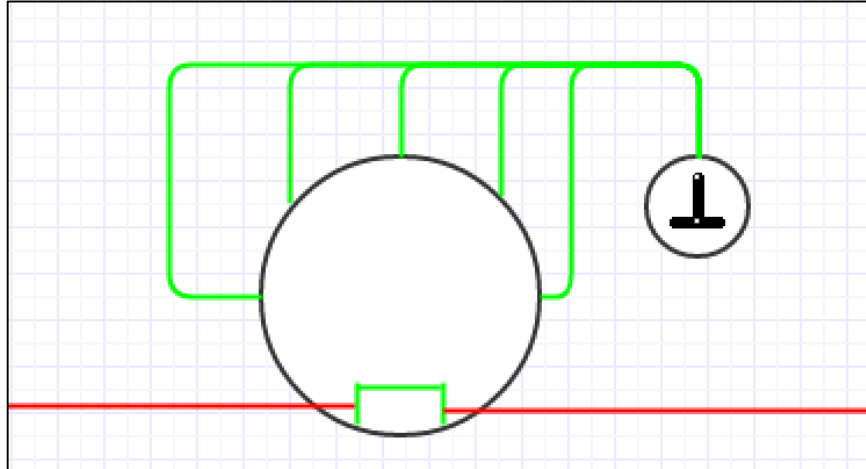


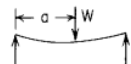
**Figure 9.10. Upper longerons (including T-beam cross section) and main floor beam.**

The main loads in the fuselage are the axial loads induced by the pressure different of the pressurized cabin relative to the atmospheric pressure at the service ceiling conditions. We derive this the limit load for axial stress by the approximation of a pressure vessel, as shown below:

$$\sigma_{axial} = \frac{\text{Frontal Area} * \Delta P}{(\text{Area}_{longerons} + \text{Area}_{floor})} \quad (6)$$

$$\sigma_{axial} = \frac{\left(\frac{\pi}{4} * \text{diameter}_{fuselage}^2 * (P_{cabin} - P_{serviceceiling})\right)}{(\text{Area}_{longerons} + \text{Area}_{floor})}$$

The second primary loading on the fuselage is the bending of the fuselage, which can be approximated to be a length-wise beam, with free support on each of the ends, corresponding to the forward and aft limits of the aircraft, with a point load being applied at the center of the main wings with an amplitude equal to that of max lift at landing. The free-body diagram and corresponding solids mechanics equations can be seen in Figure 9.11 below.

<p>e. Left end simply supported, right end simply supported</p> 	$R_A = \frac{W}{l}(l - a) \quad M_A = 0$ $\theta_A = \frac{-Wa}{6EI}(2l - a)(l - a) \quad y_A = 0$ $R_B = \frac{Wa}{l} \quad M_B = 0$ $\theta_B = \frac{Wa}{6EI}(l^2 - a^2) \quad y_B = 0$	$\text{Max } M = R_A a \text{ at } x = a; \text{ max possible value} = \frac{Wl}{4} \text{ when } a = \frac{l}{2}$ $\text{Max } y = \frac{-Wa}{3EI} \left(\frac{l^2 - a^2}{3}\right)^{3/2} \text{ at } x = l - \left(\frac{l^2 - a^2}{3}\right)^{1/2} \text{ when } a < \frac{l}{2}; \text{ max possible value} = \frac{-Wl^3}{48EI} \text{ at } x = \frac{l}{2} \text{ when } a = \frac{l}{2}$ $\text{Max } \theta = \theta_A \text{ when } a < \frac{l}{2}; \text{ max possible value} = -0.0642 \frac{Wl^2}{EI} \text{ when } a = 0.423l$
---	--	--

**Figure 9.11. Fuselage bending diagram [19].**

The beams were designed with two considerations in mind. First, the axial loads were designed to be taken purely by the longerons, thus leading to a conservative margin of safety. The cross-sectional area of the sum of all five beams was derived using the same iterative and automated solver, like the wing primary structures design, and an initial aspect ratio of  $AR = 1$  was chosen for the T-beam. After this, the dimensions of the floor C-channel were chosen. The strong dimensions, corresponding to ‘Dim B’ and ‘Dim H’ in Figure 9.12, were constrained by the configuration group as part of the main internal floor geometry, but we are still left with the wall thicknesses as a variable. The area moment of inertia of the ‘fuselage beam’ is approximated using the parallel axis theorem and linear superposition, with an approximated neutral axis running through the C-channel since  $I_{floor} \gg \sum I_{longerons}$ .

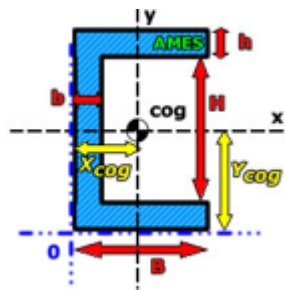


**Figure 9.12. Primary C-channel dimensions and geometry.**

The final dimensions for each of the beams are tabulated below, as well as maximum longitudinal deflections set at  $\delta_{max} \leq 0.5 \text{ inches}$ . The margins of safety for the longerons are set at  $MOS = 0.5$ , but since they are designed to support the full axial load, the floor beam ultimately increases the effect margin of safety for the overall axial support structure.

**Table 9.2. Primary Longeron Dimensions**

Notation	Value	Units
B	1	[in]
b	0.25	[in]
H	1.25	[in]
h	0.25	[in]

**Table 9.3. Primary Floor Beam Dimensions**

Notation	Value	Units
B	6	[in]
b	0.3	[in]
H	16	[in]
h	0.3	[in]

**Table 9.4. Fuselage Margins and Limit Load Deflections**

Notation	Value
$MOS_{longerons}$	0.5
$\delta_{max}$	-0.04 in (at longitudinal limits under max lift at landing)

### 9.3.2 Stringers and Skins

The second primary section of the fuselage structures are the stringers and skin. The primary intent of the stringers is to provide longitudinal bending stiffness, when coupled with the longerons and floor, and to interface with other primary structures such as the wing, window, and tail section interfaces. The radial sections are designed in the same twofold manner as the length-wise sections. The skin is designed to support the maximum hoop stress induced by the limiting pressure differential, but these are also reinforced by stringers which are spaced to support other interfacing primary structures. A simplified systems-level diagram is shown below in Figure 9.13.

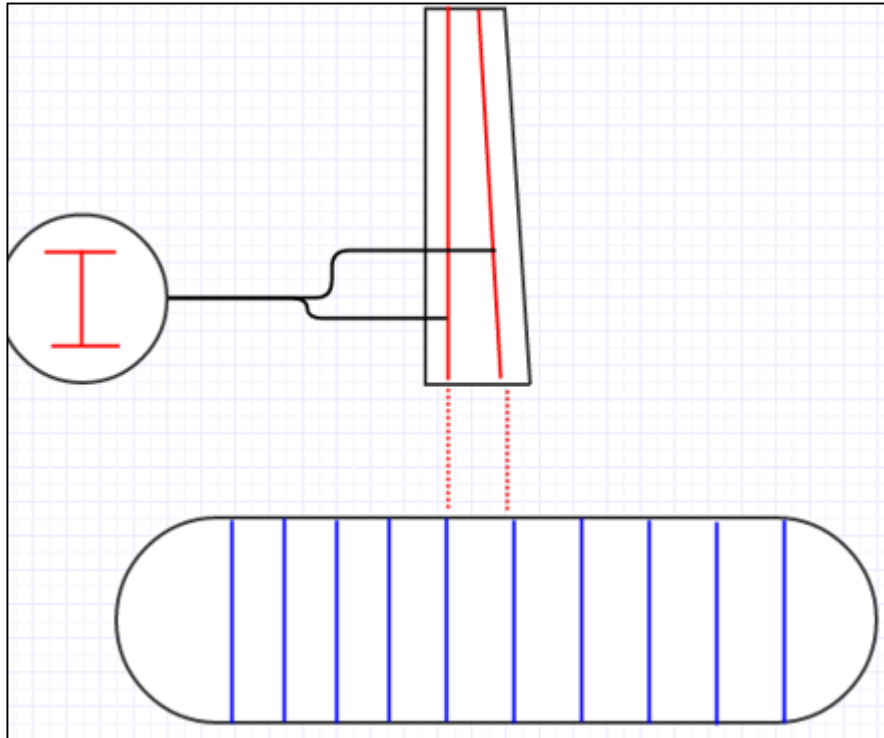


**Figure 9.13. Stringer spacing diagram and interfaces.**

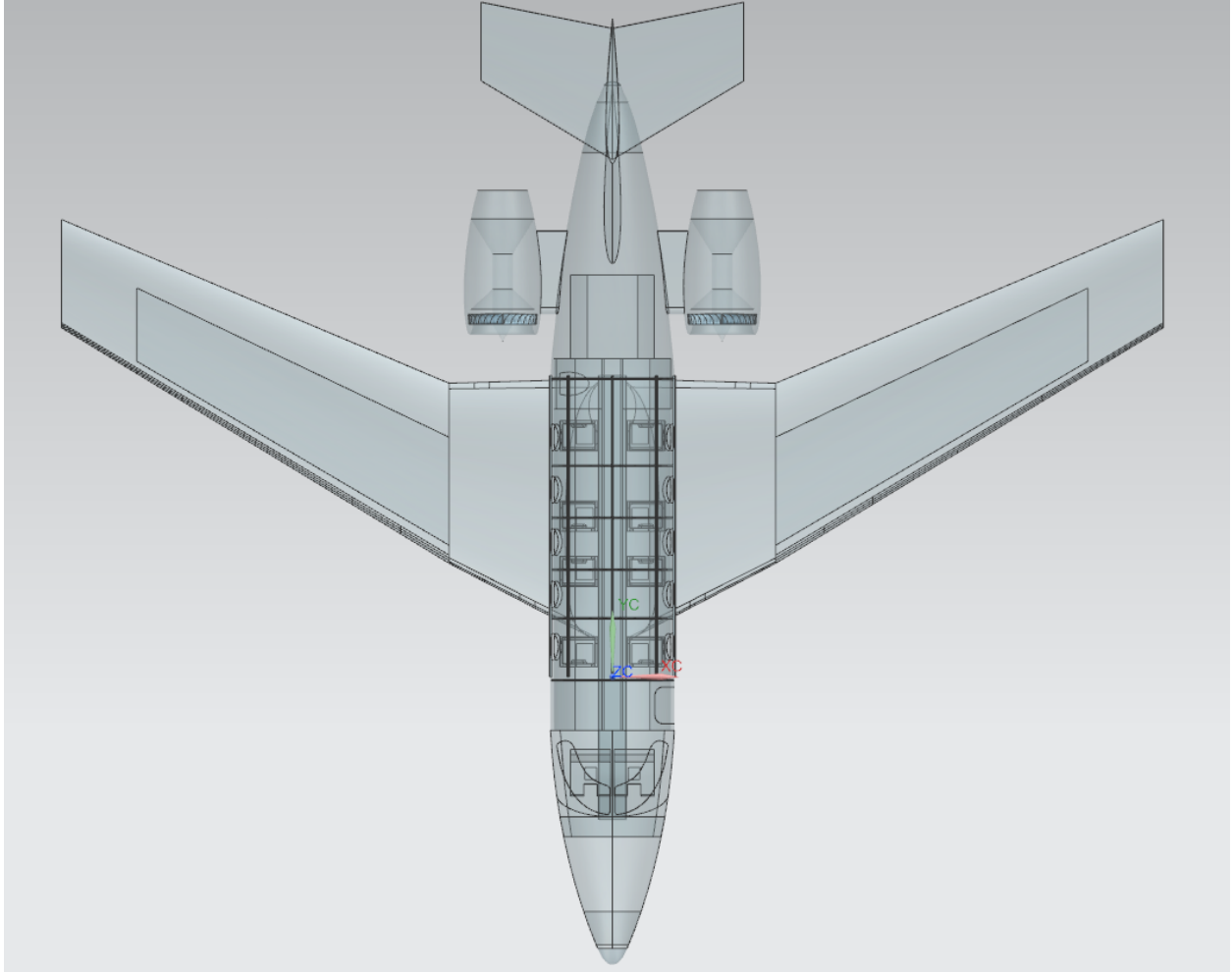


**Figure 9.14. Top view of fuselage structures.**

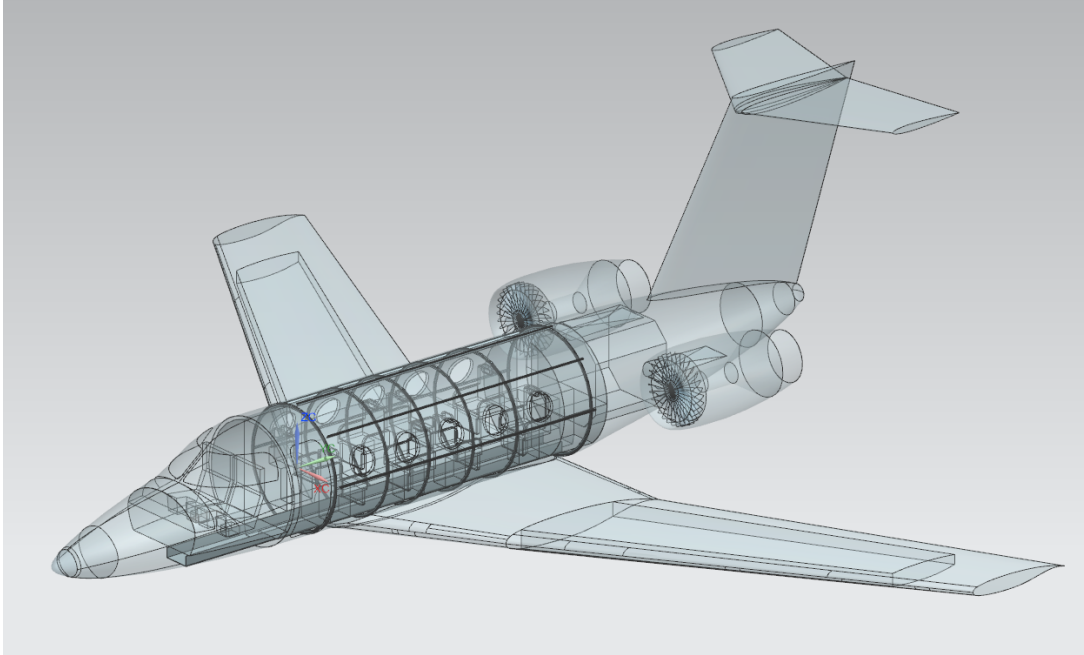


**Figure 9.15. Isometric view of fuselage structures.**

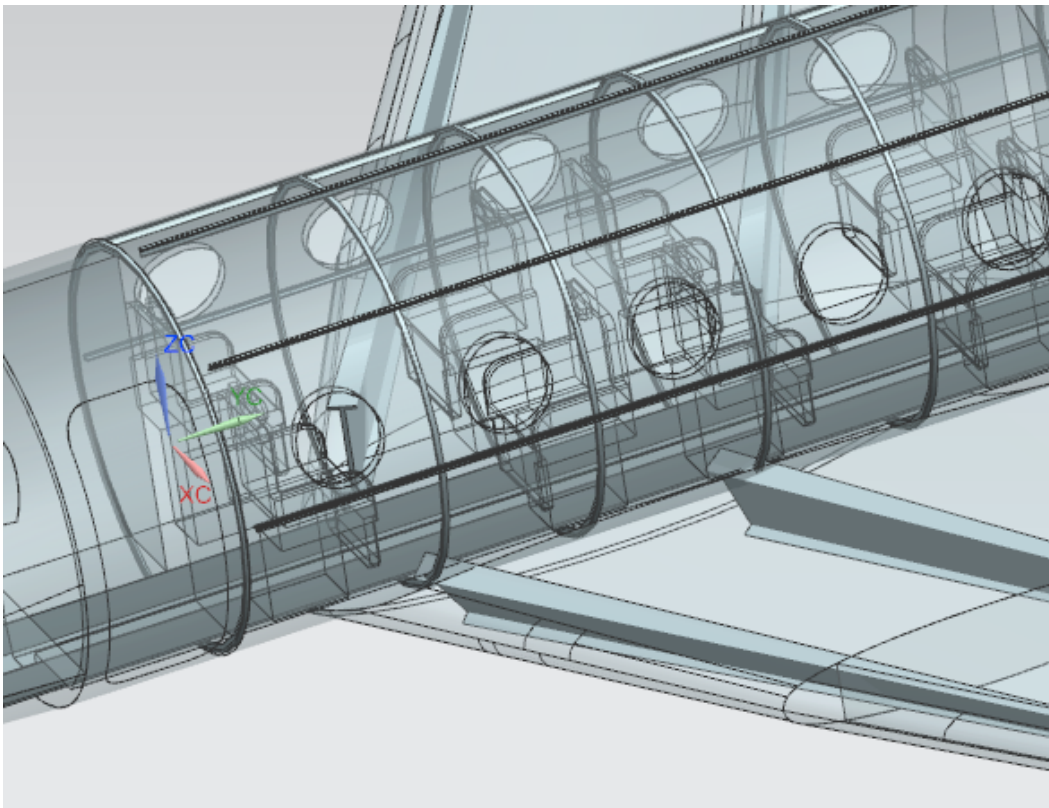


**Figure 9.16. Detailed view of wing spar and fuselage interfaces.**

The skin is designed to support hoop stress induced by the pressure difference at service ceiling conditions. This is calculated through Equation (7). Using the iterative and automated solver coupled with a constrained  $MOS = 0.5$ , a skin thickness of  $t_{skin} = 0.0154 \text{ inches}$  was derived. The thickness is increased to  $t_{skin} = 0.02 \text{ inches}$  due to unimplemented stress concentrators that result from joint interfaces. This also aids in the primary goal of designing towards ease of manufacturing by specifying a common gauge of sheet aluminum.

$$\sigma_{hoop} = \frac{\Delta P * Thickness_{skin}}{4 * Diameter_{fuselage}} \quad (7)$$

The stringer was sized to support loads at interfaces rather than being designed as a critical loading bearing structures needing to make a minimum MOS. The spacing of the stringers is variable along the length of the fuselage, and primarily placed at the interfaces where the wing primary beams connect, as well as supporting windows at locations of seats per the configuration group's requirements. The dimensions of the T-beam used in the stringers are identical to the longerons, such that tooling and manufacturing costs are kept low, as well as allowing commonality between the two aircraft in the family. The dimensions can be found in **Error! Reference source not found.** and a systems-level of all the primary and secondary fuselage structures in Figure 9.16 above.

### 9.3.3 Cockpit and Empennage Structures

The structures for the cockpit follow the same design and analysis regime as for the fuselage. Using the linearity and superposition relationships of Equation (5), Equation (6) and Equation (7), we can appropriately size and scale the longerons and stringers proportional to the diameters of the fuselage and other load-bearing structures. The cross-sections, geometries, and materials of each corresponding beam and structure are kept identical to the fuselage, resulting in primary dimensions being the only variables. The sole exception to this constraint and design

methodology is that the forward part of the floor beam is kept identical to the fuselage dimensions, but the aft section is tapered appropriately. This is due to the cockpit configuration being analogous to the passenger compartment.

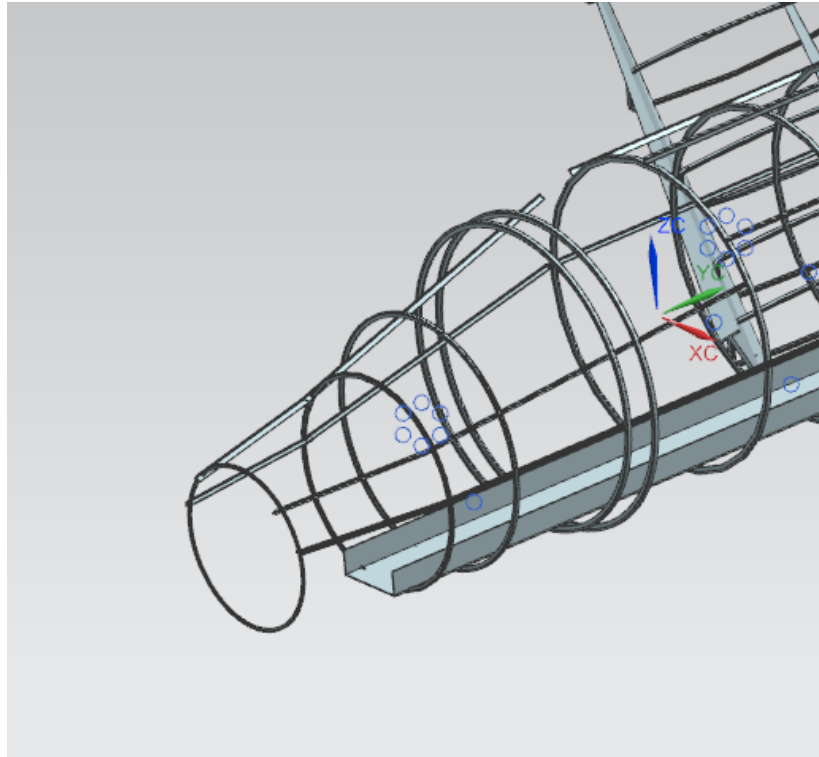


**Figure 9.17. Detailed isometric view of cockpit primary and secondary structures.**

The spacing of stringers in the cockpit is constrained to a maximum inter-stringer distance of 36 in. Locations of the stringers are chosen to support primary components of the cockpit, such as the forward and aft supports of the main forward windows, front bulkhead, and the interfaces to the main fuselage section. The same design methodology is implemented for the spacing and placement of the stringers in the empennage with intended supports being for the vertical tail and horizontal stabilizers.



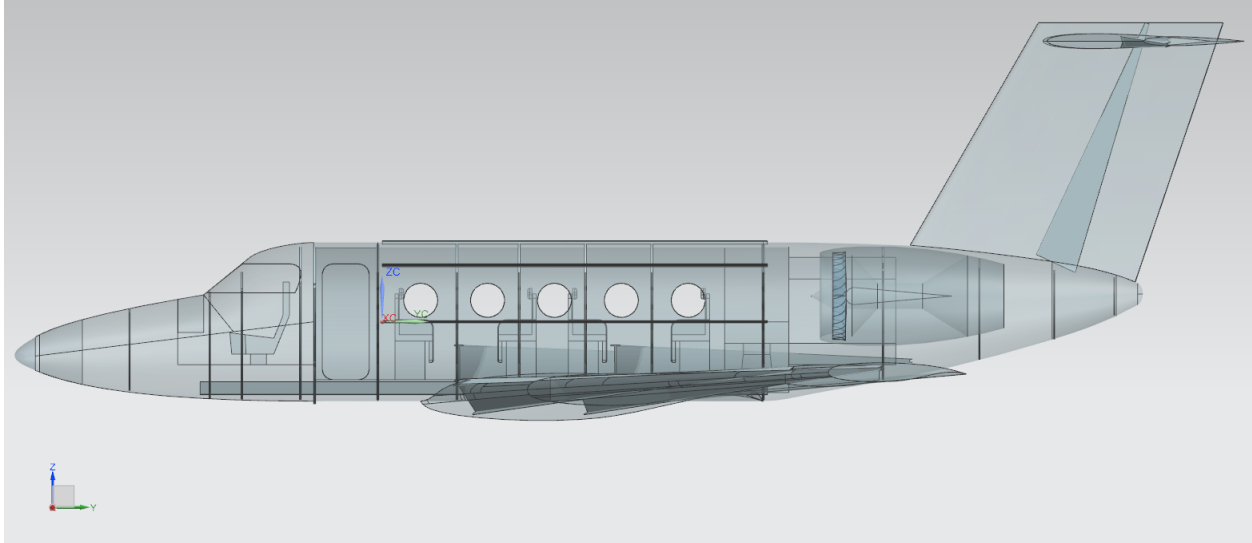


**Figure 9.18. Stringer locations for cockpit, fuselage, and empennage.**

### **9.3.4 Vertical Tail and Horizontal Stabilizer Structures**

To decrease cost, expedite the manufacturing and tooling timelines, and to aid in structures commonality, the tail and stabilizer structures are derived from the primary and secondary wing structures. Each will have a single, rather than double, beam implemented and these will interface directly to the empennage longerons and stringers. Sections will be cut from the tapered ends of the wing beams and from the rib sections. This is attainable due to the lift and drag forces being lesser than those of the main wings and the stresses are lesser due to the linearity of Equation (5). The skins are also kept uniform and identical to that of the fuselage and main wings to decrease tooling and resource costs, as well as having common manufacturing practices throughout a wide variety of sections of each aircraft variant.

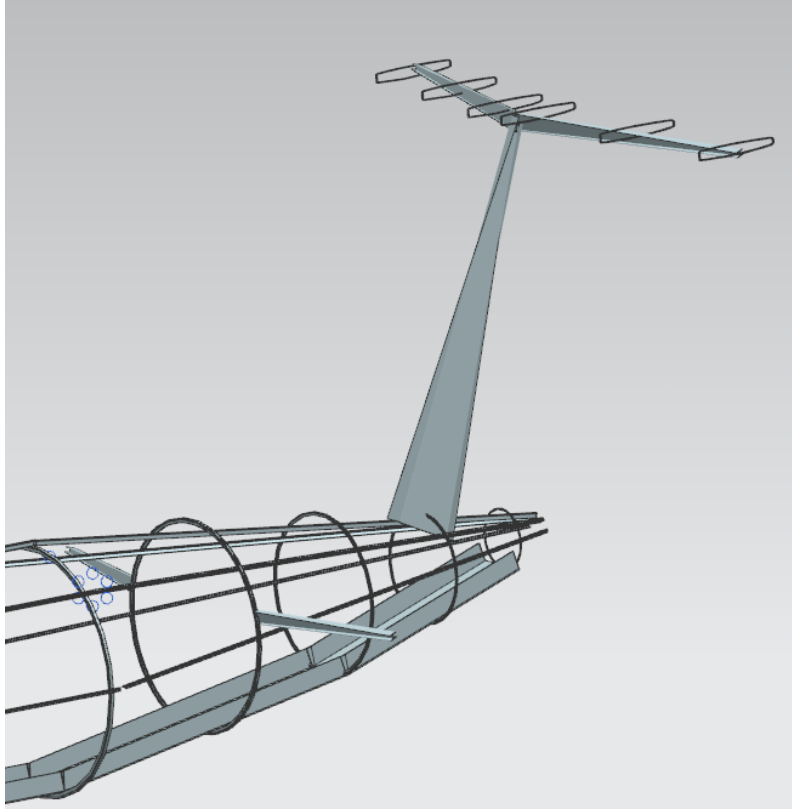


**Figure 9.19. Tail section primary and secondary structures.**

#### **9.4 Primary Structures Commonality Design**

As per the constraints of 70 percent structures and configuration commonality between the family of aircraft, each of the primary structures have been designed to limit loads corresponding to the Commander. The Chief will use the same configuration of wing structures, longerons, and floor and cockpit/empennage structures. The main difference between the two aircraft variations is that the Chief will have one less fuselage stringer section which will eliminate a window support and corresponding row of seats. This methodology of implementing a high degree of structures commonality will allow tooling and manufacturing for the aircraft to be created from a single set of processes with slight length-wise dimensional changes being needed only for the fuselage longerons. The fuselage will be manufactured in two sections, one being forward of the wing centerline and the other being after of the centerline. For the Commander, there will be an

additional stringer section manufactured independently and joined between the two primary sections giving the additional length and seating configuration.

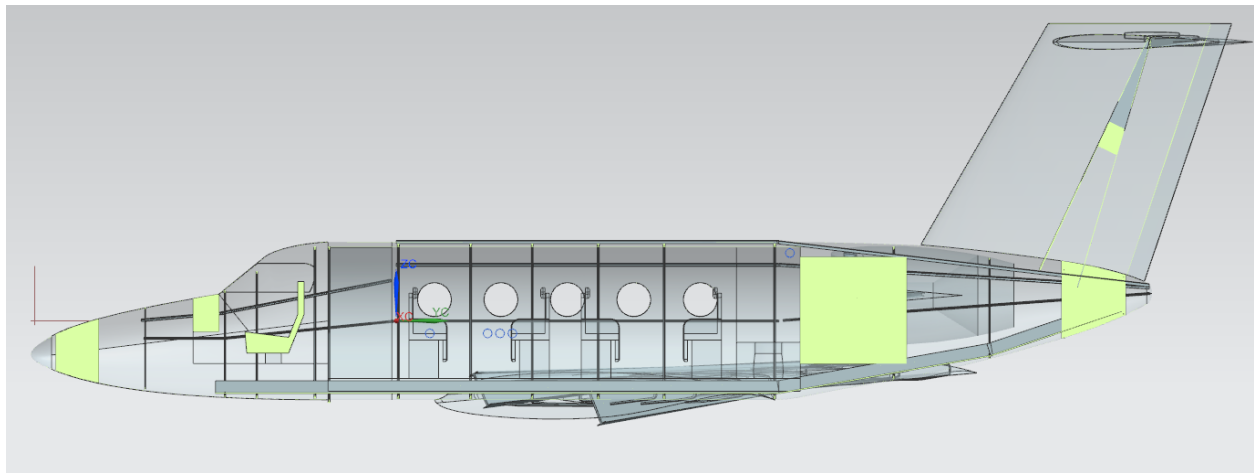


**Figure 9.20. Section view of primary structures design and integration within full aircraft assembly.**

### **9.5 Primary Structures Summary and Weight Analysis**

Weight consciousness was one of the primary objectives and constraints, along with an expedited design and manufacturing timeline and commonality between aircraft variants. Using the independently design and created iterative solver each section was designed to a set of hard constraints, such as dimensions specified by the configuration group, as well as the hitting the minimum mandated margin of safety. Examples of the user-created tool are shown below in Figure 9.21 and Figure 9.22. The tool features an overview page where primary input parameters can be specified with automatic feedback for safety margins and weights. More detailed analysis pages are also included such that parameters for certain structures can be independently tuned and verified. This leads to optimal geometries and efficient structures, and ultimately resulted in a low structural weight for the aircraft. A table of structural weight for the aircraft weight is shown below in **Error! Reference source not found.**, along with critical margins of safety for primary load bearing structures.

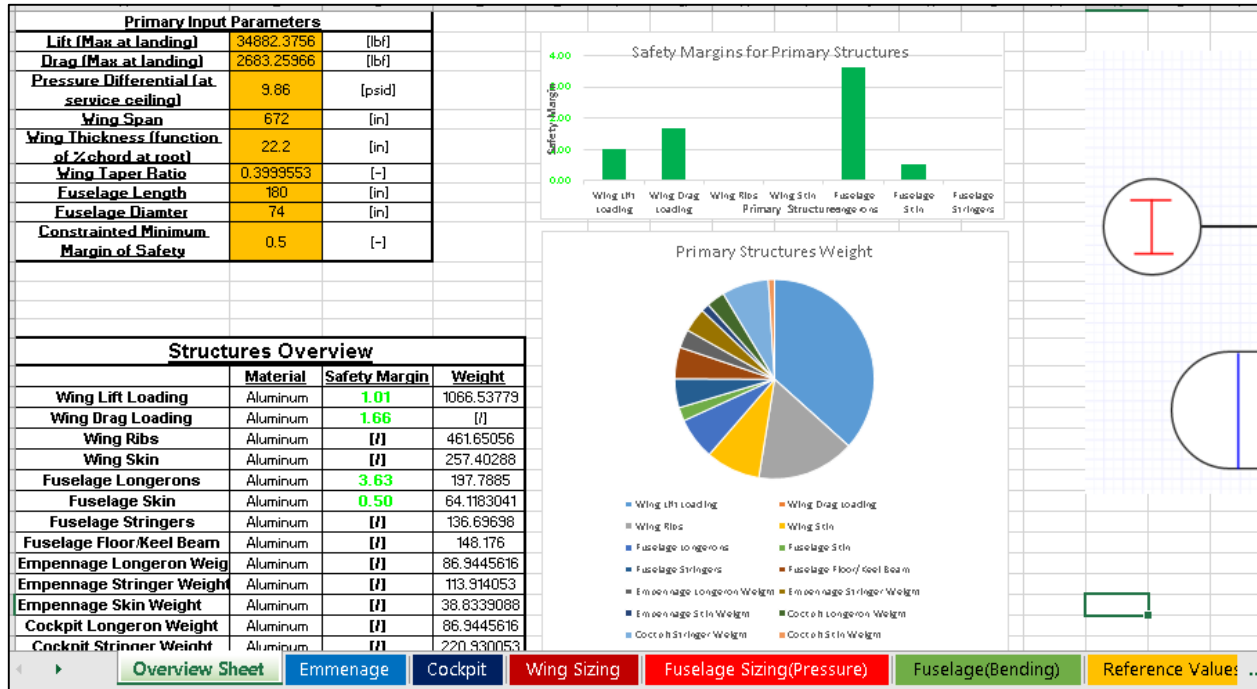


Figure 9.21. User-created iterative solver and automated design tool input screen.

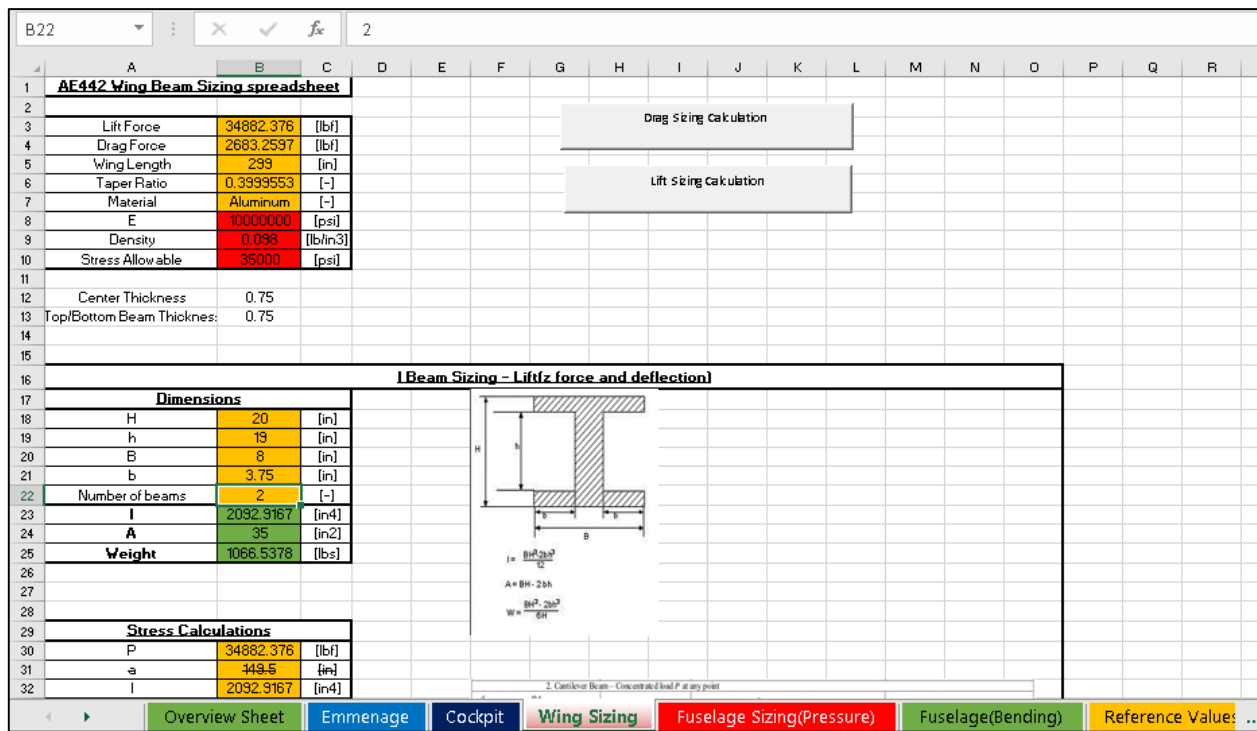
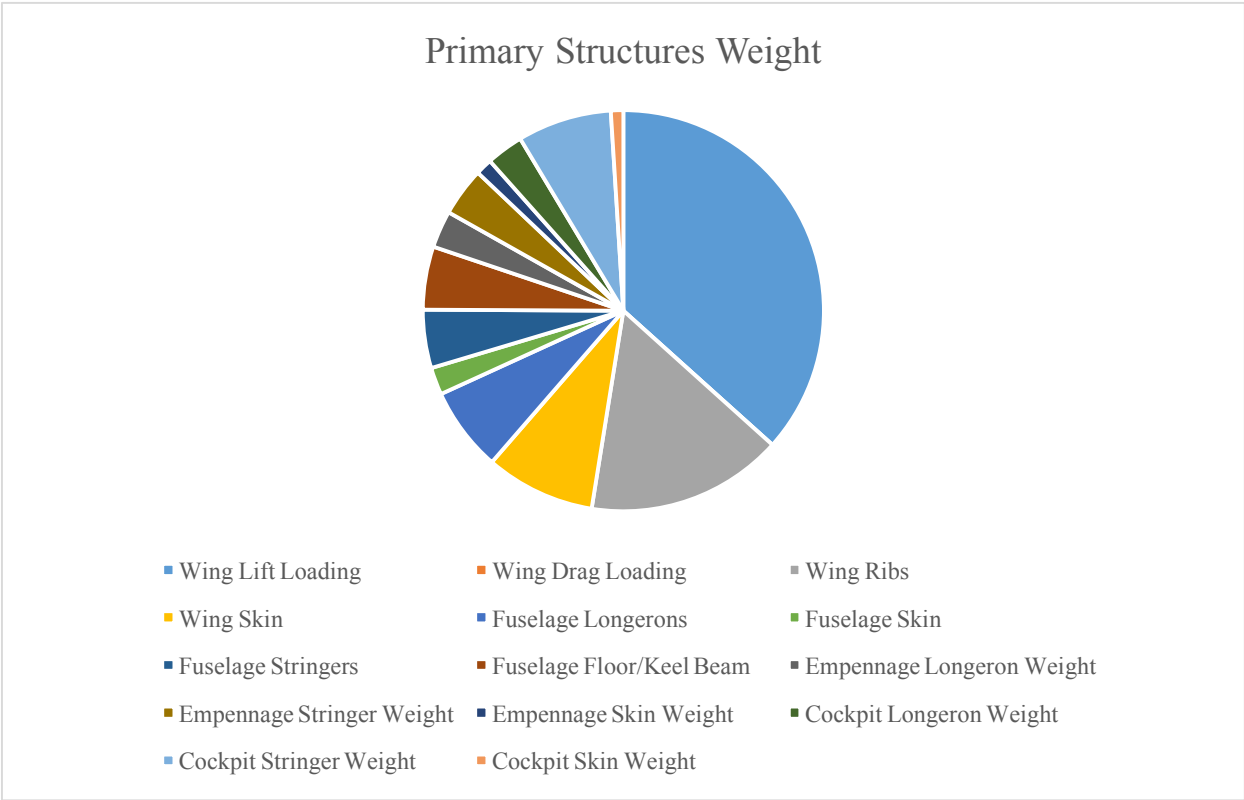


Figure 9.22. User-created iterative solver and automated design tool detailed analysis screen.

**Table 9.5. Tabulated Weights and Margins of Safety for all Primary and Secondary Structures**

<b>Item</b>	<b>Material</b>	<b>Safety Margin [-]</b>	<b>Weight [lb]</b>
Wing Lift Loading	Aluminum	1.01	1066.54
Wing Drag Loading	Aluminum	1.66	[/]
Wing Ribs	Aluminum	[/]	461.65
Wing Skin	Aluminum	[/]	257.41
Fuselage Longerons	Aluminum	3.63	197.79
Fuselage Skin	Aluminum	0.50	64.118
Fuselage Stringers	Aluminum	[/]	136.69
Fuselage Floor/Keel Beam	Aluminum	[/]	148.18
Empennage Longeron Weight	Aluminum	[/]	86.945
Empennage Stringer Weight	Aluminum	[/]	113.91
Empennage Skin Weight	Aluminum	[/]	38.834
Cockpit Longeron Weight	Aluminum	[/]	86.945
Cockpit Stringer Weight	Aluminum	[/]	220.93
Cockpit Skin Weight	Aluminum	[/]	29.149
Total	[-]	[-]	2572.06

This is only a partial list of weights as it does not include fasteners, joints interfaces, gussets and stiffeners. However, each section is representative of the distribution of weights for each section of the aircraft, and the distribution of weights relative to each other can be seen in Figure 9.23. The weights shown are for the Commander, but the Chief would be similar, with a reduction in weight only decreased by the weight of a single fuselage stringer section and the decreased length of the corresponding longeron, floor section, and outside skin.



**Figure 9.23. Relative weight distribution for primary and secondary structures.**

**9.6 V-n Diagram**

A V-n diagram compares the airspeed and load factor prescribes an aircraft can withstand. Loads greater than the positive load factor, loads smaller than the negative load factor, airspeed faster than the dive speed or slower than the positive and negative stall speeds will lose structural integrity and will incur structural damage and structural failure. To prevent structural failure, the aircraft must remain within the aircraft’s maneuvering envelope as shown below in Figure 9.24.

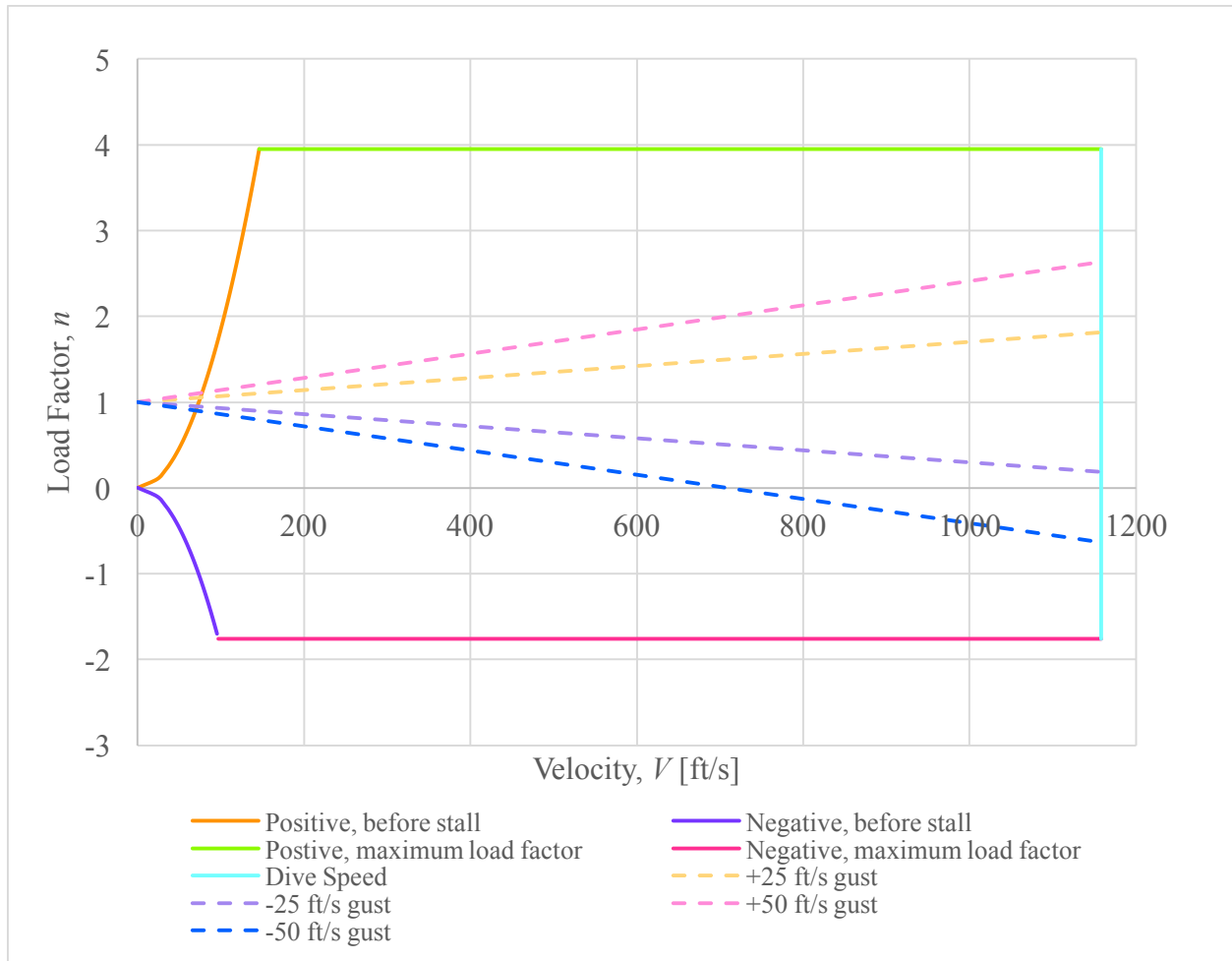


**Figure 9.24. V-n diagram.**

Using velocities from zero to the stall speed, the dark orange and dark purple curves calculate the aerodynamic limits of the load factor and is derived from the stall equation [1] as shown in Equation (8).

$$V = \sqrt{\frac{2nmg}{\rho S C_{L_{max}}}} \quad (8)$$

$$n = \frac{V^2 \rho S C_{L_{max}}}{2mg}$$

As shown in Figure 9.24, the maximum positive load factor is 3.951 and the maximum negative load factor is -1.032. Per FAR 23 and FAR 25 standards, calculated values are within the acceptable load factors and are consistent with load factors for business jets.

At the intersection of the dark orange and lime green curve lies the maneuver point. The maneuver point is the highest load factor and lift coefficient the aircraft can reach and the velocity corresponds to the corner velocity and is expressed as the following equation:

$$V^* = \sqrt{\frac{2n_{max} W}{\rho C_{Lmax} S}} \quad (9)$$

For  $V < V^*$ ,  $n < n_{max}$  and the maneuver envelope is limited by stall and for  $V > V^*$ ,  $n = n_{max}$  and the maneuver envelope is limited to the maximum acceptable positive loading of 3.951 and is shown by the lime green line. Similarly, for the negative load factor at  $n = n_{max}$ , the maneuver envelope is limited to the maximum negative loading of -1.032 and is shown by the hot pink line. For flight above the maximum acceptable positive loading and below the minimum acceptable positive loading, the aircraft will sustain structural damage.

The maximum positive and negative loading values will remain constant until the high speed limit is reached. The high speed limit is defined as the dive speed and per FAR standards, the dive speed must be greater than 1.4 times the cruise speed. For our aircraft, the calculated dive speed is 1158 ft/s and is shown by the sky blue line. For airspeeds greater than 1158 ft/s, we will encounter permanent deformation and failure.

Gusts in the atmosphere is inevitable and we need to account for them in our V-n diagram analysis. They change the load factor and we must add the gust load to the maneuver load to determine a safe and structurally acceptable flight. As shown in Figure 9.24, the gust load is within the maneuver load of the four analyzed gusts: +25 ft/s (light orange line), -25 ft/s (light purple



line), +50 ft/s (light pink line) and -50 ft/s (dark blue line). The aircraft is susceptible to high gusts further than the four analyzed and will not see structural damage for high upward and downward gust conditions.

## 9.7 Landing Gear

### 9.7.1 Gear Configuration Trade Study

Three landing gear configurations were considered for the Commander and the Chief: taildragger, bicycle and tricycle.

A taildragger landing gear configuration has two main landing gears forward of the aircraft's center of gravity and one small landing gear below the tail of the aircraft as shown in Figure 9.25. The main landing gears will carry 80-90% of the load whereas the tail landing gear will carry 10-20% of the load. This three-wheel support provides stability on the ground, but directional instability during ground maneuvers. With the two different tire sizes, the cabin floor will be uneven. The on-board experience for passengers will be uncomfortable; cargo and baggage storage will be difficult and inefficient. This landing gear configuration will require a high angle of attack during ground roll which will yield low runway visibility for the pilot.

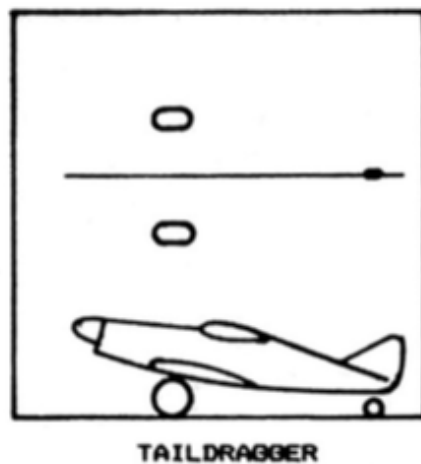


**Figure 9.25. Taildragger landing gear configuration [17].**

Next, the bicycle configuration was studied. The bicycle landing gear configuration has two main landing gears as shown in Figure 9.26. The first gear is forward of the aircraft's center of gravity and the second gear is aft of the aircraft's center of gravity. Small outrigger wheels are attached below the wing to prevent the aircraft from tipping sideways. To compensate for low runway visibility, the aft landing gear is placed further aft of the aircraft's center of gravity. This will create an even cabin floor and require a low angle of attack during ground roll to yield the highest amount of lift. This design is ideal for aircrafts with a narrow fuselage and a wide wing span. It is also a simple, lightweight and cheap candidate compared to the taildragger configuration.

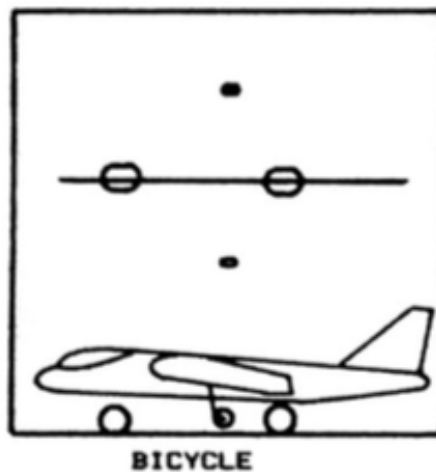


**Figure 9.26. Bicycle landing gear configuration [17].**

Lastly, the tricycle configuration was analyzed. The tricycle landing gear configuration has two main landing gears near the aircraft's center of gravity and a nose landing gear near the cockpit as shown in Figure 9.27. Similar to the bicycle configuration, the main landing gears will carry 80-90% of the load whereas the nose landing gear will carry 10-20% of the load. The main landing gear has larger wheels, but the nose and main landing gears will still have the same height. Unlike the taildragger, this configuration is directionally stable on the ground and during ground maneuvers.

Not considered in the taildragger and bicycle configurations, the placement of the main landing gear aft allows the aircraft to land with a large crab angle. Crab angles are commonly seen during crosswind landings where the nose is not aligned with the runway.

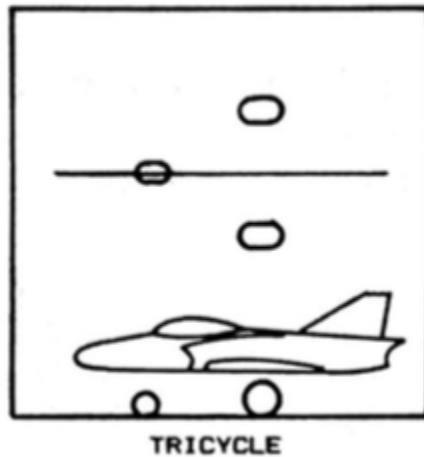


**Figure 9.27. Tricycle landing gear configuration [17].**

After studying all three landing gear configurations, the tricycle configuration was chosen for the Commander and the Chief because it was the solution to the problems presented in the taildragger and bicycle landing gear configuration. The placement of the gear yields a flat cabin floor and provides the best pilot visibility during takeoff and landing. With the presence of wind during landings, the ability to crab the aircraft is a desirable feature. The nose landing gear will be placed 76.462 in aft of the tip of the radome and directly under the fuselage for both the Commander and the Chief. The main landing gears will be placed 38.683 in and 32.754 in aft of the aircraft's center of gravity for the Chief and the Commander, respectively, and  $\pm 50$  in along the  $y$ -direction.

## **9.7.2 Shock Absorption Trade Study**

After determining the landing gear configuration, the type of shock strut for the Commander and the Chief was assessed. Three gear and shock absorption methods were considered: rigid axle, solid spring and oleo shock strut.

The rigid axle configuration is the original shock absorption method. The landing gear wheels are welded to the airframe. While this configuration is structurally sound, the shock from an imperfect landing is transferred to the fuselage. This would be felt by the pilot and passengers and would make it an uncomfortable in-flight experience.

Next, spring struts were analyzed and is another simple method to absorb shock. When the aircraft lands, the strut flexes upwards and when it returns to its original position, the forces are dissipated through the airframe. Spring struts are typically made from steel and aluminum materials and most recently, composites. Using composite materials, springs struts yield extremely lightweight gears. In terms of maintenance, they are also economically efficient because they will not corrode compared to steel and aluminum parts.

Finally, shock struts were studied. Shock struts are pneumatic and hydraulic struts that combines nitrogen and hydraulic fluid as shown in Figure 9.28. Typical shock struts contain an inner cylinder and outer cylinder assembly and the flow is regulated with a metering pin and orifice plate. When the aircraft lands, the inner cylinder moves hydraulic fluid through the outer cylinder as kinetic energy and generates heat as thermal energy. The transfer of energy forms absorbs the shock experienced by the aircraft during landings.

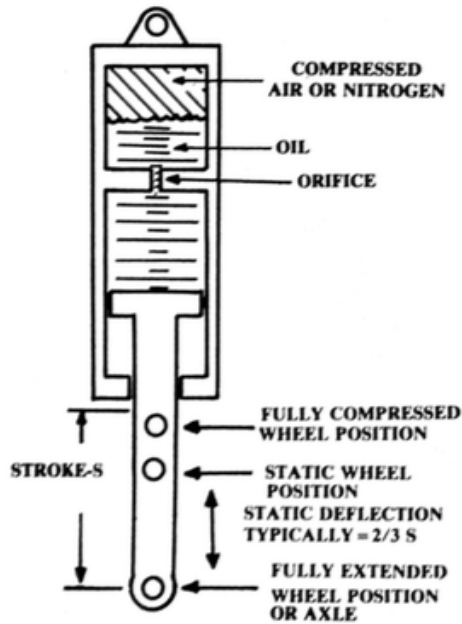


**Figure 9.28. Schematic of shock strut absorber [17].**

After studying all three shock absorption methods, the shock strut was chosen for the Commander and the Chief. While a lightweight shock strut is desirable, stronger and historically reliable materials like steel and titanium is required to support the aircraft when the aircraft is taxing and absorb the shock when the aircraft is landing. A landing gear made of composite materials could lead to a collapsed landing gear and damage the belly of the fuselage and wing tips. Unlike the rigid axle and spring struts, the shock strut absorbs shock most efficiently and will create the most comfortable passenger experience.

### **9.7.3 Components**

The desired nose and main landing gear will consist of major gear components used on commercial aviation aircrafts today. The nose landing gear will comprise of an inner cylinder and outer cylinder with an upper and lower torsion link to hinge the two components together. At the base of the outer nose gear cylinder, an upper steering plate and a lower steering plate is attached. At the two in-line bores of the plates, steering actuators are installed and is wired to the cockpit

for pilots to steer the business jet during takeoff and taxi. Three taxi lights are installed on the outer nose gear cylinder and above the steering assembly. This will provide visibility for pilots during dim and dark conditions. All assemblies mentioned above will be installed on the nose landing gear axle that is attached to the number one (left nose landing gear) tire and number two (right nose landing gear) tire.

The left and right main landing gear will take on a very similar form to the nose landing gear. They will also comprise of an inner cylinder and outer cylinder with an upper torsion link and lower torsion link to hinge the shock strut assembly together. The main landing gear outer cylinder does not have a triangular attachment like the nose gear cylinder. To better distribute the aerodynamic and braking loads along the main landing gear, a diagonal arm called the drag strut assembly is introduced. The drag strut assembly consists of a lower drag brace that is attached to the outer cylinder and an upper drag brace that is attached to the wheel well under the wing. At the hinge between the upper and lower drag brace, the drag strut assembly folds and is tucked snugly under the wing when the gear is retracted. All assemblies mentioned above will be installed on the main landing gear axles that are attached to the number three and number four (left main landing gear outboard and inboard respectively) tires and the number five and number six (right main landing gear inboard and outboard respectively) tires.

#### **9.7.4 Loads**

To calculate the static load carried by the nose landing gear, moments were summed about the main landing gear and to calculate the static load carried by the main landing gear, moments were summed about the nose landing gear. Once the static load carried by either the nose landing gear or main landing gear was determined, the following equation can be used to determine the unknown force [23]:

$$P_n + n_s P_m = W \quad (10)$$

In **Error! Reference source not found.** and **Error! Reference source not found.**, nose landing gear and main landing gear forces are tabulated at takeoff gross and empty fuel weight for the Chief and the Commander, respectively.

**Table 9.6. Nose Landing Gear and Main Landing Gear Load Calculations for the Chief**

Weight Configuration	Weight [lb]	Nose Landing Gear Load [lbf]	Main Landing Gear Load [lbf]
Takeoff Gross Weight	16329.53	2958.14	13371.39
Empty Fuel Weight	11329.53	1898.35	9431.18

**Table 9.7. Nose Landing Gear and Main Landing Gear Load Calculations for the Commander**

Weight Configuration	Weight [lb]	Nose Landing Gear Load [lbf]	Main Landing Gear Load [lbf]
Takeoff Gross Weight	19261.12	2701.39	16559.72
Empty Fuel Weight	13561.12	2077.67	11483.44

Using the tabulated values from **Error! Reference source not found.**, the nose landing gear takes on 18.115% and the main landing gear takes on 81.885% of the Chief's load at the takeoff gross weight. When the aircraft is devoid of fuel, the nose landing gear and main landing gear loads change as the center of gravity changes. Using the tabulated values from **Error! Reference source not found.**, the nose landing gear takes on 16.756% and the main landing gear takes on 83.244% of the Chief's load at the empty fuel weight. With the same calculation and analysis, the nose landing gear carries 14.025% and the main landing gear carries 85.975% of the Commander's load at the takeoff gross weight and the nose landing gear carries 15.321% and the main landing gear carries 84.679% of the Commander's load. These percentages are consistent with percentages used for transport aircraft with a tricycle configuration. With the two center of gravity values at takeoff gross weight and empty fuel weight, the percentages reflect the chosen location of our landing gears is acceptable.

### **9.7.5 Wheel Sizing**

During taxiing, takeoff roll and landing roll, tires experience severe static and dynamic loads. A wide variety of tires were analyzed to ensure the selected tire could withstand these demanding situations and the Type VII/New Design tires were chosen for the Commander and the Chief. Type VII/New Design tires are built to carry extra high pressure, carry the largest load capacity and travel at very high takeoff speeds. It also has a narrow width that will not take up an insignificant amount of space when stored in the wheel well.

As described in 9.6.3, the nose landing gear will have two total tires and the main landing gear will have four total tires. For the Commander, the nose landing gear will carry a maximum load of 2701.39 lbf and each tire will carry 1350.69 lbf. It is estimated the aircraft will grow in weight during its lifecycle and 25% is added on to the tire load to account for the weight addition [23]. As a result, each nose landing gear tire will carry 1688.37 lbf. The main landing gear will carry a maximum load of 16559.73 lbf and each tire will carry 4139.93 lbf. Accounting for the weight fluctuations, each main landing gear tire will carry 5174.91 lbf. Looking at Goodrich's tire data catalogs [23], a tubeless 14.5 in in diameter and 5.5 in in width tire was chosen for the nose landing gear. Each nose gear tire can carry a maximum load of 3550 lbf and travel at a maximum speed of 200 mph with a maximum inflation pressure of 155 psi. For the main landing gear tires, a tubeless 20 in in diameter and 5.5 in in width tire was chosen. Each main gear tire can carry a maximum load of 7200 lbf and can travel at a maximum speed of 200 mph with a maximum inflation pressure of 230 psi. To ensure the tires could support the maximum loads, the selected tires can carry more than 25% of the maximum load. The chosen tires are also sized perfectly to fit inside their respective wheel well making them a great choice for the Commander.



The same wheel sizing analysis was carried over for the Chief. The nose and main landing gear tires chosen for the Commander will be used for the Chief to maintain commonality between our variants. This continues to support our design philosophy of economizing cost and providing customers with the best product value.

### 9.7.6 Shock Strut and Height Sizing

Using the fundamental physics equation of kinetic energy as shown in Equation (11), we can calculate the vertical energy of the aircraft to determine the required dimensions of the tire and shock absorber.

$$E_t = \frac{1}{2} \left( \frac{W}{g} \right) w_t^2 \quad (11)$$

To satisfy FAR 23 standards for the Chief, a vertical touchdown rate of 10 ft/s was chosen and to satisfy FAR 25 standards for our eight passenger aircraft, a vertical touchdown rate of 12 ft/s was chosen.

To better analyze the distribution of the kinetic energies seen in the landing gear, the tire and shock absorber energies are separated and the number of struts, maximum loads and landing gear load factor are introduced. Then, the maximum kinetic energy seen by the airplane is rewritten with the following equation [23]:

$$E_t = n_s P_m N_g (\eta_t s_t + \eta_s s_s) \quad (12)$$

For the Chief, a  $N_g$  of 3.0 must be used to meet FAR 23 standards and for our eight passenger aircraft, a  $N_g$  of 1.5 to 2.0 must be used to meet FAR 25 standards. Tire and shock absorber efficiency values of 0.47 and 0.80 respectively were chosen for our tire and shock absorption method from Table 2.17 [23] to represent their typical efficiency values. Equating Equation (11) and Equation (12) and solving for  $s_s$ , we find the desired length and diameter for the shock

absorber. In **Error! Reference source not found.**, the maximum kinetic energy and desired shock absorber length and diameter are tabulated for the Commander.

**Table 9.8. Maximum Kinetic Energy and Shock Absorber Length and Diameter Calculations**

Item	Notation	Value	Units
Landing weight	$W_L$	19261.12	[lb]
Vertical touchdown weight	$w_t$	12	[ft/s]
Number of main landing gear struts	$n_s$	2	[-]
Maximum static main landing gear load (per strut)	$P_m$	8279.86	[lbf]
Landing gear load factor	$N_g$	2	[-]
Tire energy absorption efficiency	$\eta_t$	0.47	[-]
Energy absorption efficiency of the shock absorber	$\eta_s$	0.8	[-]
Maximum allowable tire deflection	$s_t$	1.475	[-]
Stroke of the shock absorber	$s_s$	18.639	[in]
Desired stroke of the shock absorber	$s_{s,desired}$	19.639	[in]
Diameter of the shock absorber	$d_s$	3.222	[in]
Maximum kinetic energy of the calculated stroke of the shock absorber	$E_t$	43068.35	[ft-lbf]

Combing the stroke of the inner cylinder and outer cylinder along with the radius of the main landing gear tire, the height of the main landing gear and wheel assembly is 50.792 in. In our design, the stroke of the nose and main landing gears are the same for consistency. Factoring in a smaller nose landing gear tire, the height of the nose landing gear and wheel assembly is 48.042 in. To maintain an even cabin floor, the main landing gear will be installed 2.75 in higher in the  $x$ -direction to account for the gear height offset.

## 9.8 Future Work

All of the calculations made were rough estimates of the actual values. Detailed computations can be done by modeling various components of the Commander and the Chief in a finite element analysis software like Abaqus to gain a better understanding of the aircraft during various structural loads. We will be able to generate pressure and stress distributions along

modelled components and see if our aircraft is structurally sound as designed or if it needs to be redesigned.

The landing gear system lacks system integration. The current nose landing gear design consists of an upper and lower steering plate, but steering actuation methods will need to be analyzed to determine what the best method to steer the aircraft. The current analysis does not contain wiring of hydraulic and fuel lines. Their purpose and locations will need to be investigated so the landing gear can extend and retract.

## **10 Costs (McHugh)**

### **10.1 Basis for Estimation**

There are various methods for estimating the cost of a proposed aircraft, each with varying degrees of complexity and accuracy. Due to the “back of the envelope” nature of our design and the limited experience of our design team in producing similar aircraft, our cost estimations were limited to statistical methods. The first method we used is an approximation based on the cost to weight ratios of other Light Jets and should only be used to give context to more accurate methods. The second method similarly compares similar jets but differs in that it then forms weighted normal distributions for several variables based upon their correlation to cost and, from this, produces a more accurate cost estimate. The final and most accurate method employs CERs developed by the RAND Corporation to estimate RDT&E cost and Flyaway cost. A comparison will be made of all three methods and will be used to frame a discussion on the optimal quantity of production and market potential for the Commander and the Chief aircraft series as well as to produce a breakdown of RDT&E plus Flyaway costs for both variants.

### **10.2 Method #1: Comparison to other Light Jets**

According to Raymer “aircraft...are bought by the lb” [18]. Using this principle, we can compare aircraft within our market segment to find an average cost for light jets per lb of empty weight. From this we can obtain an estimate of the cost of the Commander and the Chief aircrafts using their respective approximate empty weights of 12633 lb and 12116 lb.

**Table 10.1. Cost Over Weight Ratios for Light Jets**

<b>Model</b>	<b>W<sub>e</sub> (lb)</b>	<b>Cost (USD)</b>	<b>W<sub>e</sub> Cost Ratio (USD/lb)</b>
Cessna Citation CJ3+	8,185	8,300,000	1014.05
Syberjet SJ30	8,500	7,900,000	929.42
Cessna Citation CJ4	6,765	9,000,000	1330.38
Embraer Phenom 300	14,000	8,760,000	625.71
Learjet 70	13,890	11,300,000	813.53
Average	[-]	[-]	942.62 USD/lb
The Commander	12,633	11,900,000	[-]
The Chief	12,116	11,400,000	[-]

This cost estimate of \$11,900,000 and \$11,400,000 are reasonable values. However, a closer examination of the method shows that it has significant flaws. Firstly, the limited sample size and wide range of cost ratios give a misrepresentative distribution values. Secondly, there seems to be less correlation between empty weight and cost than assumed; it is possible that other variables are more directly related to the aircraft cost. It is probable that these errors are a result of the lower weights of light business jets compared to other aircraft for which this method is more accurate. These low weight values mean that the proportional differences in weight lead to greater variance in the cost compared to larger commercial jets thus creating both of the aforementioned flaws.

### **10.3 Method #2: Weighted Normal Distribution of Comparable Jets**

Given the shortcomings of the previous method there is an opportunity for deeper statistical analysis. As such, an original method for cost estimation was developed with a broader sample size and more dependent variables. We expanded the sample size by including very light jets and

mid-sized jets. MTOW and seating capacity were chosen as the additional dependent variables, along with empty weight, for their apparent high correlation to cost.

**Table 10.2. Multi-Variable Comparison of Similar Jets**

Model	Seats	MTOW [lb]	W <sub>e</sub> [lb]	Cost [USD]
Cessna Citation CJ3+	8.5	13870	8,185	8,300,000
Syberjet SJ30	5.5	13950	8,500	7,900,000
Cessna Citation CJ4	8.5	17110	6,765	9,000,000
Embraer Phenom 300	8.5	17968	14,000	8,760,000
Learjet 70	6.5	21500	13,890	11,300,000
Cessna Citation M2	7	10700	6,746	4,500,000
HondaJet	5.5	9963	7,203	4,500,000
Phenom 100E	6	10582	7,132	4,200,000
Learjet 75	8.5	21500	13,890	13,800,000
Sample Set Values				
Average	7.25	17242	9,590	8,886,000
Z-score	0.60984 / -1.0164	0.95358 / 0.17378	0.67064 / 1.4151	[-]
Correlation Coefficient	0.53783	0.94898	0.77662	[-]
Weighted Z-score	0.14494	0.39988	0.23015	[-]
Cost Estimates				
The Commander	8	21,300	12,633	11,667,000
The Chief	6	18,500	12,116	9,312,000

By relating all three variables (seats, maximum takeoff weight and empty weight) to the cost for each aircraft we can determine each variables influence on the cost and thus weight our cost estimation accordingly. Specifically, for each variable's sample set we calculate a mean, standard deviation and correlation coefficient (vs cost). With these values we produce weighted z-scores which we sum to finally calculate the X value of the cost sample. These X values of \$11,667,000 and \$9,312,000 are reasonable cost estimates for the Commander and the Chief aircrafts respectively.

#### **10.4 Method #3: RAND Corporation's Cost Estimating Relationships**

Given our resources the most accurate method for estimating aircraft cost is to employ the cost estimating relationships published by the RAND Corporation. This method still relies upon

simple variables but uses curve fitting programs based on cost data from other aircraft to produce an accurate estimation. In our case we will leave the variable  $Q$ , quantity of aircraft produced, undefined, and vary it from 50 to 2000 allowing us to find the optimal production quantity. Using Raymer as a guideline, we can proceed through these calculations. It is necessary to convert the hourly wages given in this text to 2016 USD using the Consumer Price Index and to convert the purchase prices calculated in previous methods, used in the figure below as comparative values, into production costs (RDT&E plus flyaway costs) using an investment cost factor.

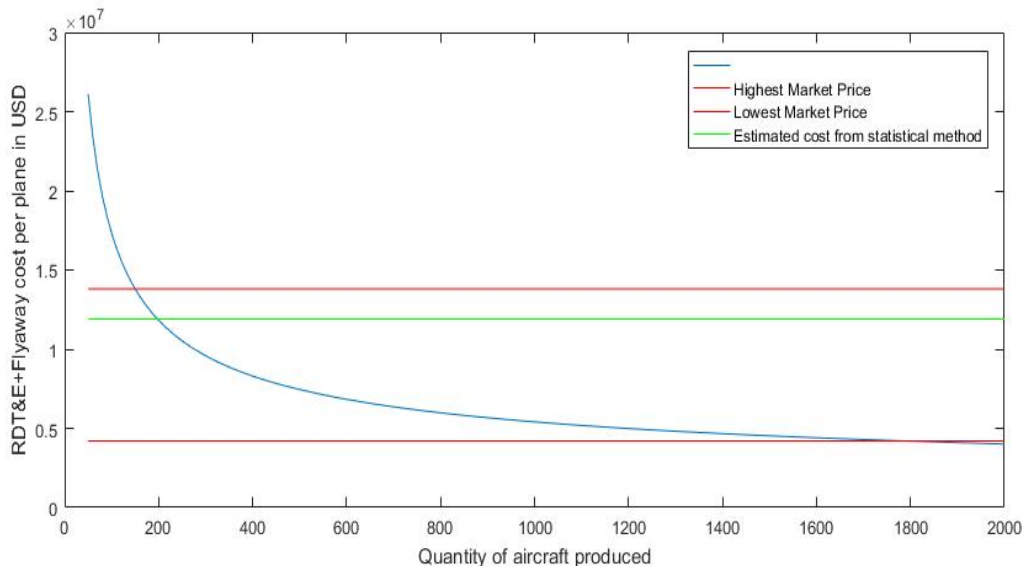


**Figure 10.1. Quantity of aircraft produced versus RDT&E plus flyaway costs for the Commander.**

**Error! Reference source not found.** shows the relationship between quantity of aircraft produced and aircraft costs (RDT&E plus Flyaway costs) for the Commander. The highest and lowest prices on the market, converted to costs, are shown for reference alongside the cost estimate given by the previous method. The benefit of varying  $Q$  when applying this CRE method is that it displays the range of feasible production quantities. In the case of the Commander, it is implausible to compete with the low end of the market no matter how many aircraft we can produce. It would also be unreasonable to expect either aircraft to compete at the high end of the market given their

specifications. In order to sell at a price in between these two extremes it is necessary to produce more than 150 aircraft. Based on these conclusions, it seems that the ideal strategy for both aircraft would be to list at purchase prices below the price points of \$11,667,000 and \$9,312,000 which the previous method suggests as being reasonable for aircrafts of similar specifications. This strategy would market the Commander and the Chief aircraft series as value purchases but would also require higher than expected production quantities. Meeting this requirement would depend on investors' assessments of the current market for light jets and their willingness to assume the financial risk of a high production quantity.

### **10.5 Market Analysis**

In order to justify any production quantity, it is necessary to understand the potential of the market segment for light jets. Competition analysis shows that a typical annual production quantity is between 20 and 80 aircraft. Over the lifetime of a light jet as many as 500 units might be produced although more often that number is around 200. These values were often lower at the beginning of a product's life cycle, which shows an average potential for 200 sales within the first four years of its release.

In general, it is advisable to project production quantities conservatively due to the high investment risk associated with bringing any concept aircraft to production. However, consideration of external factors which were present in the market at the time of data collection suggests there may be cause for some optimism regarding the market potential of the Commander and the Chief aircrafts. The data was collected in the early 2010's at a time when the weakened Euro had created a buyer's market. Furthermore, the comparative data on new product releases was collected at a time of economic downturn which would suggest that production quantities over 200 are now possible. Additionally, as a US based company we have inside access to 52% of the

total market for business jets. These three insights suggest a great enough demand for our aircrafts to justify a more aggressive marketing strategy than typical in this industry. By considering both this optimism about the potential for the light jet market segment and the typically conservative approach to this high risk investment we arrive at a projected quantity of 300 units.

## 10.6 RDT&E and Flyaway Costs

By inserting this production quantity value of 300 into the CERs used in the third method we can obtain a final cost estimate, estimate a purchase price and breakdown the total RDT&E and flyaway costs according to various project, parts and labor costs. Due to the interrelated nature of RDT&E costs and flyaway costs within each category it is very difficult to separate them. For example, engineering hours encompasses both time spent designing the aircraft and time producing it.

**Table 10.3. Breakdown of RDT&E Plus Flyaway Costs for the Commander**

<b>Cost (USD)</b>		<b>Variable</b>		<b>Total (USD)</b>
Engineering Hours	4,506,000	Engineering wrap rate	130.35	587357100
Tooling Hours	2,884,700	Tooling wrap rate	133.88	386203636
Manufacturing Hours	12,347,000	Manufacturing wrap rate	110.50	1364343500
Quality Control Hours	1,642,100	Quality Control wrap rate	122.19	200648199
Development Support Costs	51,762,000	[-]	[-]	51762000
Flight Test Costs	9,774,700	[-]	[-]	9774700
Manufacturing Materials Costs	272,840,000	[-]	[-]	272840000
Engine Production Costs	3,164	Number of engines	600	1898400
Avionics Costs	2,627,400	[-]	[-]	2627400
<b>Total RDT&amp;E + Flyaway Costs</b>	[-]	[-]	[-]	2,875,531,034
<b>Cost per Aircraft</b>	[-]	[-]	[-]	9,585,103
<b>Purchase Price</b>	[-]	[-]	[-]	11,000,000



The results of this breakdown are in line with goals set out following market analysis. The high production quantity of 300 units leads to a low cost per aircraft of \$9,600,000 for the Commander and \$9,200,000 for the Chief. By approximating an investment cost factor of 1.15 we can estimate our purchase prices to be \$11,000,000 and \$10,500,000, respectively. These price points will position both aircraft perfectly within our market segment of light jets to take advantage of what is our high projections for demand in the 2020's.

## **11 Avionics (Balsu)**

### **11.1 Introduction**

Avionics have become a critical component of the 21<sup>st</sup> century aircraft; it is unthinkable to design an airplane without considering avionics integration and support beforehand. The role of avionics is becoming increasingly diverse and demanding: pilots expect to do more with fewer gestures and screens cluttering the cockpit. As such, pilot comfort and user experience has become the centerpiece of designing avionics systems. In implementing an avionics package for both iterations of the aircraft, it was decided that an integrated approach was best, i.e., rely on one vendor for the whole avionics package instead of mixing and matching components from different vendors. Even though customers can expect to pay a higher premium for a one-vendor solution, this offsets the chance of a critical system failure or software error due to component incompatibilities from different vendors. As such, keeping in mind the safety of all passengers and crew on board, a one-vendor solution was decided upon.

### **11.2 Avionics Cockpit Package**

The most attractive avionics package for the aircraft was determined to be the Rockwell Collins Pro Line 21<sup>™</sup>. This provides a myriad variety of avionics solutions that empower a pilot to do more with less, and includes features like:

- Rockwell Collins flight guidance system
- Large AMLCDs (Active Matrix Liquid Crystal Displays)
- Weather radar
- TCAS
- TAWS
- Electronic checklist
- 3-D flight plan maps
- Electronic charts
- Digital data-links
- Real time weather graphics (which allow for a high degree of situational awareness)
- Mature designs (higher dispatchability)
- Upgradeability
  - Synthetic Vision System (SVS)
- Designed with growth in mind

The latter point is especially important because of future retrofitting/software upgrades to the system, which will benefit the customer due to an increase in product life. As such, this satisfies the design philosophy of providing the best possible value to customers. Yet another selling point was the extreme flexibility of the package: Rockwell Collins will fit the avionics according to the designs of the aircraft's cockpit area and volume, which makes it a fantastic solution for the needs of the team.

### **11.3 Connectivity Package**

Another crucial feature in today's increasingly data-hungry and information-centric business traveler is the constant presence of internet connectivity. At the heart of the strategy to provide customers with a reliable, high-speed, connection link to the Internet is the Rockwell Collins ARINCdirect Inmarsat Jet Connex Services solution. This package contains the following:

- Seamless global coverage for continuous, consistent service
- Upgradeable bandwidth for new devices and applications
- Airborne Data Router (ADR) for next gen connectivity from the flight deck to the cabin
- One price for a complete connectivity package
- One invoice for all service calls
- One phone number for technical, customer, and billing support
- Upgradeability
  - Stage<sup>TM</sup> digital entertainment service

- Live TV

This package was chosen for its high-speed capacity and due to further integration with Rockwell Collins as a trusted avionics partner. As such, given that a one-vendor avionics solution has been important in the design of this business jet, this partnership with Rockwell Collins may be fruitful and may even lead to discount purchases, leading to an overall cost reduction for the customer.

#### **11.4 Upgrades**

The customer will also be able to purchase upgrades to the basic avionics kit, as indicated above. These upgrades will ensure a premium experience for the customer, which will increase overall product satisfaction.

#### **12 Conclusion**

The Chief and Commander meet and exceed the requirements set out by the Request for Proposal, and they provide convenient, affordable, and fast transportation from coast-to-coast. Further optimization of the aircraft designs will serve to improve their performance and make the family of light business jets even more competitive with similar aircraft that are on the market. The Chief and Commander designs allow for the development of a higher-capacity variant in the future because the common fuselage structure allows the cabin to be easily extended or shortened to seat different numbers of passengers and offer a variety amenities.

#### **References**

[1] Ansell, P. J., “Lecture 14”, Spring 2016 – AE 419 – Aerospace Flight Mechanics – Section A1, University of Illinois at Urbana-Champaign, Feb. 2016.

[2] ARINCDirect, R. C., “Rockwell Collins' ARINCDirect | Jet ConneX (JX),” *Rockwell Collins' ARINCDirect*. [<http://www.arincdirect.com/what-we-do/cabin-communications/inmarsat-jet-connex-jx-services> Accessed 11/18/16.]

- [3] “Civil Turbojet/Turbofan Specifications,” *Civil Turbojet/Turbofan Specifications*. [<http://www.jet-engine.net/civtfspec.html> Accessed 11/10/16.]
- [4] D’Urso, S. J., “Avionic Data for Business Jets”, AE 442 Reference Materials, Aug. 2016
- [5] D’Urso, S. J., *Constraint Analysis I*, Sep. 2016.
- [6] D’Urso, S. J., *Constraint Analysis II*, Sep. 2016.
- [7] D’Urso, S. J., *Constraint Additional Notes*, Sep. 2016.
- [8] D’Urso, S. J., “2016-2017 Aircraft Design Team Project RFP: Light Business Jet Family,” Fall 2016 – AE 442 – Aerospace Systems Design I – Section A1, University of Illinois at Urbana-Champaign, Oct. 2016.
- [9] “FJ44-4,” *FJ44-4 - Products - Williams International*. [<http://www.williams-int.com/products/fj44-4> Accessed 10/30/16.]
- [10] “Garrett TFE731-3 Cutaway Drawing as a Licensed Media,” *FlightGlobal Image Store*. [<http://www.flightglobalimages.com/garrett-tfe731-3-cutaway-drawing/print/1569729.html> Accessed 11/20/16.]
- [11] Mattingly, J. D., *Elements of Propulsion*, American Institute of Aeronautics and Astronautics, Inc., Reston, VA, 2006.
- [12] *Metals Handbook, Vol. 2 - Properties and Selection: Nonferrous Alloys and Special-Purpose Materials*, ASM International, 10th ed., 1990.
- [13] Munson, K., and Taylor, J. W. R., *Jane's All the World's Aircraft*, Jane’s Information Group, London, England, 1987.
- [14] “Pro Line 21™ Integrated Avionics System,” *Rockwell Collins, Pro Line 21*. [[https://www.rockwellcollins.com/Data/Products/Integrated\\_Systems/Flight\\_Deck/Pro\\_Line\\_21\\_Integrated\\_Avionics\\_System.aspx](https://www.rockwellcollins.com/Data/Products/Integrated_Systems/Flight_Deck/Pro_Line_21_Integrated_Avionics_System.aspx) Accessed 11/18/16.]
- [15] “PW300,” *PW300 | Pratt & Whitney Canada*. [<http://www.pwc.ca/en/engines/pw300> Accessed 10/20/16.]
- [16] “PW500,” *PW500 | Pratt & Whitney Canada*. [<http://www.pwc.ca/en/engines/pw500> Accessed 10/20/16.]
- [17] Raymer, D. P., *Aircraft Design: A Conceptual Approach*, 2nd ed., American Institute of Aeronautics and Astronautics, Inc., Reston, VA, 1992.
- [18] Raymer, D. P., *Aircraft Design: A Conceptual Approach*, 5nd ed., American Institute of Aeronautics and Astronautics, Inc., Reston, VA, 2012.

- [19] Roark, R. J., Young, W. C., and Budynas, R. G., *Roark's Formulas for Stress and Strain*, McGraw-Hill, New York, NY, 2002.
- [20] Roskam, J., *Airplane Design, Part I: Preliminary Sizing of Airplanes*, DARcorporation, Lawrence, KS, 2005.
- [21] Roskam, J., *Airplane Design, Part II: Preliminary Configuration Design and Integration of the Propulsion System*, DARcorporation, Lawrence, KS, 2004.
- [22] Roskam, J., *Airplane Design, Part III: Layout Design of Cockpit, Fuselage, Wing and Empennage: Cutaways and Inboard Profiles*, DARcorporation, Lawrence, KS, 2011.
- [23] Roskam, J., *Airplane Design, Part IV: Layout of Landing Gear and Systems*, DARcorporation, Lawrence, KS, 1985.
- [24] Roskam, J., *Airplane Design, Part V: Component Weight Estimation*, DARcorporation, Lawrence, KS, 2003.
- [25] Roskam, J., *Airplane Design, Part VII: Determination of Stability, Control and Performance Characteristics: FAR and Military Requirements*, DARcorporation, Lawrence, KS, 2006.
- [26] Sadraey, M., *Aircraft Design: A Systems Engineering Approach*, John Wiley & Sons, Ltd, West Sussex, United Kingdom, 2013.
- [27] Staff, "Flying Offices: Staying connected on a private jet", *CorporateJetInvestor*, Feb. 2015. [<http://corporatejetinvestor.com/articles/flying-offices-staying-connected-private-jet-836/> Accessed 11/18/16.]
- [28] "TFE731 Turbofan Engine," *TFE731*. [<https://aerospace.honeywell.com/en/products/engines/tfe731-turbofan-engine> Accessed 10/19/16.]